TAMPEREEN TEKNILLINEN YLIOPISTO
TAMPERE UNIVERSITY OF TECHNOLOGY

TONI LIIMATTA

INKJET PRINTING IN MANUFACTURING OF STRETCHABLE INTERCONNECTS

Master's thesis

Examiner: Assist. Prof. Matti Mäntysalo
Examiner and topic approved by the Faculty Council of the Faculty of Computing and Electrical Engineering on 9th October 2013.

ABSTRACT

TAMPERE UNIVERSITY OF TECHNOLOGY
Master's Degree Programme in Electrical Engineering
LIIMATTA, TONI: Inkjet printing in Manufacturing of Stretchable Interconnects
Master of Science Thesis, 77 pages, 1 Appendix page
March 2014
Major: Electronics Product Design
Examiner: Assist. Prof. Matti Mäntysalo
Keywords: inkjet printing, stretchable electronics, printed electronics, digital manufacturing, elastic substrate materials, functional inks, nanotechnology

Smaller form factors and dynamic applications have made flexible circuits an essential part of today's electronic devices. Although flexible electronics is well established and constantly growing industry, this technology has its limitations. Flexible circuits can typically bend along one axis and cannot therefore conform to arbitrary shapes like for example human skin. The transition to stretchable electronics is an alternative, which can enable bending in any direction simultaneously and in addition dynamically changing the surface area of device. However, manufacturing of stretchable electronics sets new challenges for manufacturing technology due to significantly different material properties of stretchable substrates and therefore new manufacturing methods must be introduced.

Inkjet printing is an emerging technology for printed electronics and due to the digital control of the printing process the adaptation to different circuit board layouts is easy and fast. Therefore inkjet printing is especially suitable for small volume manufacturing, prototyping and research purposes of transferring conventional flexible circuits to printing technology. Since inkjet technology has already been proven feasible with flexible circuits, this thesis focuses on evaluating feasibility of inkjet printing in manufacturing of stretchable electronics. Advantages of inkjet technology like contactless deposition, low process temperatures and low use of chemicals are very beneficial when stretchable substrate materials are considered.

The feasibility of inkjet printing in manufacturing of stretchable circuits is studied in this thesis through literature review and experimental analysis. Different manufacturing methods for stretchable electronics are reviewed and based on this; a method for manufacturing stretchable devices utilizing inkjet printing and stretchable interconnects is presented. This thesis describes optimizing process of manufacturing process parameters and development of strain testing system to analyze manufactured structures. Peak strain of inkjet-printed conductors on stretchable substrate is found to be modest, but conductivity is observed to be almost fully reversible when strain is released. Based on the knowledge accumulated during this work, suggestions for improving performance of inkjet-printed interconnects on stretchable substrate are given.

TIIVISTELMÄ

TAMPEREEN TEKNILLINEN YLIOPISTO
Sähkötekniikan koulutusohjelma
LIIMATTA, TONI: Mustesuihkutulostus venytettävien johtimien valmistuksessa
Diplomityö, 77 sivua, 1 liitesivu
Maaliskuu 2014
Pääaine: Elektroniikan tuotesuunnittelu
Tarkastaja: Assist. Prof. Matti Mäntysalo
Avainsanat: mustesuihkutulostus, venytettävä elektroniikka, painettava elektroniikka, digitaalinen valmistus, elastiset alustamateriaalit, funktionaaliset musteet, nanoteknologia

Elektroniikkalaitteiden yhä pienenevä koko ja liikkuvia osia sisältävät sovellukset ovat tehneet taipuisista piirilevyistä olennaisen osan nykyisiä elektroniikkatuotteita. Vaikka taipuvien piirilevyjen valmistus on vakiintunut ja jatkuvasti kasvava teollisuudenala, tällä tekniikalla on omat rajoituksensa. Taipuisat piirilevyt voivat tyypillisesti taipua vain yhteen suuntaan kerrallaan, eivätkä ne näin ollen pysty mukautumaan monimutkaisiin muotoihin kuten esimerkiksi ihmisen iholle. Siirtymällä venytettävään elektroniikkaan taipuisuus voidaan saavuttaa yhtä aikaa mihin tahansa suuntaan ja lisäksi laitteen pinta-alaa voidaan muuttaa dynaamisesti. Venytettävän elektroniikan valmistus aiheuttaa kuitenkin uusia haasteita tuotantomenetelmille, koska venytettävien alustamateriaalien ominaisuudet poikkeavat merkittävästi totutuista materiaaleista. Tämän takia uusia valmistusmenetelmiä on kehitettävä.

Mustesuihkutulostus on nouseva teknologia painettavassa elektroniikassa ja digitaalisesti ohjatun valmistusprosessin ansiosta se mukautuu helposti ja nopeasti erilaisiin piirilevymalleihin. Mustesuihkutulostus sopii siis erityisesti pieniin valmistussarjoihin, prototyyppien valmistukseen ja tutkimuskäytössä tavallisten piirilevymallien siirtämiseen painomenetelmillä valmistettaviksi. Koska mustesuihkutulostus on osoitettu käyttökelpoiseksi menetelmäksi taipuisien piirilevyjen valmistuksessa, tässä diplomityössä keskitytään mustesuihkutulostuksen käyttöön venytettävän elektroniikan valmistuksessa. Mustesuihkutekniikan erityisiä etuja venyvien alustamateriaalien kohdalla ovat muun muassa painomenetelmän kontaktittomuus, matalat prosessilämpötilat ja vähäinen kemikaalien käyttö.

Tässä diplomityössä tutkitaan mustesuihkutulostuksen käyttöä venytettävän elektroniikan valmistuksessa kirjallisuusselvityksen sekä kokeellisten menetelmien avulla. Diplomityössä käsitellään kirjallisuudessa esitettyjä venytettävän elektroniikan valmistusmenetelmiä ja tämän pohjalta esitetään venytettävien elektroniikkalaitteiden valmistukseen menetelmä, joka hyödyntää mustesuihkutulostusta ja venytettäviä johtimia. Menetelmän valmistusprosessin parametrit optimoidaan ja valmistettujen rakenteiden venytystestaukseen kehitetään järjestelmä. Venyvälle alustamateriaalille mustesuihkutulostettujen johtimien suurimmat saavutetut venymät huomattiin melko vaatimattomiksi, mutta niiden johtavuuden todettiin palautuvan lähes täysin, kun venytys vapautetaan. Työn aikana kerääntyneen tiedon pohjalta annetaan ehdotuksia, joilla mustesuihkutulostettujen johtimien suorituskykyä voitaisiin parantaa.

PREFACE

This Master's thesis was done at Department of Electronics and Communications Engineering at Tampere University of Technology during 2013. Work was carried out as a part of HealthSens –project, which is a 2-year project funded by the Finnish Funding Agency for Technology and Innovation (Tekes).

I would like to thank my thesis examiner Assist. Professor Matti Mäntysalo for guidance and valuable feedback. I would also like to thank my supervisor D.Sc. Eerik Halonen and M.Sc. Juha Niittynen in the TUT Printable Electronics research group for advice and ideas during this work and M.Sc. Miao Li for providing evaporated samples, which I used as reference samples in strain testing.

In addition, I would like to thank all the personnel in the Department of Electronics and Communications Engineering for this enjoyable working environment.

Lastly, I would like to thank my family and friends for the support during this work and my studies.

Tampere, February 2014

Toni Liimatta

CONTENTS

LIST OF ABBREVIATIONS

1-wire	Serial communication bus with possibility of using only one data wire and ground wire.
ACA	Anisotropic conductive adhesive
ADC	Analog to digital conversion/converter
AWG	American wire gauge
CAN	Controller area network. A robust serial communication bus consisting 4 wires: Power, ground and 2 signal wires for differential operation.
CIJ	Continuous inkjet
CNT	Carbon nanotube
CPU	Central processing unit
CTE	Coefficient of thermal expansion
DC	Direct current
DoD	Drop-on-demand
dpi	Drops per inch
DUT	Device under test
ECG	Electrocardiogram
EMG	Electromyography
FR-4	Flame retardant 4. A common dielectric material for printed circuit boards.
I2C	Inter-integrated circuit. A serial communication bus consisting of data signal, clock signal and ground.
IC	Integrated circuit
ICA	Isotropic conductive adhesive
LED	Light-emitting diode
LSB	Least significant bit
MCU	Microcontroller unit
OLED	Organic light-emitting diode
PAR	Polyacrylate
PC	Personal computer
PCB	Printed circuit board
PCO	Polycyclic olefin
PDMS	Polydimethylsiloxane
PEN	Polyethylene naphthalate
PES	polyethersulphone
PET	Polyethylene terephthalate
PI	Polyimide
P-PDMS	Photosensitive polydimethylsiloxane
PU	Polyurethane
RF	Radio frequency

RFID	Radio frequency identification
RTC	Real time clock
SoC	System on chip
TPU	Thermoplastic polyurethane
UV	Ultraviolet (light)
WLCSP	Wafer level chip scale package

1 INTRODUCTION

Flexible circuits have become a key enabling technology for dynamic and flex-to-fit applications in today's electronic devices. At the same time there has been growing interest for new manufacturing technologies which would enable cost-effective, fast and environmentally friendly production of flexible circuits. Printed electronics can revolutionize the electronics industry by offering these benefits due to printing technology's additive nature and feasibility for mass production, but have replaced traditional manufacturing methods only in a few applications. Hindering factors for the growth rate of printed electronics seem to be the inability of suppliers to reduce costs and the fact that it is challenging to displace traditional manufacturing methods when there is strong existing infrastructure and the new manufacturing method would require development and implementation of new design solutions. New applications utilizing printing technology are for example radio-frequency identification (RFID) and organic light-emitting diode (OLED). [1.]

Inkjet printing is an emerging technology for printed electronics and due to the digital control of the printing process the adaptation to different circuit board layouts is easy and fast. Therefore inkjet printing is especially suitable for small volume manufacturing, prototyping and research purposes of transferring conventional flexible circuits to printing technology. Applicability of inkjet printing for manufacturing flexible circuits has been demonstrated for example through a demonstrator case in which a flexible circuit board of a mobile phone was transferred to inkjet printing technology and performance of manufactured prototypes was found to be close to original devices [2.].

Although flexible electronics is well established and constantly growing industry, this technology has its limitations. Flexible circuits can typically bend along one axis and cannot therefore conform to arbitrary shapes like for example human skin. The introduction of stretchable electronics is a change, which is comparable to transition from conventional rigid circuit boards to flexible circuit boards. Stretchable circuits can enable bending in any direction simultaneously and in addition dynamically changing the surface area of device. Since the idea of stretchable electronics is to conform to arbitrary shapes like human skin, the driving force has been applications related to wearable or near-body electronics. However, most of the stretchable applications presented have not yet been seen as commercial products. Concept of stretchable circuit itself is not a new one - applications like spring shaped telephone cord or flexible circuits folded in to a shape like accordion bellows have been around for decades. The novelty in stretchable electronics is manufacturing whole electronic device on stretchable thin film, thus making the whole device stretchable. [1; 3.]

Manufacturing of stretchable electronics sets new challenges for manufacturing technology due to significantly different material properties of stretchable substrates. Conventional methods and existing infrastructure are inefficient or completely incapable in handling these materials and therefore new manufacturing methods must be introduced. Since inkjet technology has already been proven feasible with flexible circuits, this thesis focuses on evaluating feasibility of inkjet printing in manufacturing of stretchable electronics. Advantages of inkjet technology like contactless deposition, low process temperatures and low use of chemicals are very beneficial when stretchable substrate materials are considered.

The feasibility of inkjet printing in manufacturing of stretchable circuits is studied in this thesis through literature review and experimental analysis. Chapter 2 describes inkjet technology and its advantages in manufacturing flexible electronics. This is followed by Chapter 3, which presents basic principles of stretchable electronics, main manufacturing methods and applications. Based on this literature review, challenges of using inkjet technology in manufacturing of stretchable circuits is also discussed. Chapter 4 presents experimental methods for optimizing printing process for stretchable substrate materials in viewpoint of printability and electrical performance. Equipment and methods for testing stretchability of printed circuits is also presented. In Chapter 5 results of the experiments are presented and discussed, and lastly conclusions of feasibility evaluation through these methods are presented in Chapter 6.

2 INKJET-PRINTED ELECTRONICS

Printing technologies are often addressed as novel manufacturing methods for electronics. However, the industry in fact began with additive processes and one of the first methods was described by Thomas Edison in the early 1900s. Edison did not exactly mention printing, but his method for producing conductive traces on paper could easily be adapted to printing processes. During the following decades subtractive photolithography was taken as the industry standard and it still continues as the dominant circuit manufacturing method. [4.]

Since photolithography is mature and widely used technology for electronics manufacturing, the need for continuous development of processes has created an increasing demand for new manufacturing methods. Printing technologies, such as flexography, gravure, inkjet or screen printing, are subjects of interest due to their additive nature and reduced number of process steps. Screen printing is a simple printing method, which is mostly used in electronics manufacturing for printing solder pastes, solder masks and PCB markings. Figure 1A illustrates the operating principle of screen printing. As can

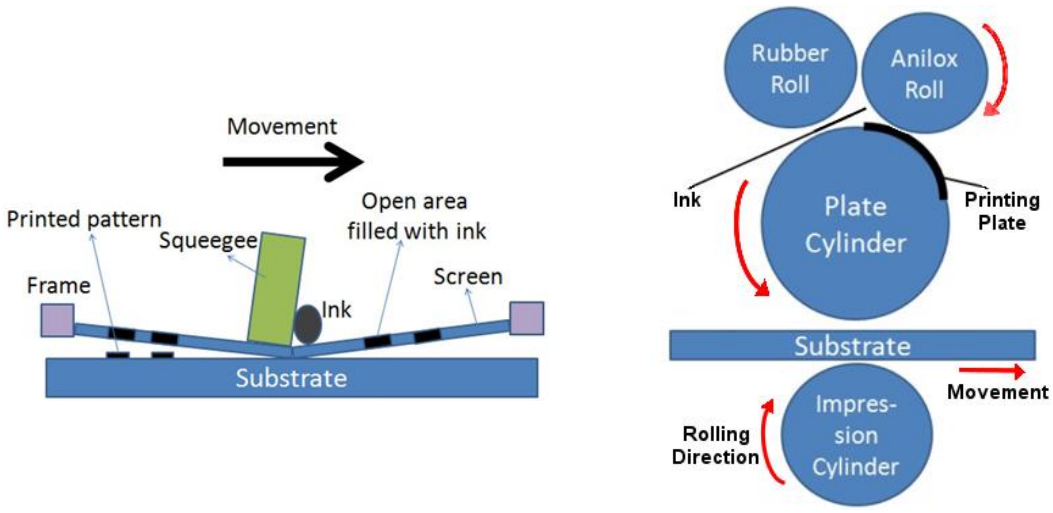

(A) **(B)**

Figure 1. *Operating principles of (A) screen printing and (B) flexography printing.[5.]*

be seen in Figure 1A, screen printing includes a screen, which is patterned with holes or open areas. Ink is placed on top of this screen and it is moved across whole patterned screen with a squeegee blade while pressing the screen against substrate material. This forces ink through the holes or open areas and it is transported on the substrate material. Amount of ink is determined by the thickness of screen. [5; 6.]

Another common printing method is flexography printing, which is illustrated in Figure 1B. In flexography printing the ink is applied to anilox roll, which is full of engraved little cups. These cups are filled with ink and therefore the amount of deposited ink is controlled by the size of these cups. Ink is transported via anilox roll on to a plate roll, which holds separate engraved printing plates. Printed pattern is determined by these engraved plates and ink is deposited on areas, which have not been recessed. Print plates then transport the ink on to substrate material. Impression cylinder is used to control the pressure between substrate and printing plate. Gravure printing is also quite similar technique as flexography printing, but the main difference is fewer number of process rolls. This is achieved by combining anilox roll and print plates to a single gravure roll, which contains little ink cups only in areas where ink is to be deposited. Gravure roll transports ink directly on to substrate and pressure is again controlled with an impression roll. [5; 6.]

Flexography, gravure and screen printing all include mechanical contact to substrate and manufacturing a pattern specific physical part, for example a screen, roll or print plate, which increases the starting costs for a single pattern. Inkjet printing is different from these methods in a way that it is a contactless method and pattern generation is controlled digitally. This means that substrate materials can be chosen more freely and the printed pattern can be changed simply by editing the print file on computer. Therefore inkjet printing is especially suitable for rapid prototyping, research and development of new materials and for manufacturing small production batches. [6; 7; 8.]

This thesis focuses on application of inkjet printing on novel substrate materials and the following subchapters serve as background information of inkjet printing and flexible electronics. First the main principles of inkjet technology are presented, which is followed by a survey of functional materials used in inkjet printing. Chapter 2.3 focuses on pattern generation with inkjet printing, which gives insight to different printing parameters and interaction between ink and substrate material. Chapter 2.4 presents how flexible electronics are manufactured conventionally and with inkjet technology, and also which materials can be used in manufacturing of flexible electronics.

2.1 Inkjet Technology and Equipment

Inkjet printing was first commercialized by Hewlett-Packard in 1984 and in the following years it has become very popular in especially small office and home applications. It differs in nature from the other common printing methods and therefore offers several advantages, which include for example that:

- No contact to substrate material is needed, which enables printing on novel and possibly non-flat substrate materials.
- No need for printing plates or any similar pattern specific parts, which reduces starting costs and therefore enables lower price per print even in small production batches.

- Process is digitally controlled and therefore printed pattern can be easily changed – even between every printed pattern.
- Printers are usually cheaper than conventional printing presses.
- There is very little ink wastage, since drops are generated only when needed or unused drops are recycled. This is especially beneficial if deposited materials are high cost or available amount is low.
- Process is usually highly automated and therefore requires very little or no monitoring. Automation also enables reproducible results and increases the process stability. [9; 10; 11.]

These advantages make inkjet printing very suitable for printed electronics especially in the research and development phase, and therefore inkjet printing is used as the main material deposition method in this thesis.

Inkjet technology can be mainly divided into two different classes based on the operating principle: continuous mode inkjet (CIJ) and drop-on-demand inkjet (DoD). Operating principles of DoD and CIJ are illustrated in Figure 2A and Figure 2B, respectively. In continuous mode inkjet printing a stream of ink flows through a small orifice and due to the Plateau-Rayleigh instability the stream breaks up into discrete droplets. The size of droplets and rate of droplet formation can be controlled by a transducer, which generates mechanical oscillation in the ink. This transducer is typically a piezoelectric element or alternatively a small heating element. As the name of the method sug-

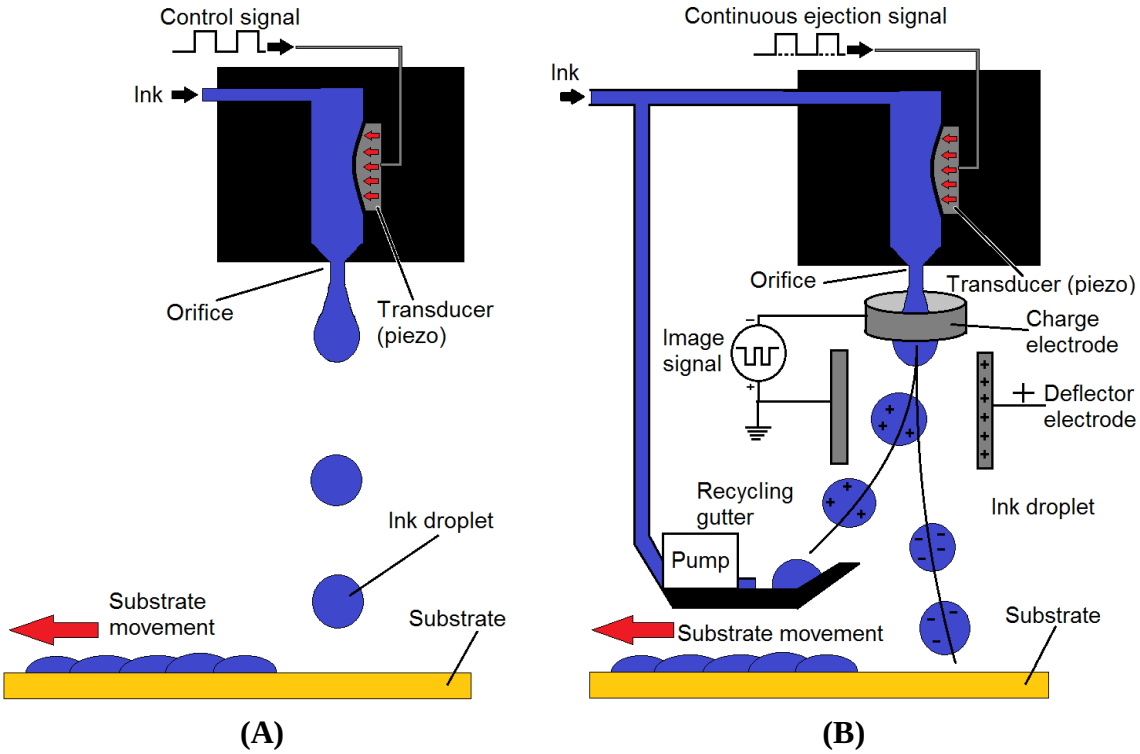

Figure 2. *Operating principle of (A) drop-on-demand inkjet printer and (B) continuous inkjet printer. [10; 11; 12.]*

gests, a CIJ printhead generates a continuous stream of individual drops, which is then passed through a charge electrode. By alternating the voltage of charge electrode each droplet can be charged differently and when the droplets enter the static electric field between high voltage deflector electrodes, flight path of each droplet is determined by the charge it carries. Therefore each generated droplet can be guided separately to land either on substrate surface or to recycling gutter. Unused droplets, which are guided to recycling gutter, are returned back to ink reservoir can be used again. [11; 12.]

The most popular technique in inkjet printing today is the drop-on-demand method. DoD method differs from the CIJ so that droplets are ejected from the printhead only when they are needed, which means that ink recycling system and electrostatic guiding system are not needed and therefore DoD printers have a simpler structure. The operation principle of a DoD inkjet printing is shown in Figure 2A. The drop formation is controlled by a transducer, which is usually thermal element in home and small-office printers and piezoelectric element in industrial inkjet systems [11]. Other techniques such as electrostatic inkjet and acoustic inkjet have also been developed, but the two aforementioned techniques are the most widely used [10]. Thermal inkjet is based on forming a bubble in the nozzle cavity by vaporizing the ink and therefore it has restrictions on the inks, which can be used. Piezoelectric transducer creates pressure waves by changing its volume when voltage is applied and therefore it does not set similar restrictions on materials as thermal inkjet. Typically DoD printhead contains tens, hundreds or thousands of nozzles, which all can be operated individually, but are typically connected to same ink reservoir. Like in the case of CIJ, drop-on-demand method relies on natural tendency of liquid stream to form individual droplets, influenced by the material properties of the liquid, but the droplet formation is enhanced and controlled by the transducer. For example in case of piezoelectric inkjet, droplet generation frequency, droplet volume and droplet speed can be controlled with waveform of voltage applied to piezoelectric element. [11.]

Although DoD inkjet is more popular and simpler in principle, there are also some benefits in CIJ technique. Continuous mode inkjet operates typically at much higher droplet generation rates and the continuous generation of droplets translates to more stable and robust droplet formation. In DoD inkjet the droplet formation is sequential, which includes droplet ejection and nozzle cavity replenishment, and this limits the maximum frequency of droplet formation. [11.] However, CIJ requires use of electrically conductive ink because the droplets need to be charged and because of the ink circulation system there is a possibility of ink contamination. Piezoelectric DoD inkjet is therefore more versatile printing method when different materials are concerned. [12.]

2.2 Materials

The variety of materials, which can be deposited with inkjet printing, is wide and constantly growing. Development of nanoparticle inks during recent years has been an enabling factor for novel applications of inkjet-technology. Whereas graphical printing uses

inks with different colors, inks for printed electronics are divided into different functionalities. The most common functional inks are conductive and dielectric, but some magnetic and semiconductor inks have also been developed. Since this thesis deals with printing conductive inks, those are discussed in more detail in this chapter.

Functional inks contain at least two basic components: a liquid component, which determines the basic rheological properties and enables printing with chosen printing method, and dispersed or dissolved component, which provides the desired functionality. Liquid main component can be for example water or organic solvent or a combination of multiple solvents, and liquid can also contain stabilizers and dispersant agents, which are needed to prevent agglomeration and precipitation of functional particles. The choice of liquid components is based on the desired viscosity, surface tension and wettability, which depend on the printhead and substrate material, because these properties determine for example jettability, drop size and wetting of the substrate. [13.] Since the diameter of printing nozzles in inkjet-printhead is very small, the size of functional particles has to be small enough so that nozzles do not get blocked. Maximum diameter of particles is in the order of 1 – 5 % of the nozzle diameter [12], but to avoid problems a lot smaller diameter is preferred. Especially with inks containing metal particles the small particle size also serves another purpose, since melting temperature of particles is strongly size-dependent [14], meaning that nano-sized particles melt at significantly lower temperatures than bulk material. As a result, conductive inks containing metal particles are typically composed of nanoparticles.

After functional ink has been deposited on a substrate, liquid component evaporates and consequently ink dries. However, additives, such as stabilizers and dispersants, still remain in the composition and prevent functional particles from coming into contact with each other. Therefore a post-process step is usually needed to form continuous structures. In the case of metal nanoparticles, this step is called sintering, which basically means welding the particles together, but it also removes the additive agents from the composition. [12; 13.] Sintering is typically achieved by exposing printed ink to heat [15] in convection oven, but other methods are for example exposure to intense light [16], microwave radiation [17], plasma [18] or electric current [19]. Sintering can also be achieved through chemical reaction [20]. As stated earlier, metal nanoparticles have significantly lowered melting temperature and for example silver nanoparticles have been successfully sintered at temperatures low as 80 °C [21], which enables a wide variety of materials, such as plastics, to be used as a substrate material.

Multiple different materials have been successfully used in inkjet printing to form conductors. Most of the research has focused on noble metals, such as silver, gold and copper, but for example carbon nanotubes (CNT) and conductive polymers have been used to create conductors with inkjet. [22.] Silver nanoparticle inks for inkjet printing are currently commercially available from more than 10 vendors, such as Harima Chemicals Group [23], NovaCentrix [24] and Applied Nanotech Holdings [25]. Copper nanoparticle ink [26; 25] and gold nanoparticle ink [23] are also commercially available.

2.3 Inkjet-Printed Pattern Generation

Inkjet printers use typically bitmap images as source files for printing patterns. This means that every pixel in an image file represents a single droplet, which printer will deposit on substrate surface. If the actual size of a droplet on substrate surface is smaller than the pixel in bitmap image, adjacent droplets will not touch and generated pattern will be discontinuous. However, if size of the droplet is larger than the pixel in bitmap image, adjacent droplets will somewhat overlap and generated pattern is continuous. For naked eye there is no significant difference if the droplets touch each other or not, but for electric current it is crucial. This describes the essential difference between graphical printing and inkjet-printed electronics.

The ratio of drop size and drop spacing is perhaps the most important factor in inkjet printing. Basically it can be controlled by altering image resolution of source file or by altering the surface energy of the substrate. Image resolution is typically measured in drops-per-inch, dpi, and it is inversely proportional to drop spacing: higher resolution means smaller drop spacing. Since the volume of droplets is constant in most cases during printing, image resolution will determine the volume of ink deposited per surface area, which also determines the layer thickness. Soltman and Subramanian have presented the effects of drop spacing in the case of a single line [27].

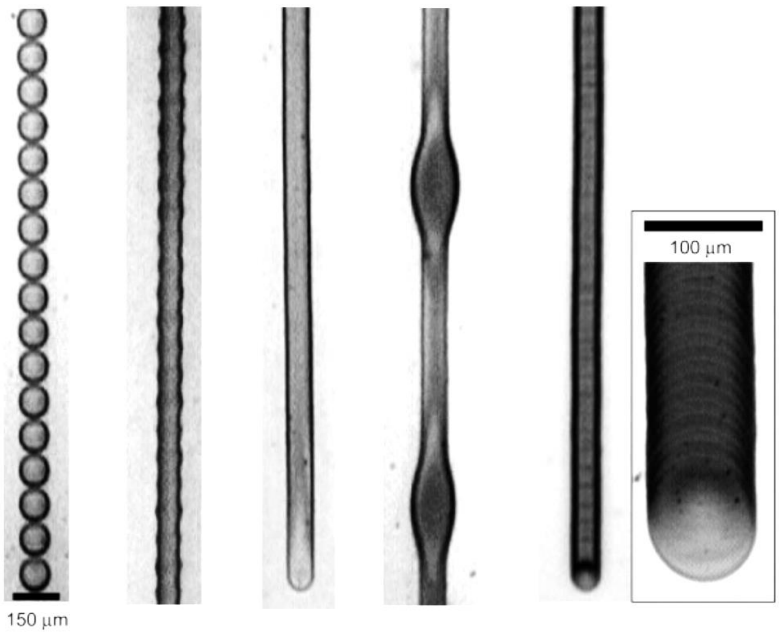

Figure 3. *The effects of drop spacing in a single line. Drop spacing decreases from (A) to (E). In (A) to (D) delay between drops is constant and in (E) delay is increased. Reprinted with permission from [27]. Copyright 2008 American Chemical Society.*

As can be seen in Figure 3A, drops will form a bead, if drop spacing is too big compared to drop size. When drop spacing is decreased, overlapped drops will form a continuous line, but the edges are scalloped. By decreasing drop spacing even more, a uni-

form line is formed, which can be seen in Figure 3C. However, if drop spacing is further decreased from this optimal state, contact line along the edges does not stay pinned and consequently edges will flood, which is also called bulging. Flooding can be prevented by increasing drop spacing or by increasing the evaporation rate of ink with respect to delay between jetted adjacent droplets. Hence, longer delay between droplets or faster evaporation will cause the individual droplets to dry before adjacent droplets are placed and it produces so called "stacked-coin"-structure, which can be seen in Figure 3E. [27.] The longer delay can be achieved by slowing down printhead movement or by altering image file to change the printing sequence, which is possible for example by using higher resolution image and masking algorithm [2]. Soltman and Subramanian also noted that increasing substrate temperature and consequently increasing evaporation rate of ink has the same effect as increasing delay between droplets [27]. Although stacked-coin-structure enables use of smaller drop spacing and consequently depositing thicker layer, the surface quality of printed line is not as homogenous as with uniform lines [28].

As noted before, ratio between drop spacing and drop size is an important factor in inkjet printing and it can be controlled through image resolution, but printing speed and temperature of substrate can be used to increase the usable resolution range. Another way is to modify the surface energy of substrate, which changes the contact angle of ink and substrate, and thereby changes the drop size. For bigger drop size and therefore better wetting there are multiple different hydrophilic surface treatments available, such as corona discharge treatment, oxygen plasma treatment, flame-pyrolytic surface silicating or UV-ozone treatment. [28; 29; 30.] If a smaller drop size is needed, then surface treatment needs to be hydrophobic. There are multiple different hydrophobic coatings and treatments available, but they can be basically divided into two methods: coating a surface with naturally hydrophobic material or roughening the surface with very small scale features [31]. An example of a hydrophobic coating material is EGC-1720, which contains fluorosilane polymer in a hydrofluoroether solvent [32]. Decreasing the drop size enables the use of smaller drop spacing and also decreases the smallest possible line width which can be achieved. On the other hand bigger drop size enables faster coating of large areas, since a smaller resolution can be used to produce continuous surface.

2.4 Flexible Printed Electronics

Flexible circuits have been one of the fastest growing market segments for interconnection products in the last several years, which is due to the wide range of applications enabled by flexibility. Like conventional rigid circuit boards, flexible circuits can be single-sided, double-sided or multilayered, but for example most of the manufactured flexible circuits in 2008 were single-sided or double-sided. Applications of flexible circuits can be roughly divided into two categories: dynamic and flex-to-fit. In dynamic applications flexibility enables movement and changing form factors, whereas in flex-to-fit applications flexibility is needed only in the assembly phase to fit circuit board in

such form factor, which is not possible with rigid planar boards. A typical example of a flex-to-fit application is shown in Figure 4, which illustrates the use of flexible circuit board in a digital camera. Naturally these two main application categories have quite different mechanical requirements, which also cause different limitations. For example the minimum bending radius, which is typically achievable for a static single layer flexible circuit board, is approximately 3 to 6 times the circuit board thickness, whereas the minimum bending radius in dynamic applications needs to be 20 to 40 times the circuit board thickness and lifetime of the circuit can be increased with larger bend radius. Flexible circuits offer many advantages over conventional rigid circuit boards in addition to flexibility. Flexible circuit boards are manufactured on thinnest available dielectric substrates, which in addition to formability help to reduce size of the package. Thinner circuit board and smaller package result in reduced package weight. Replacing conventional wires between rigid PCBs with flexible circuits makes assembly easier and faster, and also offers benefits in signal integrity and heat dissipation. [1.]

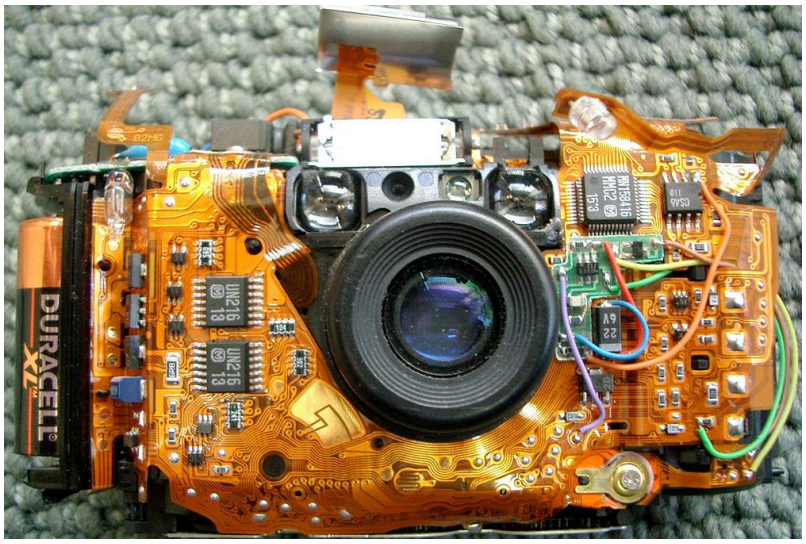

Figure 4. *Olympus Stylus camera with covers removed showing flexible circuit board wrapped around camera frame.[33.]*

Conventional method for manufacturing flexible circuits is quite similar to manufacturing rigid PCBs. Substrate material is typically covered with copper foil and circuit patterning is done with subtractive methods, i.e. photolithography. Copper can be electrodeposited, wrought, electroplated, sputtered or evaporated, and it is typically attached to substrate material via adhesive. Component attachment can be done by soldering, but this limits the substrate material choices to high-temperature resistant materials, such as polyimide, PI. Photolithography also sets requirements for chemical resistance of substrate materials. [1.]

As mentioned earlier, printing technology has several advantages over conventional manufacturing methods and the same benefits apply to manufacturing flexible circuits with printing technology. Smaller material waste and reduced process steps result in

cost savings. Reduced process temperatures in addition to less harmful chemicals enable a wider range of materials, which can be used as substrate, resulting in savings in material costs. Typically printing technology produces thinner dielectric and conductive layers, which is especially beneficial in flexible circuits. Inkjet-printed conductors have been reported [34] to have a significantly longer lifetime in dynamic bending than conventional flexible circuits due to the thinner layer and possibly due to some benefits from the porous structure of printed conductors. Inkjet printing in manufacturing of flexible circuits has also been successfully demonstrated by Koskinen *et al.* [2] by manufacturing an existing flexible circuit board from a mobile phone with inkjet technology.

2.4.1 Materials for Flexible Printed Electronics

Inkjet technology enables wider range of materials to be used as substrates due to low chemical exposure, low curing temperature and contactless nature of deposition. Naturally the same substrate materials used in conventionally manufactured flexible circuits can also be used with printing technology, but wider range of polymers and organic materials, such as paper [35], are enabled with printing technology. Polymers for flexible substrates are for example: polyethylene terephtalate (PET), polyethylene naphthalate (PEN), polyimide (PI), polycarbonate (PC), polyethersulphone (PES), polyacrylates (PAR) and polycyclic olefin (PCO) [36]. Most of the research has however focused on PEN, PET and PI, since they offer relatively small CTEs and good chemical resistance. [1.] Table 1 shows some basic properties of these materials compared to conventional rigid substrate material FR-4.

Table 1. *Properties of typical flexible substrate materials compared to traditional rigid substrate FR-4. [1; 36; 37; 38; 39; 40.]*

Substrate material	**Maximum process temperature [°C]**	**Coefficient of thermal expansion [ppm/°C]**	**Dielectric constant**	**Moisture absorption [%]**	**Young's modulus [GPa]**
PEN	200	13	2.9	1.0	4 – 5.4
PET	150	15	3.2	< 0.08	3 - 4
PI	350	16	3.5	1.3 – 3.0	4 - 5
FR-4	240	15	3.6 – 4.7	0.15	22 - 27

In order to fully utilize substrate materials, which tolerate lower process temperatures, component attachment and contacting cannot be done by soldering. If solder is replaced with conductive adhesive, component assembly can be done in similar fashion as with conventional solder paste. Conductive adhesives typically contain epoxy or other adhesive and a high weight load of metal flakes, such as silver, and conductivity can be isotropic or anisotropic. Isotropic conductive adhesives (ICA) are conductive in every direction, whereas anisotropic conductive adhesives (ACA) are conductive along one

axis only. Advantage of anisotropic conductivity is that very fine pitch connections are enabled even without high precision control for adhesive volume and placement, since adhesive forms conductive path only in direction perpendicular to substrate surface and consequently does not form short circuits between component pads. Conductive adhesives can be deposited with same methods as solder paste and therefore screen printing or dispensing can be used. Similarly as solder paste, conductive adhesive needs to be cured after component assembly, but curing temperature can be as low as 80 °C and typically ACA requires also some level of pressure during curing. Disadvantages of conductive adhesive compared to solder paste are lack of self-alignment phenomenon, somewhat lower conductivity and lower mechanical adhesion, which means that additional adhesive, such as epoxy underfill, may be required in some applications. [41; 42.]

2.4.2 Flexible Demonstrator Device

This thesis was done as a part of the HealthSens –project which seeks to develop technology for novel miniaturized biosensors. An essential part of this project is a plaster-like measurement device, which attaches to skin and measures physiological signals. Measurement device is connected wirelessly to a mobile device using Bluetooth LE technology and measured data can be viewed with the mobile device or further sent to a cloud server through mobile data connection. At time of this thesis prototype design of this device had been built on FR-4 using conventional manufacturing methods to demonstrate the capability of measuring electrocardiogram signal, analyzing measured signal to calculate heart rate and sending it further to a mobile device. This chapter describes manufacturing of miniaturized version of the wireless sensor device on flexible substrate. However, this early prototype design does not include electrodes and differential amplifier, which are needed to actually measure ECG, and its purpose is to demonstrate capability of manufacturing wireless sensor design on flexible substrate with inkjet technology and capability of wireless connection in near-body applications.

Demonstrator device design includes an integrated circuit nRF51822 from Nordic Semiconductor, which is a system-on-chip (SoC) integrated circuit containing 2.4 GHz transceiver and 32-bit ARM Cortex CPU with relevant accessories [43]. nRF51822 is in a wafer level chip scale package, WLCSP, having ball pitch of 400 µm and the few passive components, which are needed around aforementioned SoC, are in 0201, 0402 and 0603 sized packages. Since circuit layout is single-sided, some traces are routed between WLCSP contact pads consequently reducing thinnest line width to 75 – 100 µm. Circuit layout also contains a 2.4 GHz antenna optimized to be operational as near as 300 µm from human body. Size of the whole circuit layout is approximately 45 mm by 22 mm and it rectangular shaped.

Demonstrator device circuit was inkjet-printed with Dimatix DMP-2831 using Harima NPS-JL silver nanoparticle ink on 50 µm thick PEN film. Before printing PEN film was cleaned with isopropyl alcohol and it was coated with 3M Novec EGC-1720 to produce a hydrophobic surface. Surface treatment was observed to be necessary to ena-

ble printing of finest details by reducing drop size. Printing parameters are shown in Table 2.

Table 2. *Printing parameters for flexible demonstrator device.*

Drop volume (nominal)	10 pl
Printing resolution	1270 dpi
Nozzle plate temperature	43 °C
Vacuum plate temperature	60 °C
Jetting frequency	7 kHz
Droplet ejection voltage	23 V
Nozzles in use	1

Source image was also divided into four sub-images to increase delay between adjacent drops in order to avoid flooding [7; 27]. Since printing was done with only one nozzle and four sub-images, some challenges were faced due to instability of printing process during long printing runs. This was at least partly assumed to be caused by rising nozzle plate temperature near hotter vacuum plate, which changes viscosity of the ink and affects droplet formation. Sintering of printed circuits was performed in convection oven at temperature 180 °C for 60 minutes. Figure 5A shows the printed circuit after sintering and Figure 5B illustrates flexibility of printed circuit and substrate film. It can be seen in Figure 5A that surface of large printed areas, such as ground plane, is not perfectly smooth even in macroscopic scale. This is due to the sequential printing by using four sub-images, which typically produces somewhat stacked-coin structure, but allows fine lines and large areas to be printed with same parameters.

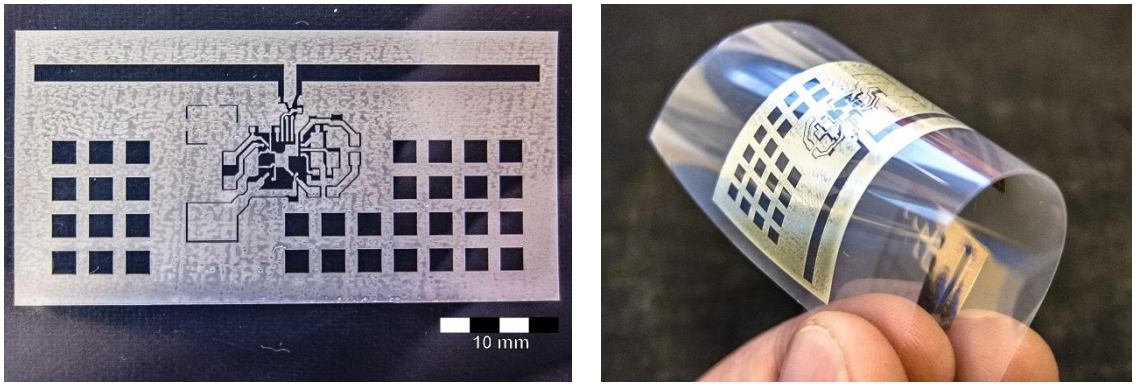

(A) **(B)**

Figure 5. *Printed flexible circuit for demonstrator device.*

Components were attached to printed circuits using isotropic conductive adhesive Creative 124-08C, which was applied to contact pads using hand-held dispenser. Small scale of contact pads made it difficult to accurately control adhesive volume and placement with hand-held dispenser and therefore screen printing was also tried. However,

due to thixotropic nature of ICA and manual screen printing device, screen printing was not successful. It was observed that ICA had tendency to flow under screen printing stencil and consequently flood over contact pads. Optimizing screen printing process was not considered as key focus area at this point and hand-held dispensing was therefore continued. Component assembly was done with Finetech Fineplacer, which enabled accurate component alignment and placement. Curing of ICA was performed in convection oven at temperature 120 °C for 15 minutes. In order to enhance mechanical durability of component attachment, Epotek OE121 epoxy underfill was applied with hand-held dispenser around the components and cured in convection oven at temperature 120 °C for 15 minutes. Figure 6A shows the component assembly of demonstrator device and Figure 6B shows the whole assembled device. Large contact pads on the left side of component assembly are meant for a battery or some other power source, but since sufficiently capable, thin and small battery was not available at this point, it was left unassembled.

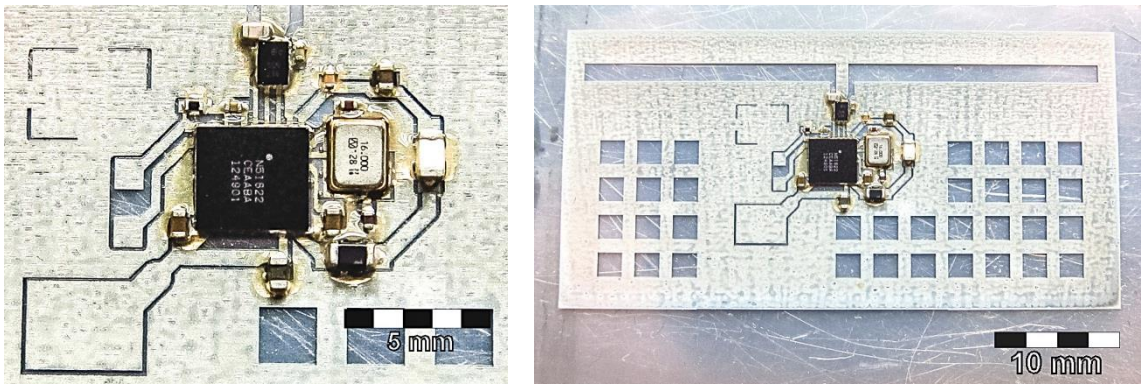

(A) **(B)**

Figure 6. *Photo of demonstrator device (A) component assembly and (B) whole device.*

Flexible demonstrator device shown in Figure 6B was successfully programmed using custom made fixture with spring-loaded needles for contacting power and programming pads. Software used in nRF51822 was a test program, which sends increasing sequence of heart rate values via Bluetooth. Initially connection to iPhone 5 manufactured by Apple Inc. could not be established, but this was identified as an issue with compatibility of hardware and software. The initial program version used external crystal oscillator as clock source for real time clock (RTC), whereas integrated flexible demonstrator device did not contain external crystal. After receiving a program code, which used internal RC-oscillator of nRF51822, a connection was established only for approximately 5 seconds. This was due to inaccuracy of internal RC-oscillator, which caused RTC and main clock to creep out-of-sync after 5 seconds and consequently dropping connection. The third software version used main clock signal to synthesize RTC, and with this software demonstrator device was successfully connected via Bluetooth to iPhone 5 and an increasing sequence of heart rate values was seen in test application supplied by Nordic Semiconductor. The connection was observed to be stable over extensive time periods in free air and near human body. Connection range for de-

monstrator device near human body was observed to be well over 5 meters, which was sufficient, since mobile device is assumed to be located in close proximity of measured subject.

This manufactured device demonstrates feasibility of using inkjet technology to manufacture flexible sensor platform for measuring physiological signals wirelessly. The next development steps will include integrating the actual sensor part consisting of electrodes and differential amplifier to this platform and further developing the device to be more imperceptible on skin contact by introducing elastic substrate materials. This thesis will focus on the latter development step in next chapters, but it is worth noting that this wireless platform could also be used to host a wide variety of sensors, such as accelerometers, gyroscopes, temperature and humidity sensors, which opens up multiple different application areas for further research.

3 STRETCHABLE ELECTRONICS

Making stretchable electronics is mainly branched in two directions, which both have their pros and cons. The first method is to use intrinsically stretchable materials, like conductive polymers or organic semiconductors, which have relatively poor electrical performance compared to conventional inorganic electronic materials. The second method is to use conventional electronic materials and make the system stretchable. This way good electrical performance is achieved, but the stretching is more challenging, since conventional semiconductors, like silicon, are hard and brittle. If rigid areas with silicon-based semiconductors are kept small and the interconnections between them are made stretchable, resulting system appears stretchable macroscopically. Figure 7 illustrates the different approaches to manufacturing stretchable electronics. [3.]

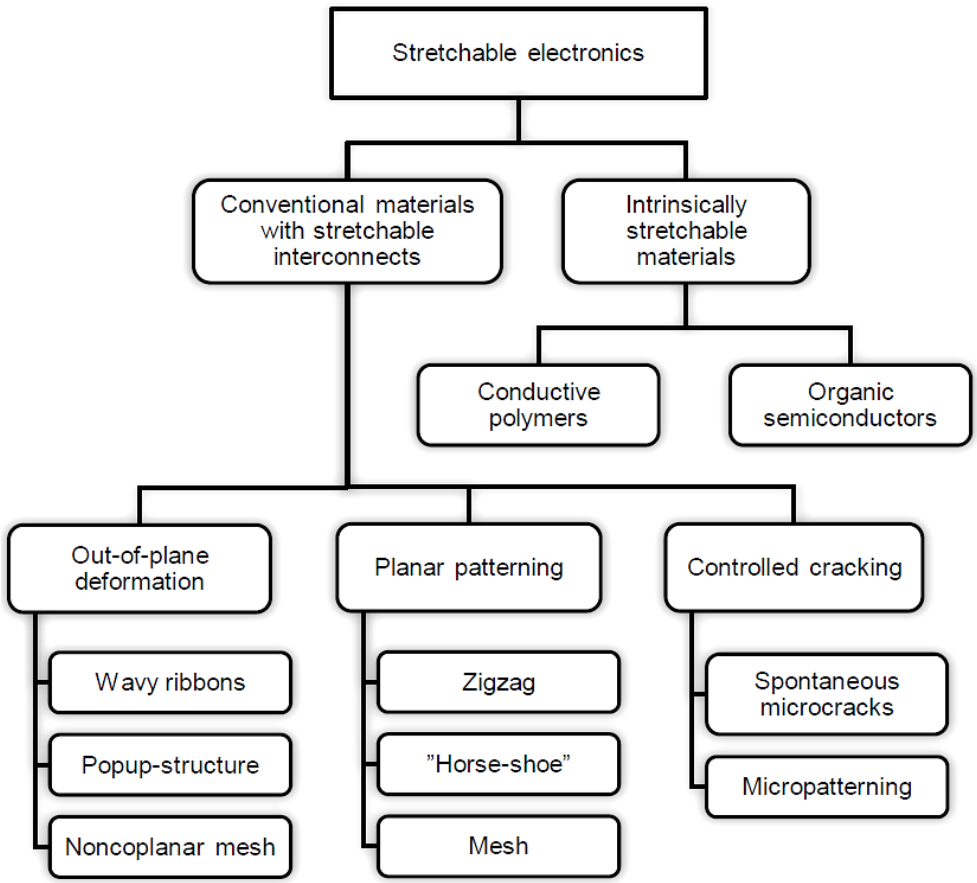

Figure 7. *Options for manufacturing stretchable electronics.*

Stretchable interconnects are usually made by exploiting out-of-plane deformation or planar patterning which help to reduce stresses caused by stretching. Basically the actual length of conductors is increased while dimensions along one or two axis are pre-

served. Consequently this converts stretching to bending for strains between the actual length of conductor and the relaxed state of conductor. Other methods for producing stretchable interconnects rely on thin films and forming of microscopic cracks, which serve as strain relief and form a conductive network. [3; 44.]

This chapter focuses mainly on using conventional conductor and semiconductor materials for fabrication of stretchable electronics. Since conventional substrate materials are hard and rigid, novel substrate materials, which are suitable for conventional fabrication methods, must be introduced. Chapter 3.1 presents novel materials for fabrication of stretchable electronics, but also covers properties of some conventional materials from stretchability viewpoint. Theory behind stretchable interconnects is presented in Chapter 3.2, which is followed by fabrication processes of stretchable interconnects in Chapter 3.3. Applications of stretchable electronics are presented in Chapter 3.4. Lastly, the challenges concerning inkjet-printed electronics on stretchable substrates are discussed in Chapter 3.5.

3.1 Materials for Stretchable Electronics

A material is defined as elastic, if it can be deformed by applying a certain mechanical stress, and it returns to its initial dimensions once stress is removed. Many materials exhibit some level of elastic behavior, but particularly elastomers, which are rubber-like polymers, can undergo large elastic deformations and are therefore prime candidates for stretchable substrate materials. Manufacturing processes for flexible thin film electronics are relatively well established, but introducing elastomeric substrates brings completely new challenges in compatibility of standard microfabrication processes, reproducibility, suitable probing methods and patterning accuracy. In addition to challenges in manufacturing process, elastomeric materials have significant differences in physical properties when compared to conventional materials used in for example electronic components. While conventional device materials have relatively low CTE and are hard and brittle, elastomers can expand several times their initial length reversibly and have high CTE. Most of the research on elastomeric substrates has focused on silicone rubbers and polyurethane elastomers - more precisely on polydimethylsiloxane (PDMS) and thermoplastic polyurethane (TPU). Therefore these two materials are examined in this chapter in more detail. [3; 44.]

Elastomers are composed of long-chain molecules, which are linked together forming a network of chains. Elastic behavior results from each chain acting as a mechanical spring when external force is applied. Organic elastomers, such as natural rubber and nitrile rubber are composed of carbon-carbon polymer chains, whereas silicone elastomers contain silicon-oxygen chains. The strong silicon-oxygen bond is the reason for silicone elastomers' outstanding heat and ozone resistance. By adding different functional side groups to silicon-oxygen backbone, properties such as curing conditions of silicone elastomers can be modified. However, the bulk mechanical properties of cross-linked pure polysiloxane are rather poor and therefore manufacturers usually mix pol-

ysiloxanes with fillers, such as precipitated or fumed silica, which reinforce the structure of silicones considerably and for example tensile strength can be increased by a factor of 100. As can be seen in Table 3, physical properties of PDMS, which represents silicone elastomers, are significantly different from typical conductor materials used in electronic devices. It is an excellent dielectric material, which can be deformed easily by significant amounts, but its thermal expansion is over 10 times higher than for example copper. The main advantages of silicone elastomers are:

- Wide operation temperature range: from -50°C up to +200°C and short times up to +300°C.
- Highly constant mechanical properties over operation temperature range.
- High transparency.
- Chemical inertness.
- High biocompatibility.
- High resistance to chemical, ozone, UV and X-ray exposure.

However, there are also some disadvantages such as low tear resistance, high swelling in organic solvents and very high gas permeability. PDMS is the most researched substrate material candidate and it is easy to cast in different molds or apply by spin-coating. Some photosensitive silicones (P-PDMS) are also commercially available. [3.]

Table 3. *Physical properties of typical conductor materials and elastomers. Listed values are for bulk materials. Large variations exist between different deposition methods and compositions, and chosen values are only for illustrating differences between materials. [45; 46; 47; 48.]*

	Si	**Cu**	**Ag**	**Au**	**PDMS**	**TPU** (average)
Young's modulus [GPa]	112.4	110	82.5	77.2	$3.6 \cdot 10^{-4}$ – $8.7 \cdot 10^{-4}$	0.0196
Yield strength [MPa]	120	333	40 - 55	-	-	16.1
Ultimate tensile strength [MPa]	120	344	140	120	1.55 – 9.0	34.9
Poisson's ratio	0.280	0.364	0.364	0.420	0.5	-
Elongation at break [%]	-	14	-	30	430 - 725	584
Electrical resistivity [Ω·cm]	0.01	$1.72 \cdot 10^{-6}$	$1.59 \cdot 10^{-6}$	$2.44 \cdot 10^{-6}$	$2.4 \cdot 10^{14}$ – $15 \cdot 10^{14}$	$3.01 \cdot 10^{11}$
Dielectric constant	11.8	-	-	-	2.77 – 3.69	6.34
CTE [ppm/°C]	2.49	16.4	19.6	14.4	197 - 263	153

Polyurethanes (PU) are the second group of materials, which appear as potential substrate material for stretchable electronics. Polyurethane chemistry is very versatile and therefore it has a wide range of applications such as cast systems, rigid and soft foams, dispersions, lacquers and varnishes. However, specific group of polyurethanes, namely thermoplastic polyurethanes, are elastomers suitable for elastic substrates. The structure of TPUs has two distinct parts: soft and flexible segment of polyether or polyester and a stiff part formed by diisocyanate and glycol. Size of the hard phases are in the range 10 – 50 nm, but the whole chain of soft and hard segments is significantly longer. Harder varieties of TPUs are usually turbid or milky, which is caused by the long soft-hard segment chains, which tend to crystallize and form spherulites. The dual structure of TPUs enables high tensile strength and abrasion resistance in addition to high elasticity. Chemical resistance of TPU is dominated by soft segments, since hard segments are very stable, but generally TPUs are very stable against nonpolar substances. Thermoforming of TPUs is enabled by melting of hard segments, which crystallize again when cooled down. Softening range can be adjusted by different selection of substances forming the hard segment. Typically operation temperature range for thermoplastic polyurethanes starts from as low as -60°C and can be up to +150°C after which mechanical properties start to decay rapidly. The main advantages of TPUs are:

- High abrasion resistance
- Oil resistance
- Ozone resistance
- Biocompatibility
- Well glueable due to high surface energy.

Due to thermoformability of TPU it can be laminated on various surfaces. Thermoplastic polyurethanes are already used in textile industry to enhance fabric properties and to attach fabrics together. This makes TPU an attractive option for substrate material in wearable electronic applications. [3.]

Similarly as silicones, polyurethanes can be modified by introducing additives or fillers. Carbon black filled polyurethanes have been used in antistatic shielding and as glob top encapsulating for electronic components. However, during European STELLA –project elastic TPU was filled with different conductive fillers to form conductive tracks on various substrate materials. Although conductivity of these conductive TPUs was significantly lower than conventional conductor materials, it offers an interesting option for forming intrinsically stretchable conductors. [3, p.182-184]

3.2 Mechanics of Stretchable Materials

To understand the concept of stretching, one needs to understand some fundamental aspects of mechanics of materials. A material can be deformed, when it is exposed to sufficient mechanical *stress*, which is defined as force *F* per surface area *A*. If stretching is considered, the acting force must be a pulling force and the resulting stress is called *tensile stress* σ. The deformation caused by a stress is called *strain* ϵ and it is expressed as deformation per unit length. Therefore strain can be calculated:

$$\epsilon = \frac{L - L_0}{L_0} = \frac{\Delta L}{L_0} \tag{1}$$

Where L_0 is the original length of an object, L is the new length of object and ΔL is the change in length due to tensile stress. Tensile strain is also often called *elongation*. If deformation is elastic, i.e. reversible, the relationship between strain and stress can be described by Hooke's Law:

$$\sigma = E\epsilon \tag{2}$$

Where σ is tensile stress applied to material, ϵ is strain and *E* is *Young's modulus*, which often also called *modulus of elasticity*. However, all materials do not follow Hooke's Law: for example rubbers are usually nonlinearly elastic. [49.]

When a stress applied to material is high enough to cause permanent deformation, material is said to yield and the stress needed to cause yielding is called *yield stress*. As a material property yield stress is often also addressed as *yield strength*. Since it is often difficult to define exact point when material starts to yield, yield stress is often specified as a stress needed to cause a specific amount of permanent strain, such as 0.2%. The highest stress that a material can endure is called *ultimate tensile strength*, after which the material begins to soften due to accumulated damage. If a material is known to be linearly elastic and its yield strength and Young's modulus are known, materials maximum elastic strain can be solved from Hooke's Law:

$$\epsilon = \frac{\sigma_\gamma}{E} \tag{3}$$

Where σ_γ denotes yield strength. [49.] Tensile strain can further be used to predict durability of a material when it is bended along a known radius. If material with thickness *t* is bended along a radius, *r*, then the resulting strain, ϵ, at outer surface can be calculated [50; 1, p.267]:

$$\epsilon = \frac{t/2}{r + t/2} \tag{4}$$

Similarly, if thickness and maximum elastic strain of a material are known, then the minimum bending radius can be calculated:

$$r_{min} = \frac{t/\epsilon_{max} - t}{2} \tag{5}$$

For example, if a material with thickness of 50 µm is able to endure maximum elastic strain of 0.01 (or 1 %), the minimum bending radius for such material would be approximately 2.5 mm. However, Equations (4) and (5) apply only if material is homogenous. Combination of stiffer and softer material, such as metal and plastic, shifts neutral bending radius towards the stiffer material and if the stiffer material is located on outer surface, results based on Equations (4) and (5) are higher than the actual values will be.

Last concept related to elastic deformation that is presented here is the *Poisson effect*. When a material is stretched along one axis, a negative (compressive) strain will be observed along other dimensions. This can be easily observed for example by stretching a rubber band and noticing how it gets thinner the more it is stretched. This phenomenon is called *Poisson effect* and a materials tendency for this phenomenon is described by *Poisson's ratio*:

$$v = \frac{-\epsilon_{lat}}{\epsilon_{long}} \tag{6}$$

Where v is Poisson's ratio, ϵ_{lat} is the lateral strain and ϵ_{long} is the longitudinal strain. Poisson's ratio is dimensionless parameter, which also describes nicely the nature of a material. Rubbers have the highest Poisson's ratios and brittle ceramics the lowest. This means that Poisson's ratio is related to the molecular mobility of a material, since more elastic materials are able to rearrange themselves to keep their volume constant when deformed. [49.]

3.3 Fabrication Processes of Stretchable Interconnects

Typical conductor materials have Young's modulus in the order of 10^{11} Pa and yield strength in the order of 10^{8} Pa. According to Equation (3) their maximum elastic strain is therefore in the order of 0.1%. Since typical conductor materials have very limited elastic range, some special tricks are needed to enable strecthing. Typically this means converting stretching to bending by introducing more complex geometries. Most techniques for making stretchable interconnects involve pre-stretching the substrate to produce buckling in the attached conductor. Such techniques are for example stretchable wavy ribbons, popup structure, noncoplanar mesh design and noncoplanar mesh design

with serpentine interconnects. Alternative way, which doesn't include pre-stretching, is planar patterning of conductors into sinusoidal, zig-zag, horseshoe, or mesh shaped patterns. [3, p.94; 44.] These different techniques are illustrated in Figure 8.

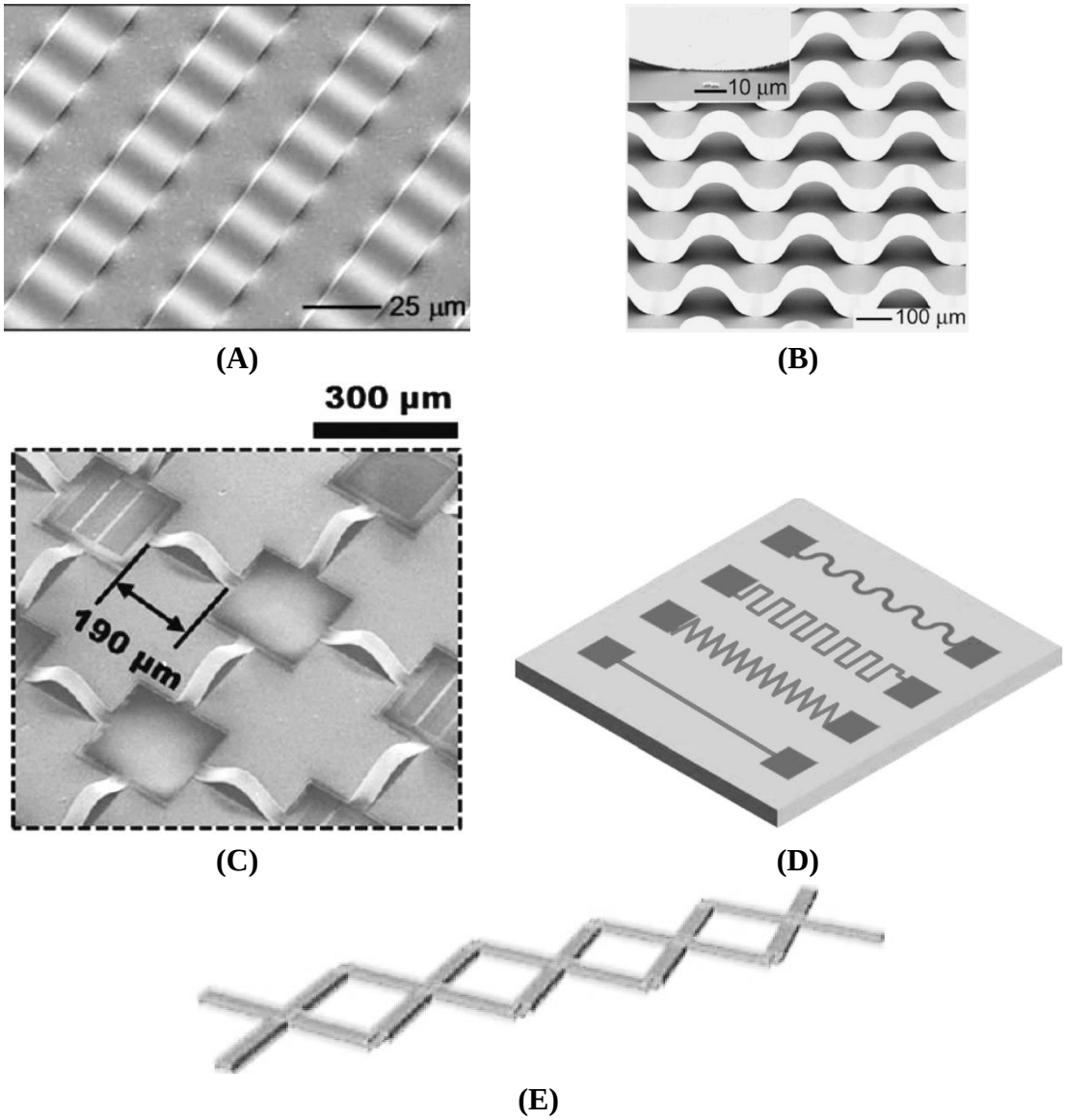

Figure 8. *(A) Stretchable wavy ribbons. From [51]. Reprinted with permission from AAAS. (B) Popup structure. Reprinted with permission from [52]. Copyright 2007, AIP Publishing LLC. (C) Noncoplanar mesh design. Reprinted with permission from [53]. Copyright 2011 American Chemical Society. (D) Different planar patterning options. Reprinted from [54], Copyright 2013, with permission from Elsevier. (E) Mesh shaped ribbon. Reprinted with permission from [55]. Copyright © 2008 WILEY-VCH Verlag GmbH & Co. KGaA, Weinheim*

Structures seen in Figure 8A – C are manufactured by first pre-stretching the substrate material to a certain strain, then attaching or depositing conductor patterns on stretched substrate. When strain of the substrate is released, conductors are exposed to compressive strain, which causes conductors to buckle. In case of wavy ribbons, seen in

Figure 8A, conductors are attached to substrate with their whole surface area and buckling produces spontaneous wavy structures. Amplitude and wave length of these structures depends on the material properties of conductor and substrate, width of ribbons and also on the amount of pre-stretch applied. When this structure is stretched, waves flatten to accommodate the applied in-plane strain. Practical levels of strain achieved with this method are in the order of 15%. [3; 44; 51; 55]

Popup structure and noncoplanar mesh design, seen in Figure 8B and C respectively, basically utilize the same idea. Both of them are manufactured in the same way as wavy ribbons, but with a difference that conductors are bonded to substrate only in certain points. This causes non-bonded areas to detach from substrate during buckling and as a result free-standing arcs are formed. Advantage in this approach is that wave length and amplitude of structures formed in buckling can be controlled with the placement of bonding points. Disadvantage is that free-standing arcs lack the mechanical support of substrate and are therefore more exposed to environmental stresses and have to be protected by some means. Practical levels of strain achieved with this approach are in the order of 100% or more, which means that even fracture limits of PDMS are approached. [3; 44; 52; 53; 56.]

Planar patterning illustrated in Figure 8D and E does not involve pre-stretching substrate, but patterns are formed on relaxed flat substrate. In-plane patterning can be done with conventional photolithography or by direct-write methods and it increases the actual length of conductors, while length along one axis is preserved. Although the ease of manufacturing is a clear advantage, planar patterning increases the footprint of conductors significantly. Several different conductor geometries have been suggested, but modeling and experimental results have shown highest achieved strain levels for horseshoe and mesh shaped designs. Performance of horseshoe shaped conductors depends highly on the ratio of conductor's curvature radius and conductor width, but in general curvature radius should be at least 10 times larger than conductor width. By optimizing conductor shape over 100% strains have been achieved with both horseshoe and mesh shaped patterns. Reliability of planar patterns can be further improved by introducing a thin polyimide layer between conductor metal and substrate material. Research on these polyimide-supported interconnects has shown, that patterned polyimide helps to bridge the gap between material differences of metal and elastomer, resulting in more uniform strain distribution in metal layer. During European STELLA –project the use of local stiffener plates formed by large conductor areas around components has been observed to increase the reliability of component contacts, when horseshoe shaped stretchable interconnects are used between components. [1; 3; 44.]

Pre-stretch method and planar patterning both have their pros and cons. In principle, pre-stretch method does not increase the footprint of conductors like planar patterning, but due to the buckling during manufacturing process conductors are left under constant stress in relaxed state of the substrate. In addition, direction of pre-stretch also determines the direction of stretchability for final structure and pre-stretching in multiple directions introduces very complex structures, which are difficult to control. Similarly,

horseshoe shaped planar patterning is stretchable only in one direction, but if meshes are introduced, stretchability can be achieved in more than one direction. However, alternative method for producing similar 3D-structures, as with pre-stretch method, is micropatterning the substrate surface before conductors are formed [57]. This enables stress-free conductors and geometries for two-dimensional stretching are more easily controlled, which is illustrated in Figure 9. Technique also enables forming of flat areas in the same process phase as wavy areas, whereas in pre-stretch method these need to be done in separate phases. The main disadvantages are naturally additional process phase of micropatterning substrate surface and additional requirements for conductor forming method, since surface is not flat during deposition of conductors.

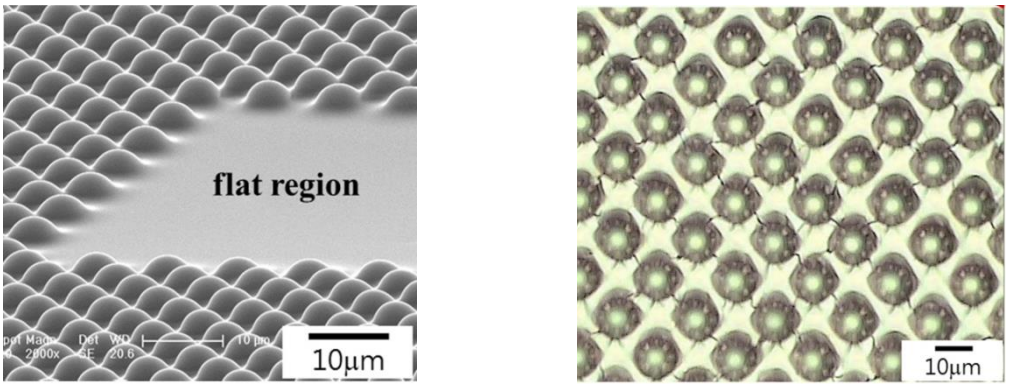

(A) **(B)**

Figure 9. *(A) Flat islands within two-dimensional wavy stucture (B) Two-dimensional wavy structure after 5 stretching cycles to 20% strain. Reprinted from [57], Copyright 2013, with permission from Elsevier.*

Whereas most fabrication processes for stretchable interconnects aim to avoid plastic deformation and thus crack formation, it can also be exploited to provide strain relief in conductor structure. Microcracking of thin gold films has been reported [58; 59; 60] to provide significant amount of strain relief, while cracked surface forms a conductive network, which maintains some level of conductivity even at strain levels of tens of percentages. Figure 10B illustrates the forming of microcracks on different strain levels in 50 nm thick evaporated gold film on smooth PDMS. Increased surface roughness has beneficial effect on stretchability by increasing the microcrack formation [59], which provides more points of strain relief, and by shortening the length of formed cracks, which helps to maintain conductive network. Although crack formation will inevitably increase the electrical resistance of conductors, it can be taken into account in circuit design. Since microcracking occurs spontaneously, apparent ease of manufacturing is an attractive feature, if sufficient strain levels are achieved for considered application.

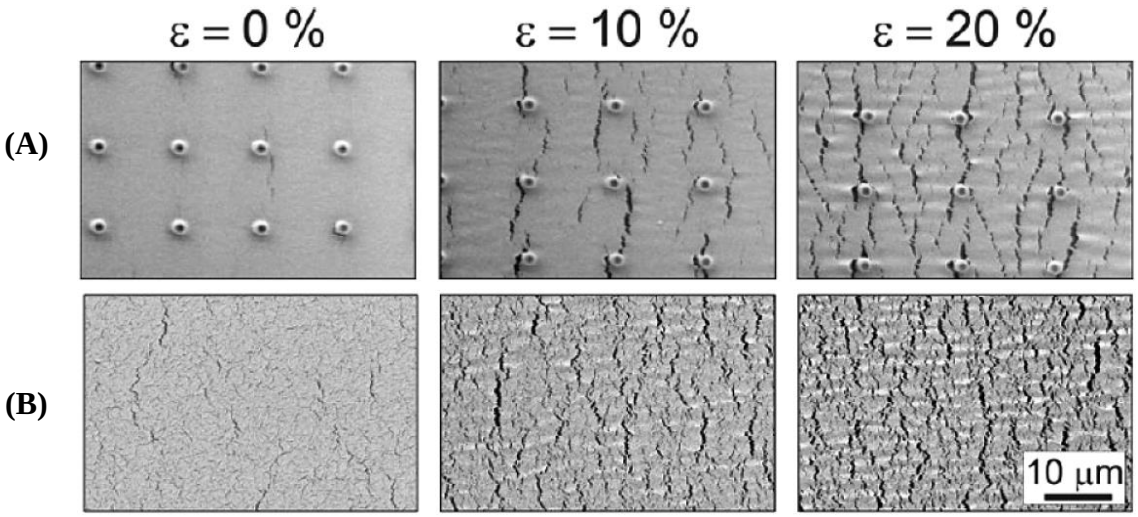

***Figure 10**. ESEM images of conductor surfaces on different strain levels: (A) Inkjet-printed silver on micropatterned PDMS. (B) 50 nm thick evaporated gold on smooth PDMS. Reprinted (adapted) with permission from [60]. Copyright 2011 American Chemical Society.*

More sophisticated approach to increased surface roughness is that microcracking can be controlled by micropatterning substrate surface. Robinson *et al.* [60] have shown that patterning substrate with micropillar arrays, shown in Figure 10A, enables control of microcrack formation in conductor and thus control of conductor stretchability. Although fabricated metal film is significantly thicker, resulting microcrack pattern is remarkably similar to one seen in thin evaporated gold films. Size and placement of micropillar arrays also enable control of wetting and pinning of fluids on substrate surface. This is highly beneficial for depositing conductive tracks with printing technologies since additional surface treatments, such as ozone or oxygen plasma, are not needed in order to produce sufficient wetting of ink on substrate surface.

3.4 Applications for Stretchable Electronics

Typical applications being researched and enabled by stretchable circuits usually involve a need to integrate a circuit on a non-flat, irregular and/or changing surface. The most common such surface is human skin and therefore the typical applications are related to monitoring functions of the human body. Conventional PCBs cannot conform to irregular shapes of human body and are not comfortable in skin contact. Although some degree of comfort can be obtained with miniaturization of the circuit so that the lateral dimensions are small enough compared to local bending radii of the surface. In some cases miniaturization is not an option; this can be due to device complexity, which prevents sufficient miniaturization, or due to nature of functionality, which requires a certain dimensions to function properly. [1; 3.] Figure 11 illustrates some applications utilizing stretchable interconnects.

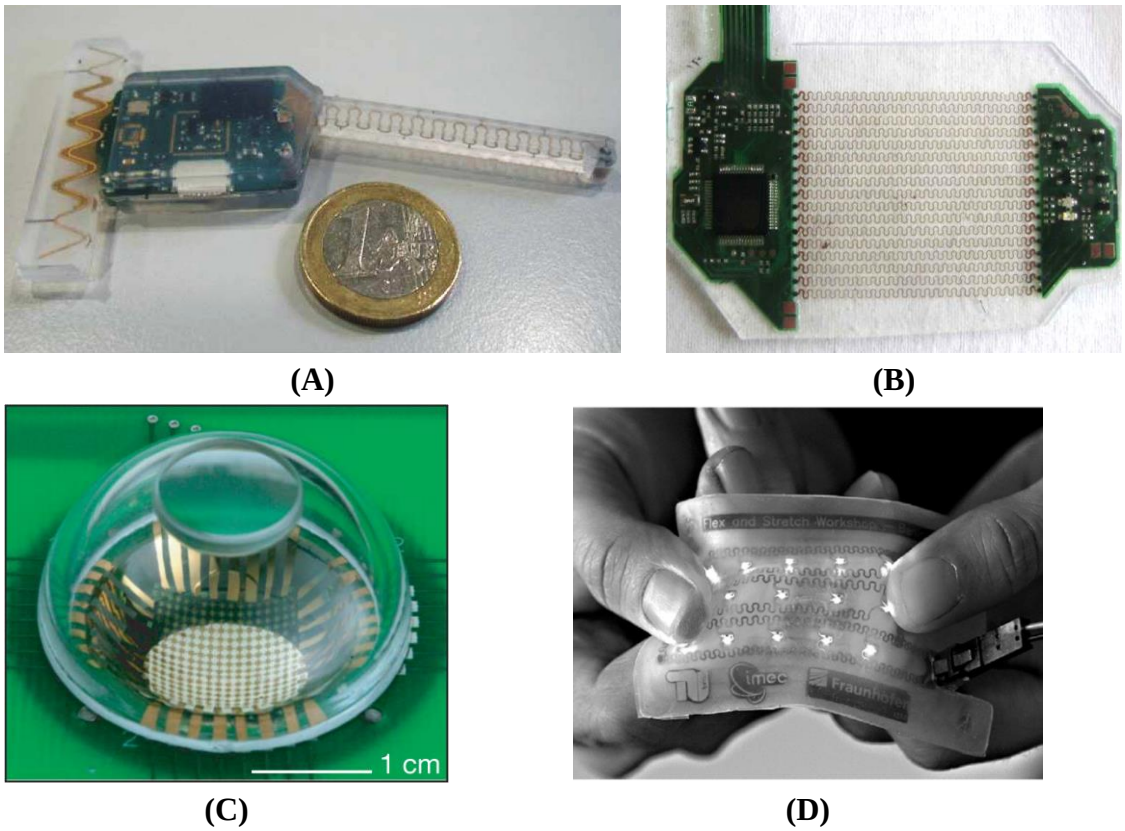

Figure 11. *Applications of stretchable interconnects: (A) ECG sensor with stretchable antenna and interconnect to second electrode. [61] © 2011 IEEE. (B)Stretchable part of a respiration monitor. [61] © 2011 IEEE. (C) Hemispherical image sensor. Reprinted by permission from Macmillan Publishers Ltd: Nature [62], copyright 2008. (D) Stretchable LED-matrix. Reprinted from [63], with permission from Elsevier.*

Figure 11A shows an electrocardiogram sensor, which is miniaturized and implemented with stretchable elements. Most of the electronics are miniaturized on a small rigid PCB, but in order to an ECG sensor to function properly, the minimum distance between electrodes needs to be 5 – 10 cm. Since this sensor is also wireless implementation, an antenna element of certain size is needed. Therefore second electrode of ECG sensor is connected with a stretchable interconnect and molded in elastic material, and similarly antenna element is made stretchable. Electrode structures and antennas are prime examples of elements, which need certain dimension, and are therefore excellent application areas for stretchable technology – especially when those elements integrated on arbitrary shapes or dynamic surfaces like human body. Another similar example is large-area network of sensors or electronic components. Applications like displays, LED-matrixes and pressure sensor networks for artificial skin need certain surface area by nature and can be enabled by stretchable interconnects. Figure 11B illustrates a stretchable LED-matrix demonstrator device, which is the first step towards stretchable displays. Different stretchable sensor networks measuring pressure or temperature have been developed by several research groups aiming to produce artificial skin, which

would enable artificial touch sense in robotic or prosthesis applications, or temperature mapping of a human patient in order to enable more accurate illness diagnosis. [1; 3.]

Part of a respiration monitor shown in Figure 11B and hemispherical image sensor shown in Figure 11C, are applications, which have a lot in common with two typical application areas of flexible electronics. In the first stretchability is needed to enable movement and in the second stretchability is needed to fit device in a certain form factor. In principle the hemispherical image sensor is only flexible, but use of stretchable interconnect schemes allows image sensor to bend in multiple directions simultaneously. Typically image sensors in digital cameras are flat and need a significant amount of optical lenses to form a picture. Hemispherical shape of image sensor brings digital imaging closer to human eye, which simplifies the needed lens structure and at the same time enables smaller cameras to be built [62].

If devices are manufactured on very thin elastic substrates using stretchable interconnects and without conventional bulky components, the resulting devices can be virtually imperceptible when attached to human skin. Figure 12 shows a demonstrator device containing wireless power coil, RF coil, ECG and EMG sensor, strain gauge and temperature sensor. This kind of device introduces a new class of electronic systems called epidermal electronics, which can be used in numerous ways to collect data from human body or to enhance functionality of skin. [64.]

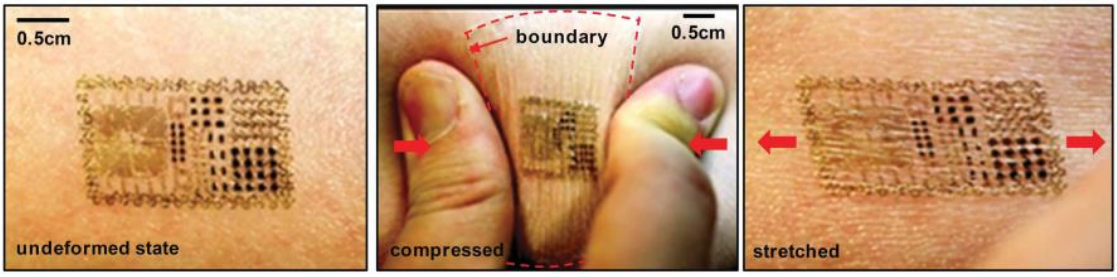

Figure 12. *Imperceptible tattoo-like stretchable sensor attached to skin. From [64]. Reprinted with permission from AAAS.*

Although multiple different applications of stretchable electronics have been demonstrated, most of these activities are currently centered in academic laboratories. Few companies like MC10 Inc. [65] are pushing inventions out of the laboratories and starting to introduce first commercial stretchable electronics. Path to commercialization is therefore just begun, but it is already clear that a wide range of new applications will be enabled by stretchable electronics.

3.5 Challenges of Inkjet-Printed Electronics on Stretchable Substrate

The most obvious challenge in using elastomers as substrate is their natural softness and instability of dimensions when compared to traditional stiff substrate materials. This causes additional challenges in every process step independent from manufacturing method. Handling of elastomers is more difficult due to lack of mechanical support and ensuring substrate flatness needed in many processes is harder to achieve. Some of these difficulties can be solved by attaching elastomers to rigid carrier plate during manufacturing, but nevertheless it causes additional work.

Advantages of inkjet technology presented in previous chapters apply similarly to manufacturing of stretchable electronics, but especially contactless deposition is highly beneficial when microstuctured substrate materials are being used. Inkjet-printed conductors have been reported to perform significantly better than conventional copper foil in bending tests [34] due to thinner layer and porous structure of sintered nanoparticle material, and it is presumable that these properties are also beneficial in stretchable applications. By comparing material properties of bulk material and porous material, some observations can be made from viewpoint of stretchability. As presented in Chapter 3.1, Young's modulus for bulk silver is 82.5 GPa and the yield strength of bulk silver is in the range 40 – 55 MPa, which suggests that the maximum elastic strain according to Hooke's Law is in the range 0.0485 – 0.0667%. However, it has been found [66] that porosity of silver not only increases resistivity, but also decreases yield strength, elastic modulus and Poisson's ratio. Experimental results for 62% dense silver have shown 20 MPa yield strength and 14 GPa elastic modulus, which would enable maximum elastic strain of 0.143%. Therefore porous structure of sintered nanoparticles can be assumed to be more elastic than bulk material, but still very brittle.

Many challenges related to material property differences of elastomer and typical conductor materials are common for all manufacturing methods for stretchable electronics. For example Poisson's ratio mismatch between metal and elastomer will cause additional compressive stresses to metal conductors during stretching. If uniaxial pre-stretch is used during manufacturing, conductors will experience tensile stress in direction perpendicular to pre-stretch direction when pre-stretch is released. CTE of elastomers is typically 10 times higher than CTE of metals, which can cause challenges in sintering phase of inkjet-printed nanometals. In addition, nanometals shrink during sintering phase, which aggravates the situation even more. This can lead to for example crack formation, wrinkling of printed layers or dimension mismatch in component assembly phase.

From printability viewpoint elastomers are challenging substrates, because they are typically very hydrophobic: for example a water droplet on PDMS has a contact angle of 116±1° [3, p.83]. Although hydrophobic surface enables finer line widths with inkjet printing, it also makes printing continuous large areas more challenging. Therefore sur-

face treatments for surface energy modification are typically needed to enable sufficient printing quality.

Most researched elastomer substrates, PDMS and TPU, are chemically fairly stable and inert. However, many polymers including PDMS and TPU typically react to solvents by swelling because of solvent absorption. The effect is temporary, but it may still cause problems in inkjet printing. Swelling can cause stresses in printed layers, which can lead to crack formation.

4 EXPERIMENTS

The goal of this thesis is to evaluate feasibility of manufacturing printed circuits on highly elastic substrates. Substrates chosen to be studied are polyurethane film, Epurex Platilon U 4201 AU, and silicone rubber sheet, NewMet NM60. Both of these materials are commercially available, can be used over a wide temperature range, offer high resistance to variety of liquids and are highly elastic. Although both films are available in a relatively wide range of thicknesses, the selected thicknesses are from the lower end of range - resulting 50 µm for Platilon and 500 µm for NM60. Material properties provided by manufacturers of chosen substrates are shown in Table 4.

Table 4. *Typical material properties for selected substrates. [67; 68]*

Property	**Epurex Platilon U 4201 AU**	**NewMet NM60**
Hardness (Shore A)	87	60 ± 5
Tensile stress at 50% strain	5 – 7 MPa	-
Tensile stress at break	60 MPa	5.5 MPa
Tensile strain at break	550 %	450 %
Temperature range	< +155 °C	-40 to +200 °C
Thickness range	0.025 – 1.000 mm	0.5 – 6.0 mm

The ink selected for experiments is Harima NPS-JL, which is a conductive ink containing silver nanoparticles. Harima NPS-JL was chosen because of its good electrical performance and sufficiently low sintering temperature for both substrates. Material properties of Harima NPS-JL are shown in Table 5.

Table 5. *Typical specifications for selected ink.[23]*

Property	**Harima NPS-JL**
Metal	Ag
Solvent	Tetradecane
Particle size (mean)	7 nm
Metal content	55 wt%
Viscosity	11 mPa·s
Min. sintering temperature	120 °C (60 min)
Volume resistivity	$6 \cdot 10^{-6}$ Ω·cm
Thickness shrinkage	87 %

Since minimum sintering temperature for Harima NPS-JL is 120 °C and maximum temperature for Epurex Platilon U 4201 AU is 155 °C, the sintering of nanoparticle ink chosen to be done at 150 °C for 60 minutes on both substrates. Sintering is performed in convection oven and samples are placed directly in oven heated at target temperature.

Printing equipment used in experiments are Dimatix DMP-2831 and iTi XY MDS 2.0 inkjet-printers. DMP-2831 is a desktop materials deposition system for jetting functional fluids and it is designed for research and development purposes. DMP-2831 can be seen in Figure 13.

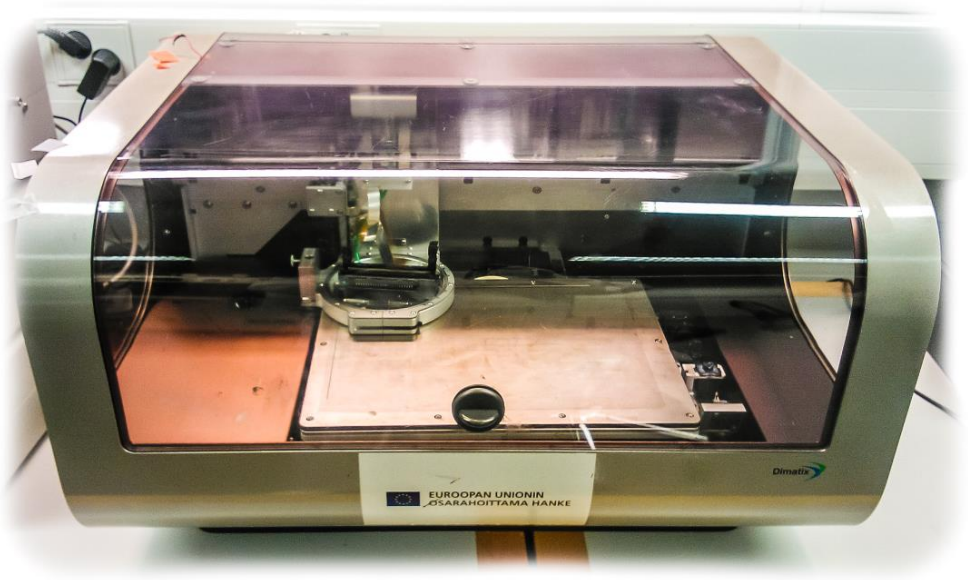

Figure 13. *Dimatix DMP-2831 desktop inkjet-printer.*

It contains a heated vacuum plate, which moves in y-direction during printing, and a cartridge carriage, which moves in x- and z-directions. DMP-2831 uses piezo-driven print heads with 1.5 ml integrated reservoir and heater. Print head contains 16 nozzles with 254 µm spacing and 10 pl nominal drop volume. Integrated drop watcher feature makes the DMP-2831 well suitable for evaluating jettability of new inks and integrated fiducial camera enables faster inspection of print quality. [69.] However, small scale of the printer limits the printing speed, which becomes problematic when multiple patterns or larger single patterns are printed. Therefore DMP-2831 is used only for preliminary tests and then the process is transferred to iTi XY MDS 2.0, which is a pilot scale inkjet printer. The main difference in iTi XY MDS 2.0 is the Spectra print head, which contains 128 nozzles with 508 µm spacing and 30 pl nominal drop volume. The print head is also stationary during printing and only the substrate is moved on a heated xy-plate.

Three main properties to be analyzed are electrical performance, mechanical performance and printability of the ink-substrate pair. Sufficient printing quality serves as a basis for electrical and mechanical performance and therefore printability analysis must be done first. When printing quality is considered sufficient with visual inspection, elec-

trical performance is measured to determine whether the conductivity of printed structures is sufficient for intended use or if the printing parameters need to be adjusted to achieve better conductivity. Lastly, the mechanical performance of printed circuits is tested from the electrical viewpoint to evaluate durability in use. Mechanical tests include evaluating adhesion between printed structures and substrate, and analyzing electrical performance under mechanical stress.

4.1 Image Printability and Manufacturing Process

Printability is the first concern when evaluating a new ink-substrate pair. If the printed pattern is continuous, bulging is minimal or non-existent and patterns dimensions are unchanged, the printability can be considered good. Fast evaluation of printability can be done visually with the aid of simple test patterns. Electronic circuit layouts usually consist of traces and gaps with different widths and lengths, and larger areas like ground planes. Therefore a simple pattern for testing ink-substrate pair printability consists of lines with different widths in process and cross-process direction, a sufficiently large solid area and also individual dots for drop size measurement. Example of such a pattern is shown in Figure 14.

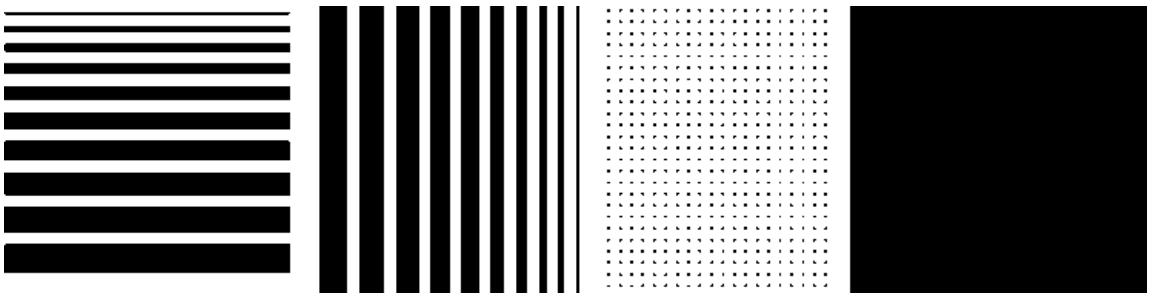

Figure 14. *Example of a test pattern for printability.*

Lines with different widths can be used to analyze continuity and bulging, but also stability of pattern dimensions. Especially with hydrophobic substrate materials large printed areas are usually prone to develop defects and cracks to the printed surface, because a larger amount of ink dries slower. Surface energies of ink and substrate have a strong influence on their interaction, but from printability viewpoint the absolute values hold little meaning whereas drop size is a good value for ink-substrate pairs' comparison. Drop size can also be used to compare different surface treatments and to determine the optimal resolution for printing. Measuring drop size is possible with a single drop, but it is advisable to measure multiple drops and use the average, because drop sizes can vary easily 10 - 20%.

In printability tests the goal is to iterate the best achievable printability by printing test patterns with different resolutions and analyzing print quality visually. If sufficient print quality is not achieved without special surface treatments, substrates surface ener-

gy can be altered with UV-ozone-treatment or anti-wetting coating. The whole manufacturing process is also evaluated and possible problems are analyzed.

4.2 Electrical Performance

Low voltage DC-measurements are widely used in semiconductor industry for characterization of material properties and process verification. Depending on the purpose of measurement, different test structures are involved. [70.] Resistivity is the most common parameter for a conductor and it describes the true performance of material. On the other hand, resistance, *R*, is much easily measured and the resistivity, ρ, can be calculated, if the dimensions of the conductor are also known:

$$\rho = \frac{A}{L}R \tag{7}$$

Where *A* is the cross-sectional area and *L* is the length of the conductor. Area *A* can be calculated by multiplying width, *w*, by thickness, *t*, of conductor. However, in the case of printed conductors, film thickness is problematic to measure because of the surface roughness and other slight distortions. [47.] This causes inaccuracy and uncertainty to resistivity calculations although the resistance can be measured accurately. Printed films are prone to crack propagation, if the amount of ink deposited at single process step is too high, and therefore the process window for film thickness is limited. Difficulty in measuring the film thickness and relatively small possible thickness variation makes the sheet resistance, R_S, a practical tool for characterization of electrical performance of printed conductors. Sheet resistance represents the resistance of a square area and it is defined:

$$R_S = \frac{\rho}{t} \tag{8}$$

If Equation (8) is combined with Equation (7), it can be seen that the resistance of conductor can be found by multiplying the sheet resistance by L/w, and resistivity can be found by multiplying the sheet resistance by thickness *t*. [70.]

In 1958, L.J. van der Pauw developed a method for measuring the resistivity or sheet resistance of arbitrary shaped disks [71], which means that problems due to incorrect knowledge of sample geometry can be avoided. One of the main error sources in this method was that the contacts are non-ideal and have finite size, but van der Pauw found that the error can be reduced if a "clover leaf" shaped samples are used. Although this method was developed for measuring large discrete samples, structures have evolved also for the scale of microelectronic devices. One of these structures is the Greek cross, which is a special case of the four-terminal van der Pauw structure. [70.] The layout of this structure is illustrated in Figure 15.

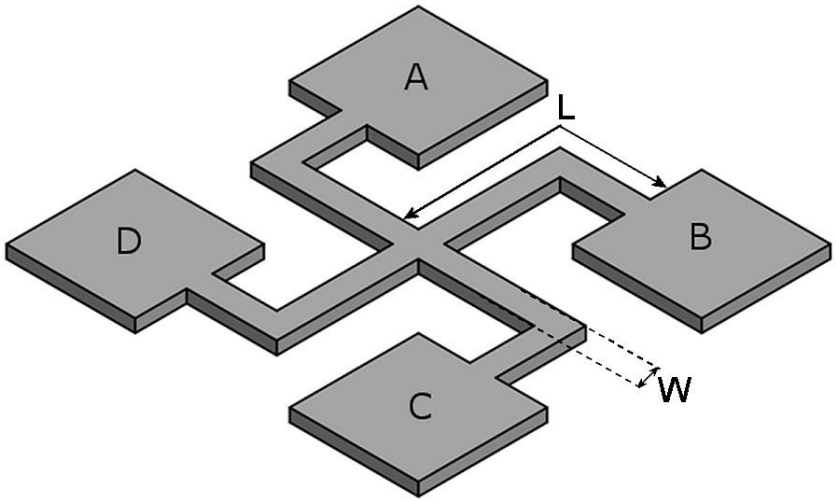

Figure 15. *Greek cross structure.*

The Greek cross is typically used for measuring sheet resistance, which is extracted at the heart of the cross [72]. The sheet resistance error depends on the ratio of arm length, *L*, to the arm width, *W*. If $L/W \geq 1$ the error is less than 1% [70], but an accuracy of better than 0,1% [72] can be achieved, provided that $L \gg W$. The sheet resistance determination is done by four measurements. First, a current is forced from pad A to B and voltage between pad D and C is measured. Then the current is reversed and voltage is measured from C to D. The resistance in this direction can be calculated:

$$R_{0^\circ} = \frac{V_{DC} - V_{CD}}{I_{AB} - I_{BA}} \tag{9}$$

After this the orientation is turned by 90° so that current is forced to pads B and C, and voltage is measured from pads A and D. Similarly as before, the resistance is calculated:

$$R_{90^\circ} = \frac{V_{AD} - V_{DA}}{I_{BC} - I_{CB}} \tag{10}$$

Then the average resistance is calculated of these two resistances as:

$$R = \frac{R_{0^\circ} + R_{90^\circ}}{2} \tag{11}$$

and finally the sheet resistance can be calculated of the average resistance:

$$R_S = f\left(\frac{\pi R}{ln(2)}\right) \ [\Omega/\square] \tag{12}$$

Where f is a correction factor for asymmetry of the structure. If the structure is homogenous, so that $R_{0°} \approx R_{90°}$, the correction factor f is effectively rounded as 1. [72.]

After sufficient printability has been achieved in previous tests, the sheet resistance of printed films is measured using the Greek cross structure, 4-point probe station and Keithley 2425 SourceMeter. If the sheet resistance is not satisfactory, printing parameters are adjusted accordingly. Basically this means increasing the amount of ink deposited on the substrate. Sufficient sheet resistance in these experiments is defined to be less than 80 mΩ/□, with less than 50% variation.

4.3 Mechanical and Electromechanical Performance

The most interesting property of stretchable circuits is naturally their electrical performance under mechanical stress, but adhesion of the ink-substrate interface is also an important part of durability. Since the substrates chosen for the experiments in this thesis are relatively soft and stretchable, commonly used cross-cut [73] or pull-off [74] tests are not suitable for testing adhesion on these substrates. Therefore adhesion is chosen to be analyzed roughly by a simple scratch test and the main focus of experiments is on the electromechanical performance.

Circuits can be stretched in three fundamental ways, i.e. in three dimensions. Linear stretching involves stretching only in one direction and is the most common example of stretchability. Linear stretching is also easiest to examine, because the test set-up is simpler and there are fewer factors to be considered. Two other stretching options are two-dimensional and three-dimensional stretching, which are usually present in real life situations, but are much harder to examine. [1, p.483.] Therefore experiments in this thesis are focused on linear stretching, which corresponds to the performance in other two dimensions, if the material is isotropic [75]. Since test samples are stretched only in one direction, test patterns to be printed can simply be a set of parallel traces with larger pads in both ends for connecting measurement wires. Such test pattern is shown in Figure 16.

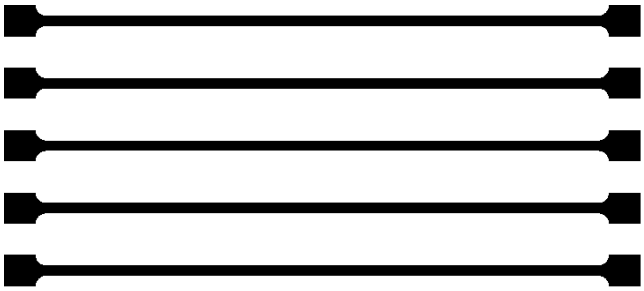

Figure 16. *Test pattern for strain testing.*

Relevant parameters for the test pattern shown in Figure 16 are trace width and thickness. Trace length can be chosen freely because strain is dimensionless i.e. measured deformation is normalized and expressed as a percentage of original length. Thick-

ness of printed trace depends on the amount of ink used, and affects the amount of strain that the trace can endure. The optimal amount of ink from printability and electrical viewpoint is determined in previous experiments and it is kept the same for the electromechanical test samples. This leaves one relevant parameter, trace width, to be decided for test samples. The narrowest reasonable trace, which can be manufactured with inkjet printing while maintaining high yield and sufficient length, is about 100 µm, and the widest trace commonly used in conventional PCBs is about 1 to 2 mm. In order to keep the number of test samples reasonable, two different trace widths are chosen to be tested: 100 µm and 1 mm. In addition to printed samples, evaporated silver lines with 50 nm thickness and 1 mm trace width are chosen to be tested for comparison, since 50 nm evaporated gold films have been reported to sustain over 15 % strain without losing conductivity due to microcrack formation [76].

The focus of the experiments in this thesis is on test-to-failure of inkjet-printed stretchable interconnects. Single elongation tests are performed to determine the peak strain that samples can endure, but also to analyze elasticity and plasticity of printed matter. Samples are analyzed visually with the aid of microscope to determine possible failure mechanisms which lead to open circuits. Cyclic elongation tests are used to evaluate products' field life, in which the estimated strain for e.g. medical applications is in the 0-20% range [3, p.209]. For safe operation, the repeated strain should therefore be larger than 20%, but it is expected that the peak strain in these experiments will be significantly below this and therefore a more suitable strain is chosen on the basis of single elongation tests. In both tests, the functionality of samples is monitored by measuring their resistance. Strain and resistance values are recorded for later analysis. The elongation speed in both tests is limited to maximum of 1.5 %/min to avoid shock effects caused by rapid changes in strain.

In order to test peak strain and life time of printed circuits on a stretchable substrate, a custom test system was designed and built. The system comprises a linear actuator, custom built test fixture, stepper motor, H-bridge motor controller, microcontroller prototyping platform and PC. The main parts of this test bench are illustrated in Figure 17.

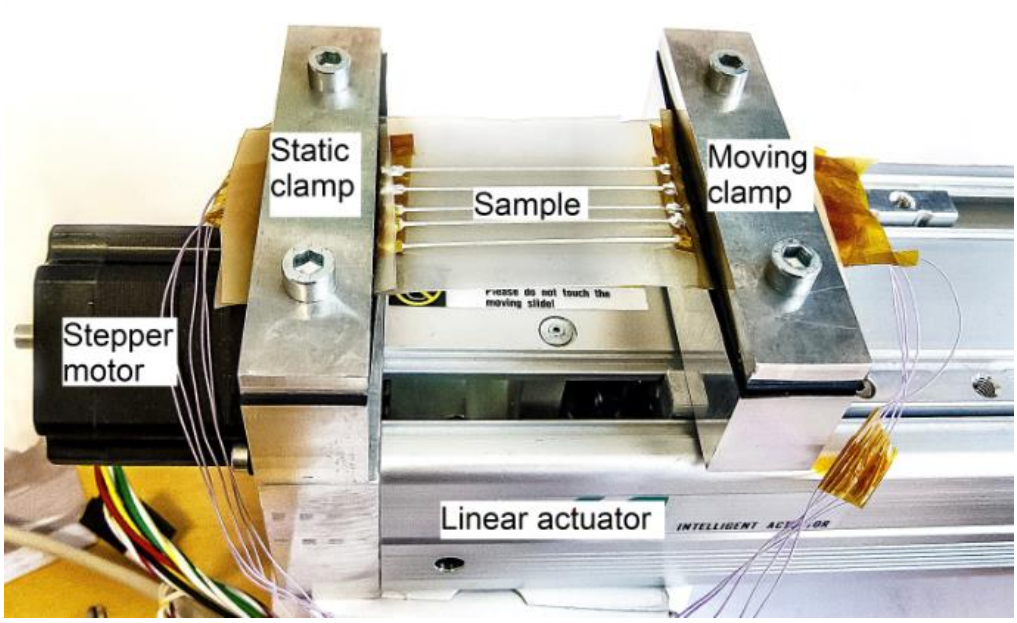

Figure 17. *Custom built test bench for linear strain tests.*

The basis of the test system is a linear actuator with 6 mm lead screw, and it is powered by a stepper motor with a maximum torque of 1 Nm [77]. The maximum linear force, which actuator can produce with such torque, can be calculated:

$$F_{max} = \frac{2\pi T_{max}}{\eta l} \qquad [78; 79] \qquad (13)$$

Where T_{max} is the maximum torque applied to screw, l is the lead of screw and η is the efficiency of screw. With 1 Nm torque, 6 mm lead and a typical 0.9 efficiency [80] for a ball screw, Equation (13) gives 1164 N for the maximum force of the linear actuator. Substrates chosen for these experiments have 60 MPa [67] and 5.5 MPa [68] tensile strengths, which means that 100 mm wide samples with thicknesses 50 µm and 500 µm, respectively, can endure 300 N and 275 N until break. Therefore the maximum force of the linear actuator is easily sufficient for stretching experiments with these substrates. The chosen stepper motor, which can be seen in Figure 17, has 400 steps per round and since the screw lead is 6 mm, this results resolution of 15 µm for the linear actuator. Minimum distance between the clamps in the test fixture is 61 mm, and with 15 µm steps the resolution for strain is at least 0.246 ‰, or smaller if longer than 61 mm samples are used. Mechanical tolerances of the screw are unknown, but since movement is needed only in one direction during measurement and samples cause stress in opposite direction, mechanical slack is minimized and therefore movement accuracy is assumed to be dominated by stepper motor resolution.

The stepper motor is driven by H-bridge motor driver, more specifically L298 dual full-bridge driver manufactured by ST Microelectronics. Motor driver is controlled by Arduino Uno microcontroller prototyping platform, which is based on the Atmel

ATmega328 8-bit microcontroller. Since ATmega328 contains a 10-bit analog-to-digital converter and 6 analog inputs, the simplest solution is to use ATmega328 also for resistance measurements, rather than setting up a separate measurement system with multiple channels. ATmega328's ADC has a maximum reference voltage of 5 V and thus one analog-to-digital-unit, ADU, translates to approximately 4.88 mV. ADC's absolute accuracy is reported ± 2 LSB, which results 9.77 mV for possible error in measurements. To achieve this accuracy, ADC must be calibrated with an accurate voltage source. [81.] The most accurate calibration can be done by measuring whole input range in small steps and storing a conversion table to the memory of microcontroller unit. However, the amount memory in small MCUs is usually very limited, and the most common errors in analog-to-digital converters are gain and offset errors, which can be corrected with two correction factors. Figure 18 illustrates the effects of gain and offset error.

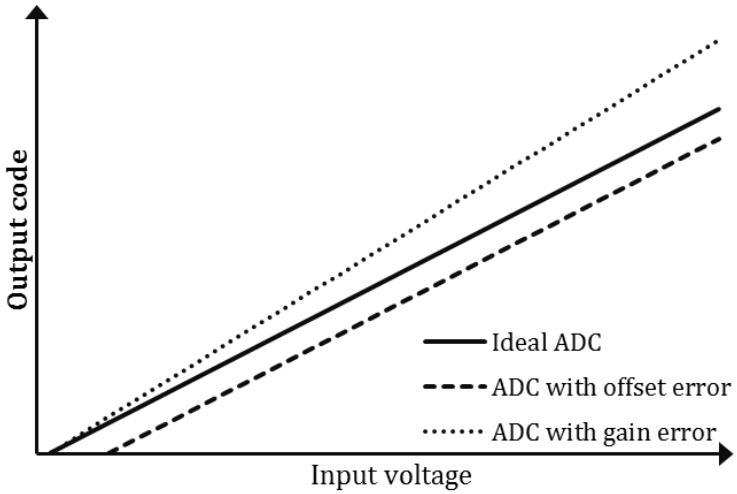

Figure 18. *Typical analog-to-digital conversion errors.*

Offset error can be corrected by adding or subtracting a constant value and gain offset can be corrected by multiplying results with a constant value. Both of these correction factors can be calculated from a single set of measurements and the implemented to the MCU's software.

Since ADC can only measure voltage, the resistance must be calculated regarding to the measurement circuit. There are two basic measurement setups for resistance measurements: constant voltage and constant current. Constant current setup includes separate current sources for every measuring channel, whereas constant voltage needs only one voltage source and voltage dividers for every channel. The drawback of constant voltage setup is that the voltage changes nonlinearly as the samples resistance changes and because the ADC's error is constant 9.77 mV, the error in calculated resistance is relatively higher at the both ends of measurement range. However, the relative error can be minimized on a certain range by choosing appropriate series resistance. Figure 19 shows the chosen measurement setup with constant voltage source.

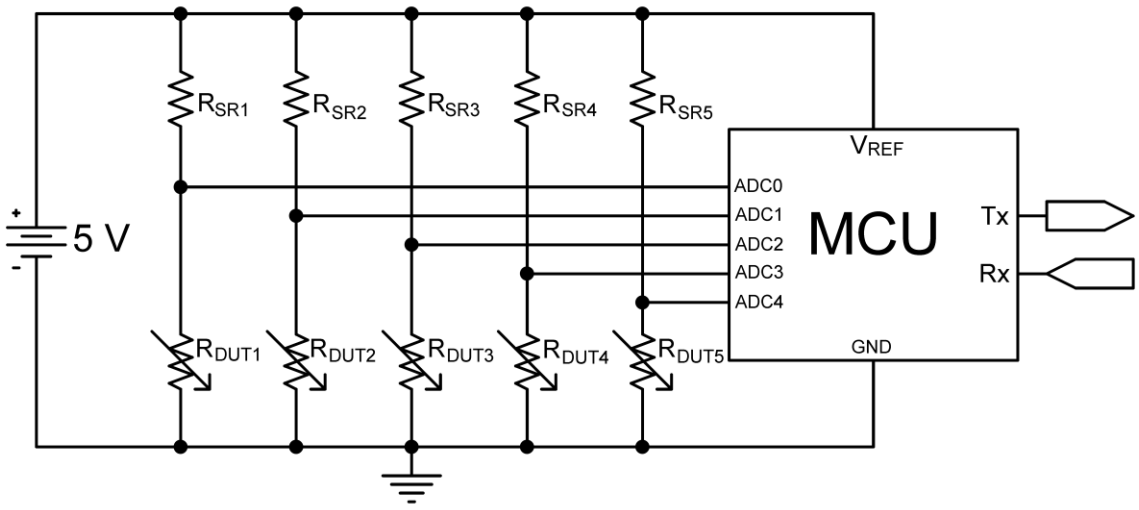

Figure 19. *Schematic of measurement setup for resistance.*

The resistance of each sample can be calculated from measured voltage with:

$$R_{DUT} = \frac{R_{SR}}{(V_{IN}/V_{OUT}) - 1} \tag{14}$$

Where R_{SR} is the resistance of series resistor, V_{IN} is the source voltage and V_{OUT} is the voltage measured by ADC. Input impedance of ADC is also connected parallel to the samples resistance, but if the measuring range is substantially lower than the input impedance, it can be ignored. ATmega328's datasheet states that the ADC is optimized for impedances 10 kΩ or less [81] and in these experiments the expected range is from few Ohms up to 1 kΩ, which is a decade lower than the upper limit of optimized impedance range. Noise also causes error in all analog-to-digital conversions, but since these measurements are not time critical, it can be effectively reduced with heavy filtering. For this reason, a fast infinite impulse response filter is implemented in the ATmega328's software and the results are calculated as an average of 100 measurements. The main source for measurement error is therefore the ADC's ± 2 LSB accuracy, which causes relatively higher errors in both ends of measurement range. Figure 20 illustrates this relative error on 0 to 500 Ω range with three different series resistors.

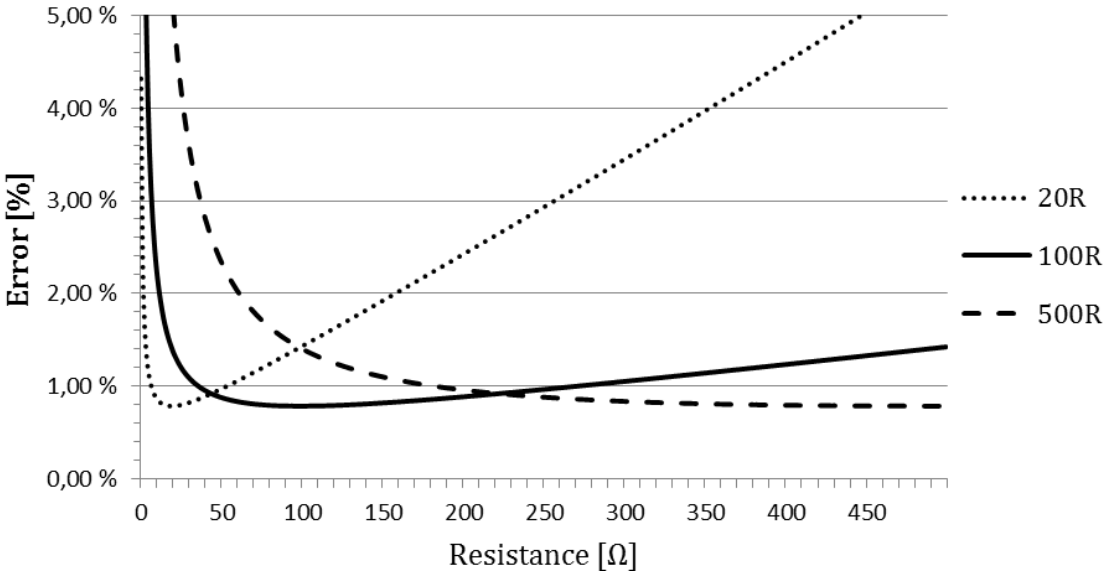

Figure 20. *Relative error with different series resistors.*

As shown in Figure 20, smaller series resistance enables more accurate results with lower sample resistances, but the range is very limited. In these experiments the initial resistances are expected to be in the range of 5 to 50 Ω and the most interesting range continues up to 5 – 10 times the initial resistance. The series resistor of 100 Ω is a good tradeoff between the low end and high end accuracy, and it gives less than 1 % relative error for measurement range 37 – 268 Ω and less than 2 % error for 13 – 791 Ω. The resistors chosen for the actual device had 5 % tolerance for resistance value, but since this is a one-of-a-kind device, the accuracy of resistances was easily assured by measuring multiple resistors with a multimeter and by "cherry-picking" the most accurate resistors.

Before the actual strain testing was done, some initial tests were performed to verify that whole test system is working like designed. Initially 61 mm long samples were attached to custom made test bench so that measurement wires were left loose over the clamps at both ends of sample and because of wires' stiffness approximately 5 mm gap was left between contact pads and clamps to prevent wires from twisting samples. Strain was increased at somewhat varying speed due to the choice in software implementation to wait for resistance to stabilize, but the maximum speed was limited to 0.9 mm/min. It was observed that the small gap between contact pads and clamps distorted results and caused measured peak strains to be higher than the actual strain in printed conductors. This is due to the fact that printed conductors and substrate material combination is stiffer than mere substrate film and therefore strain is more focused on these small gaps at both ends of samples. Measurement wires, which were left loose, also affected negatively on reproducibility of tests. An example of distorted results can be seen in Appendix A. To ensure that stretching occurs only in parts which contain conductors, measurement wires were routed through the clamps along samples, as can be seen in Figure 17, and contact pads were fixed as close to edge of clamps as possible. Strain was fur-

ther focused to conductor lines by stiffening areas around contact pads by attaching Kapton tape in reverse side of samples. Initial flatness of samples was also identified as a possible source for error and therefore a pre-stretched silicone rubber film was attached between test bench clamps to support samples and to enable reproducible initial conditions. Flatness of samples and issues in attaching samples to test bench have also been reported problematic in other studies [44].

4.4 Stretchable Demonstrator Device

In addition to tests in Chapters 4.1 – 4.3, the feasibility of an ink-substrate pair for manufacturing actual devices is demonstrated by transferring the design of the demonstrator device as described in Chapter 2.4.2 on stretchable substrate. This will transform the device to truly plaster-like, and it should be much less noticeable on skin contact, which is one of the goals in Healthsens –project.

The actual manufacturing of demonstrator device is done mostly like the manufacturing on flexible substrate. The printing is done with the optimized parameters found in previous tests. The component attachment is done with Creative 124-08C isotropically conductive adhesive and Epotek OE121 epoxy underfill, which are deposited with handheld pneumatic fluid dispenser. Components are placed with Finetech Fineplacer.

One of the main challenges in manufacturing circuits on stretchable substrate is expected to be the stability of dimensions. TPU and silicone rubber have much higher coefficient of thermal expansion than PEN, which was the previously used flexible substrate. This difference in CTE can possibly change dimensions of printed circuit and therefore cause difficulties in component assembly. Softer substrates also offer much less mechanical support for components, which may cause reliability problems. Performance of the stretchable demonstrator is further compared to the flexible demonstrator to reasonable extent.

5 RESULTS AND DISCUSSION

This chapter presents the results of experiments described in chapter 4. First the results for printability on two substrates are presented, which is followed by the results for electrical performance. These experiments yield the optimized printing parameters, which are used in manufacturing of demonstrator device and in manufacturing of test samples for electromechanical testing. A flow chart of the simplified optimization process for printing parameters is shown in Figure 21.

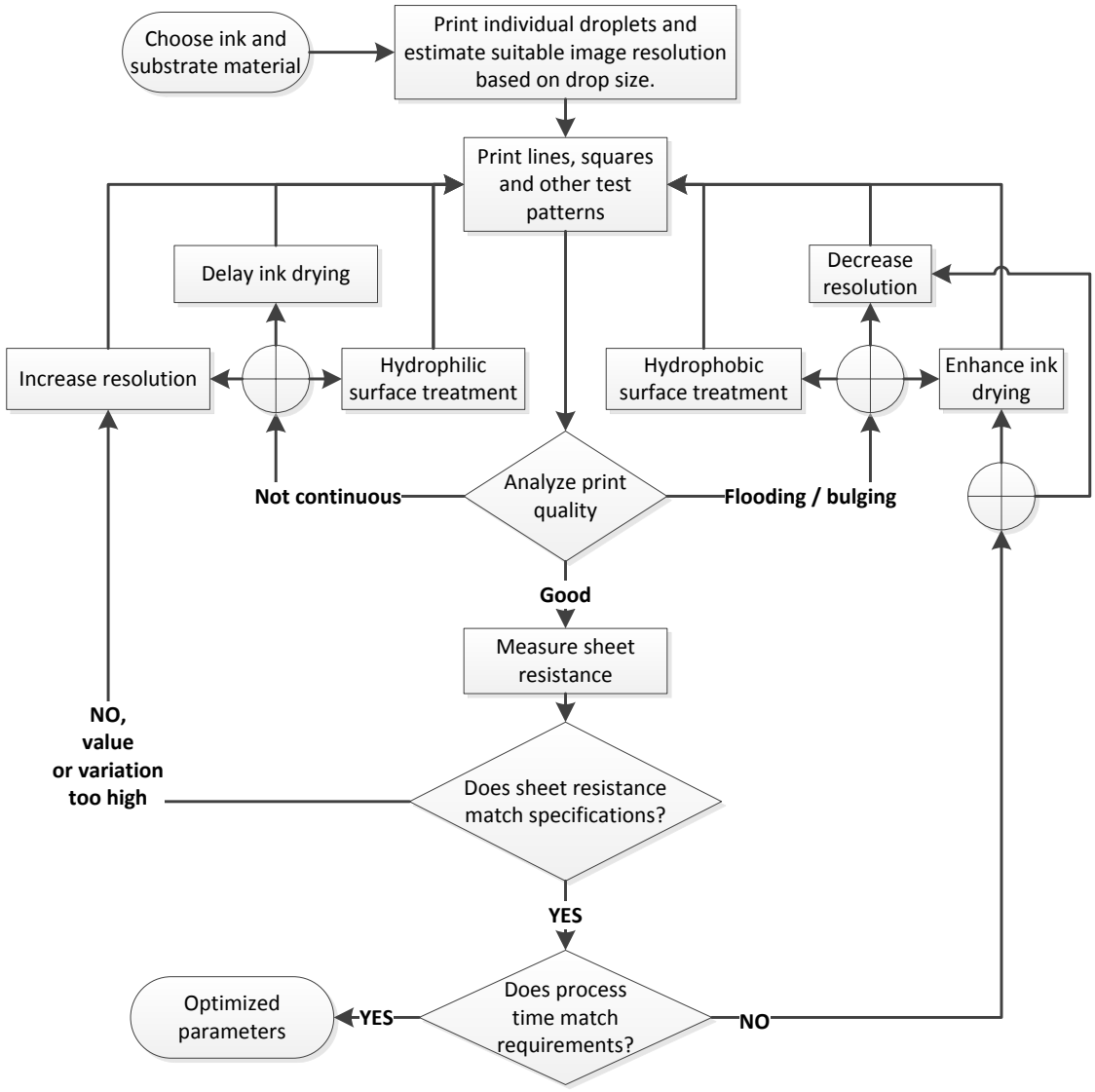

Figure 21. *Basic optimization process of printing parameters.*

As can be seen in Figure 21, the optimization process consists of multiple iteration rounds and execution of corresponding experiments is somewhat parallel. Therefore the timeline in Chapters 5.1 - 5.4 is not entirely linear. Since printing in this thesis is done with two different printers, the printing process has to be optimized for both printers separately. Small scale tests in Chapters 5.1.1 - 5.1.2 are used as a basis for printing parameters of pilot scale printer, which helps to reduce the number of iteration rounds on the second time.

5.1 Printability

Epurex Platilon U 4201 AU thermoplastic polyurethane and NewMet NM60 silicone rubber were cut into rectangular approximately 150 mm x 70 mm sized sheets and the samples were cleaned with isopropyl alcohol. It was immediately apparent that chemicals, such as isopropyl alcohol, have a pronounced effect on TPU. When a sheet of TPU was placed on a flat surface and wiped with an alcohol-dampened cloth, it immediately curled up. If the sheet was forced flat, it became wavy after isopropyl alcohol was applied to the surface. However, the effect soon faded away after the alcohol had vaporized from the surface. On NM60 silicone rubber the similar effect was noted, but the magnitude was insignificant. This effect is most probably due to absorption of solvents, which is a typical property of polymers and causes swelling.

The small scale testing with these samples are described in Chapter 5.1.1, which is followed by experiments with different surface treatments in Chapter 5.1.2. Then printing process is scaled up for a pilot class inkjet printer in Chapter 5.1.3 and finally an image masking algorithm is introduced to further improve printing process in Chapter 5.1.4.

5.1.1 Small Scale Tests

Preliminary printing trials were started with Dimatix DMP-2831 desktop printer and Harima NPS-JL ink. Pre-cleaned samples were placed on the heated vacuum plate, but the vacuum could not hold TPU samples flat against the surface. Therefore the TPU samples were secured on to a 1.5 mm thick aluminum carrier plate with Kapton tape and the carrier plate was placed on the heated vacuum plate. Initial printing parameters were chosen based on the optimal parameters for PEN substrate. Printing resolution was therefore 1270 dpi, which means 20 µm drop spacing, hot plate temperature was set to 60 °C and nozzle plate temperature to 43 °C. Drops were ejected with only one nozzle, custom waveform, 23 V amplitude and 7 kHz frequency. The printed test pattern is shown in Figure 22 and it is scaled up, since the actual size is approximately 1.2 mm x 1.2 mm. The initial printing results on TPU and silicone rubber are shown in Figure 23.

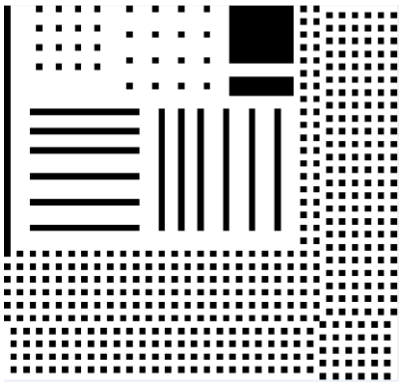

Figure 22. *Test pattern for initial printability tests.*

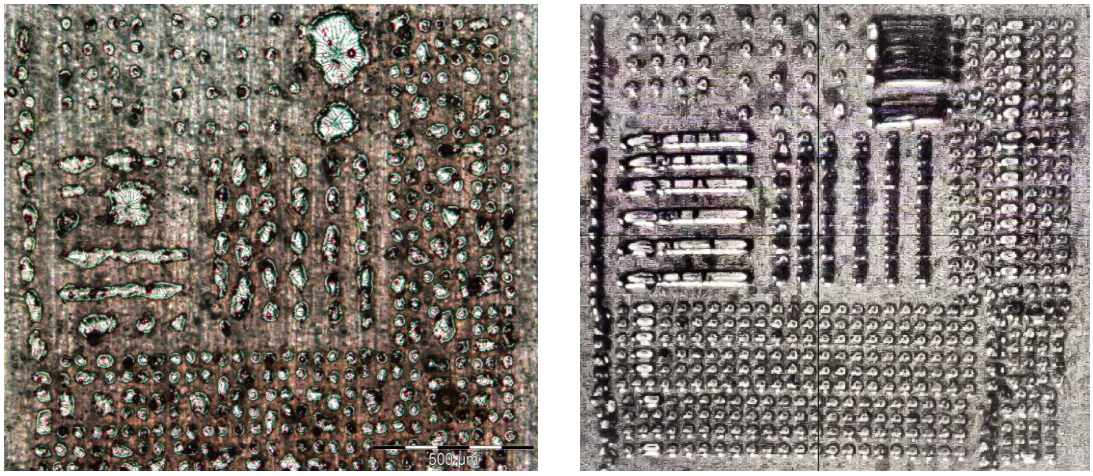

Figure 23. *Microscope image of printing results on TPU (left) and Dimatix fiducial camera image capture of printing results on silicone rubber (right).*

Figure 23 shows that the drop size on TPU and on silicone rubber is about 30 µm since the distance between drop centers in lower part of the image file is 40 µm and there is a small gap between drops. Small drop size implies hydrophobic nature of both substrates. Most of the lines on TPU have broken into beads containing 2-3 drops and the rectangular shapes have formed roundish puddles of ink, whereas all of the printed features are well formed on silicone rubber. Individual lines formed by each printing pass can even be observed in the rectangular shapes on silicone rubber. The surface defects of TPU seem to have a strong influence on drop size, shape and placement.

The second printability test was printing larger solid areas, since the rectangular shapes in the first test pattern were relatively small. Figure 24 shows microscope images of larger printed surfaces.

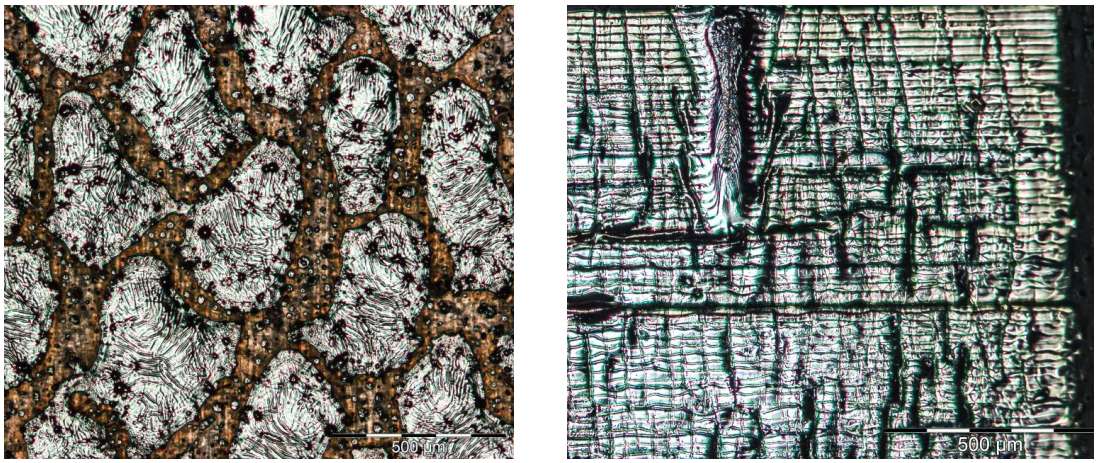

Figure 24. *Microscope images of large solid areas printed on TPU (left) and silicone rubber (right).*

With this test it became clear, that printing large solid areas in a single pass is not possible on TPU without additional surface treatments. Printed ink did not form a contiguous surface, but instead broke down into 200 – 500 µm sized puddles of ink. On the other hand, printing results on silicone rubber were similar to previous results, but with an addition of crack formation and wrinkles, which are clearly visible in Figure 24. During printing it was also noted, that TPU started to react with the solvent of ink by warping. This affects the print height and can lead to misalignment of drops or even print head touching the substrate. The warping faded away after the ink had dried, so therefore it was due to swelling of substrate material, which is caused by absorption of solvent. Similar effect of the same magnitude was not observed with silicone rubber, but this substrate is also significantly thicker, which can be a hindering factor. Swelling was therefore considered as a possible cause for the observed crack formation and wrinkling. To reduce the effects of insufficient wetting of the ink and the swelling caused by solvent-substrate interaction, drying times were increased by dividing the original printing file into 2 and 4 parts, which increased printing times to two-fold and four-fold, respectively. However, dividing image into 2 parts improved printing quality only little and even dividing image into 4 parts did not produce totally contiguous larger surfaces. As the printing time increased to four-fold, so did the possibility of a clogged nozzle and other printer related problems.

5.1.2 Surface Treatments

Insufficient printing quality of large solid areas was considered to be caused by poor wetting of ink and therefore different surface treatments were tested to enhance wetting. First, and the most obvious choice, was to treat the surface with same solvent that the ink contains and for NPS-JL that is tetradecane. Second selected treatment was UV-ozone and third was a combination of tetradecane and UV-ozone. Tetradecane treatment was carried out by applying tetradecane on substrate with a pipette, spreading it with a cleanroom wipe and at the same time wiping off excess solvent. Swelling of substrate

material was apparent on TPU, but also on silicone rubber. Tetradecane drops on silicone rubber left a visible bump, which flattened in matter of minutes. In UV-ozone treatment substrate was placed in the treatment chamber and UV-lamp was turned on for 15 minutes. After the lamp turned off, substrate was left in the chamber and let to dwell in ozone gas for 15 minutes. Combination treatment was carried out by first treating substrate first with UV-ozone and then applying tetradecane. After the surface treatments, a test pattern shown in Figure 22 was printed on each treated substrate. The results of surface treatment tests on TPU are shown in Figure 25.

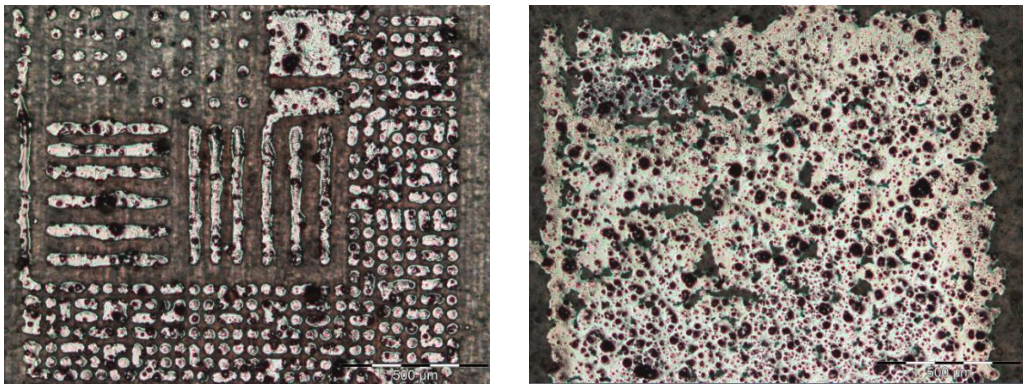

Figure 25. *Printed test patterns on TPU. Surface treated with tetradecane (left) and UV-ozone (right).*

Printing results on tetradecane-treated TPU are significantly better than without treatment. Drop size is a little bigger, which leads to more merged drops, but drops have not moved from their positions. Also some bulging is seen in rectangular areas and in some of the lines, but the lines are now continuous. On UV-ozone treated TPU the printed structures have spread extensively and it is obvious that fine patterns are impossible to print with this surface treatment. Combining UV-ozone treatment with tetradecane increased spreading even more, which caused the test pattern to merge into one continuous splotch. Based on these results, the surface treatment with tetradecane seemed as a sufficient treatment to enhance wetting and UV-ozone treatment was considered to be the second option, if the process time is shortened. Large solid areas were also printed successfully in a single pass on tetradecane-treated TPU. Interestingly these surface treatments did not have as promising results on silicone rubber as on TPU and because of that testing was increasingly focused on TPU substrate.

Although dividing printed images into 4 parts reduced swelling of substrate, it was still a problem. However, if the substrate is pre-stretched more than it swells, the substrate will remain under tension and stay flat during printing. Maintaining pre-stretch until ink is sintered may also help to balance out the CTE mismatch between substrate and ink. Therefore a pre-stretch of approximately 10% was applied to TPU substrate and printing was tried with large patterns. The results were good: substrate stayed flat during printing and no obvious cracks were formed during sintering.

After wetting and swelling problems were solved, printing was tested with greek cross patterns, which are used for electrical performance testing in Chapter 5.2, and with demonstrator device layout described in Chapter 2.4.2. With 1270 dpi printing resolution it was observed that because ink dries slowly, it flows towards the center of pattern before it dries. This causes uneven ink distribution so that pattern edges are thinner than the center. Figure 26 illustrates the ink flow on edge of a printed pattern.

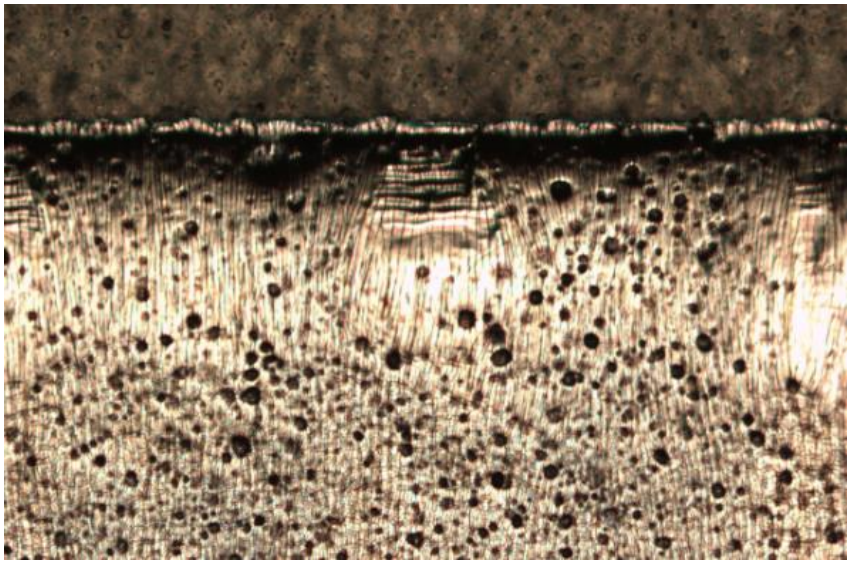

Figure 26. *Microscope image of printed patterns edge on TPU.*

Top part in Figure 26 is the substrate surface and lower part is printed ink. It can be seen that flowing of ink has a strong thinning effect on pattern edges. The effect is stronger on the edge where printing begins. Ink flow leaves crystallized-like marks on ink surface, with lines pointing towards the pattern center. In addition to uneven ink distribution, some flooding is also seen on pattern edges. Depending on the application these might not be much of a problem and therefore printing would be possible with a single pass. However, with finer circuit layouts the yield of the printing process will be reduced, which can be prevented by printing the pattern in multiple passes. In order to optimize the printing quality and the process time, different combinations were tested. With 1270 dpi and image masked into 4 files the yield of printing process was also equally low because of printing equipment related problems. Image resolution of 900 dpi and 2 layers would give roughly the same amount of ink as 1270 dpi and 1 layer, but the first layer printed with 900 dpi did not produce a continuous ink coverage, which resulted in gaps even after the second layer. Image resolution of 1016 dpi was found to be the smallest resolution, which produces continuous ink coverage in single pass, but it is not as prone to flooding as 1270 dpi. Two layers printed with 1016 dpi results in approximately 27 % more ink, which is actually better for electrical performance as will be explained in Chapter 5.2.

5.1.3 Printing Process Scale-up

At this point the printing process was moved to pilot scale inkjet-printer, iTi XY MDS 2.0, which allows much faster printing process. The only drawback is with this equipment is three times bigger nominal drop volume than with DMP-2831, which leads to larger drop size. The first step was therefore drop size measurement. Printed test pattern was a simple dot matrix and drop size was determined from 50 drops on tetradecane-treated TPU substrate. Results of drop size measurements are shown in Figure 27.

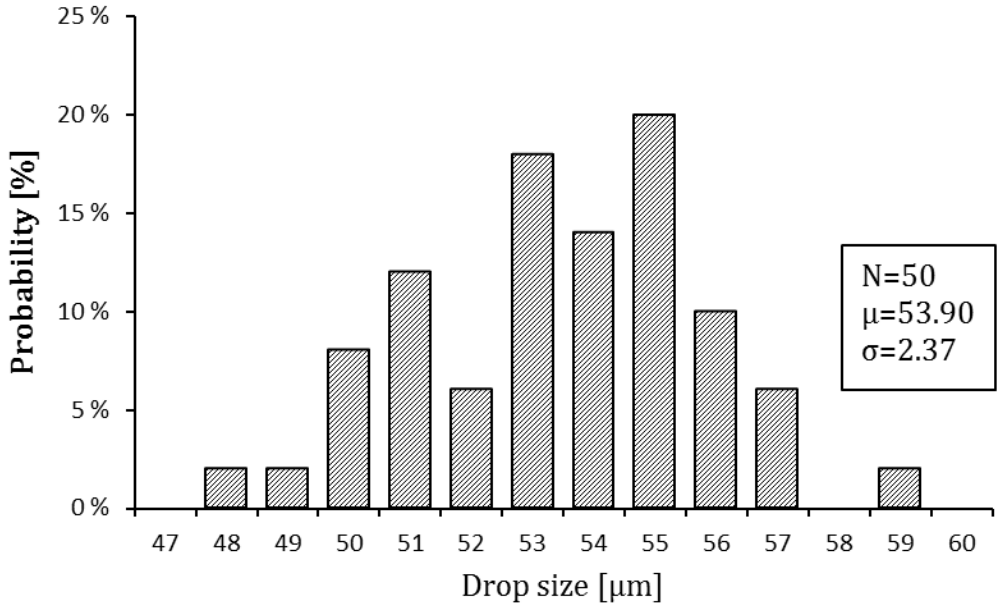

Figure 27. *Drop size distribution on TPU.*

Smallest line width in circuit layout of the demonstrator device is approximately 100 µm and the average drop size is 53.90 µm, which is not a problem. Although the best printing results with DMP-2831 on TPU were achieved with resolution 1016 dpi and two layers, the best printing results with only one layer were achieved with resolution 1270 dpi, which means drop spacing of 20 µm. The drop size with DMP-2831 on TPU was approximately 30 µm and based on this drop size and drop spacing of 20 µm proportion, the optimal printing resolution for iTi XY MDS 2.0 was estimated to be approximately 710 dpi. On the other hand, calculation of ink volume per surface area and the difference in nominal drop volumes gives an estimate of approximately 730 dpi. Resolution options of iTi printer are split in 50 dpi steps, so that closest options are 700 dpi and 750 dpi. The iteration of printing parameters with iTi XY MDS 2.0 was therefore started from image resolution of 700 dpi.

Initial printing parameters used with iTi XY MDS 2.0 were: nozzle plate temperature 34 °C, vacuum plate temperature 60 °C, printing speed 80 mm/s and ejection waveform amplitude 55 V. Printing was done in single pass with resolutions 700 dpi, 750 dpi and 800 dpi. Lines with 1-4 pixel width were printed successfully, but large solid areas failed with every resolution. Figure 28 shows typical printing result of large solid area.

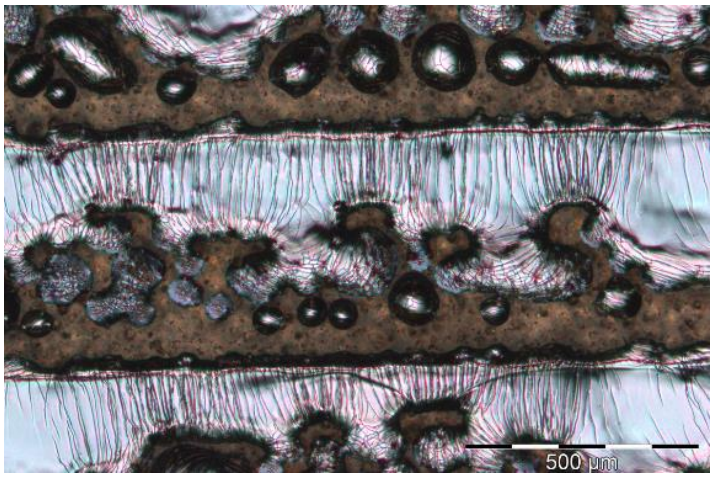

Figure 28. *Typical printing result of large solid area with iTi printer on TPU.*

In iTi XY MDS 2.0 print head always uses all nozzles, but with Dimatix DMP-2831 printing was done using only one nozzle. This basic difference in deposition method leads to discontinuous printing results as seen in Figure 28. Gaps in the printed pattern are formed according to the nozzle spacing of 508 µm in print head. Due to this drawback print pattern was again divided into 4 files in order to increase drying time and to ensure uniform ink distribution. Even though this increased printing time four-fold, the process was still faster than with DMP-2831 and a single printing pass. Vacuum plate temperature was also increased to 65 °C, which enhances ink drying. By using these parameters, all test patterns and the circuit layout of demonstrator device was successfully printed with resolutions 700 dpi, 750 dpi and 800 dpi, but with 700 dpi process yield was low due to occasional gaps. Printed surfaces were more homogenous with higher image resolutions and even resolution of 800 dpi did not produce unwanted effects, such as flooding or cracking. Higher resolutions produced also better electrical performance with smaller deviation as will be explained in Chapter 4.2.

5.1.4 Masking Algorithm

In order to further improve printing process with iTi XY MDS 2.0, a special masking algorithm was introduced. The algorithm is similar to that Santtu Koskinen presented in his Master's thesis [82] and it utilizes the full resolution of printing equipment to increase placement accuracy of drops and also to maximize drying time of individual drop before adjacent drops are deposited. This aims to a stacked coin –structure, which eliminates gaps formed by ink flow and thereby ensures uniform ink distribution. The actual masking pattern is 37 by 37 pixels in size and it contains 37 black pixels placed so that every line contains only one pixel and the distance between adjacent pixels is more than 6 pixels. With 5050 dpi maximum resolution of iTi XY MDS 2.0 the masking algorithm produces an ink amount equal to 830 dpi with full coverage. However, it was observed that evaporation rate of Harima NPS-JL with current parameters is too slow for successful printing with the masking algorithm in one layer. Vacuum plate temperature was

increased to 70 °C and printing speed was decreased to 40 mm/s, which enabled successful printing of finer structures, but with large areas droplets began to combine after approximately half of the pattern had been printed. This was presumably caused by rising solvent concentration in surrounding atmosphere, which decreases evaporation rate of solvent in ink. Therefore the mask was divided into two layers as shown in Figure 29.

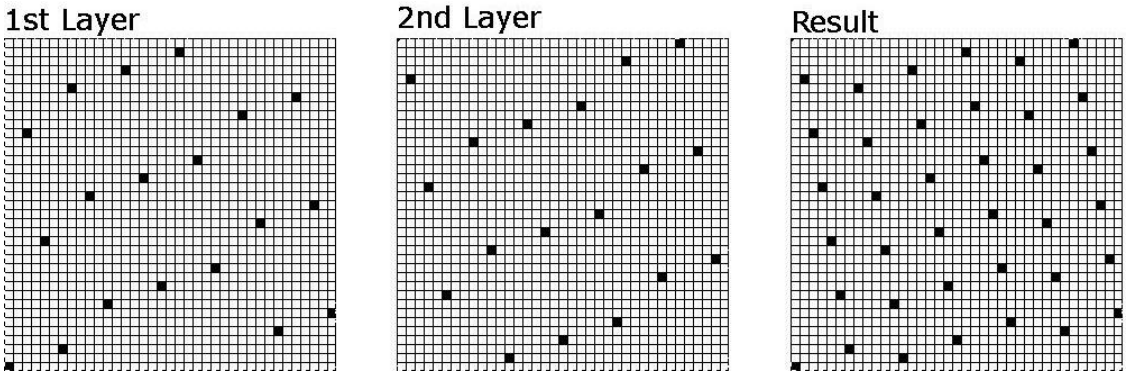

Figure 29. *Illustration of the masking algorithm with two layers.*

This solved the problem with combined droplets and produced evenly distributed stacked coin –structure. Masking algorithm with two layers proved to be robust enough that printing speed could be increased back to initially used 80 mm/s. Printing was done successfully on TPU and silicone rubber, but printed patterns wrinkled on silicone rubber as the pre-stretch was released. Also the adhesion between silver conductors and silicone rubber was inferior to adhesion on TPU as will be explained in chapter 0. However, on TPU wrinkling did not occur, which is caused by thermoforming of TPU during sintering. Microscope images of patterns printed with masking algorithm can be seen in Figure 30.

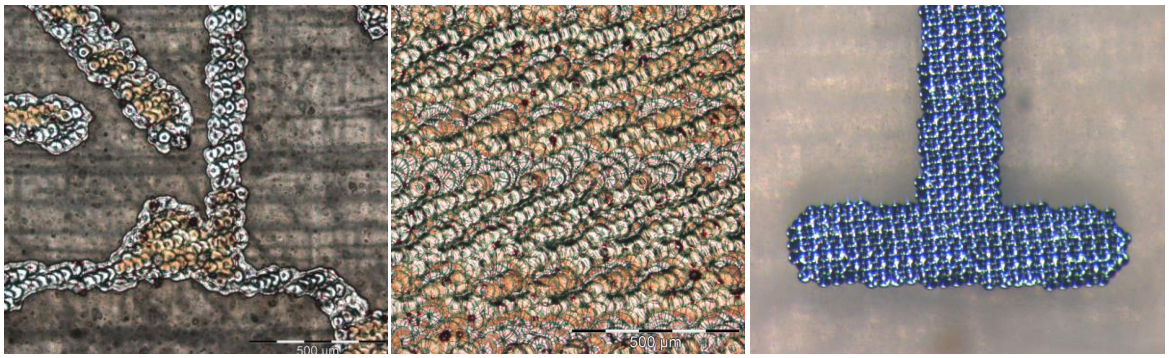

Figure 30. *Microscope images of patterns printed with masking algorithm.*

Figure 30 shows clearly how every droplet has dried individually and therefore ink distribution is exactly the same as defined by the printing file. One drawback with the masking algorithm is slightly saw tooth –patterned edges, which is most apparent on edges of straight horizontal and vertical lines. This is not a problem in most cases, but it

makes less than 100 µm wide lines more susceptible to misalignment of a single droplet, since masked lines are not uniform in width and can become connected in some parts with only 1 – 2 droplets. If problems should occur with discontinuous narrow lines, print file can be fine-tuned by adding single pixels to troublesome parts of the image.

As a conclusion, printability was at first experimented with Dimatix DMP-2831 and then process was transferred to pilot class inkjet printer iTi XY MDS 2.0. Two different ink-substrate pairs were studied: silver nanoparticle ink on thermoplastic polyurethane and on silicone rubber. Since both substrates proved to be hydrophobic, different surface treatments were tested, but wiping the surface with same solvent as the ink contains was seen as the best method. Problems with CTE mismatch and swelling of substrate material due to solvent absorption were solved by pre-stretching the substrate approximately 10 % of initial dimension. Initial testing with DMP-2831 showed that thermoplastic polyurethane was more promising candidate as a stretchable substrate for inkjet printing, but with iTi XY MDS 2.0 and the masking algorithm, which produces stacked coin –structure, both substrates were easily printable. However, inkjet-printed conductors on silicone rubber wrinkled as the pre-stretch was released and on thermoplastic polyurethane wrinkling did not occur because of thermoforming during sintering. The final printing parameters with iTi XY MDS 2.0 and 30pl Spectra printheads were: nozzle plate temperature 34 °C, vacuum plate temperature 70 °C, printing speed 80 mm/s, droplet ejection waveform amplitude 55 V and printing resolution 5050 dpi with masking algorithm, which produces ink amount equal to 830 dpi.

5.2 Electrical Performance

The electrical performance of inkjet-printed conductors was studied in parallel with the printability experiments. Greek cross patterns illustrated in Figure 15 were printed after printing quality was continuous by visual inspection and sheet resistances were measured with 4-point probe station and Keithley 2425 SourceMeter. Sheet resistances were measured from samples printed on thermoplastic polyurethane with 5 different setups and the results are shown in Figure 31. All sheet resistances were measured from 4 – 12 samples per printing setup.

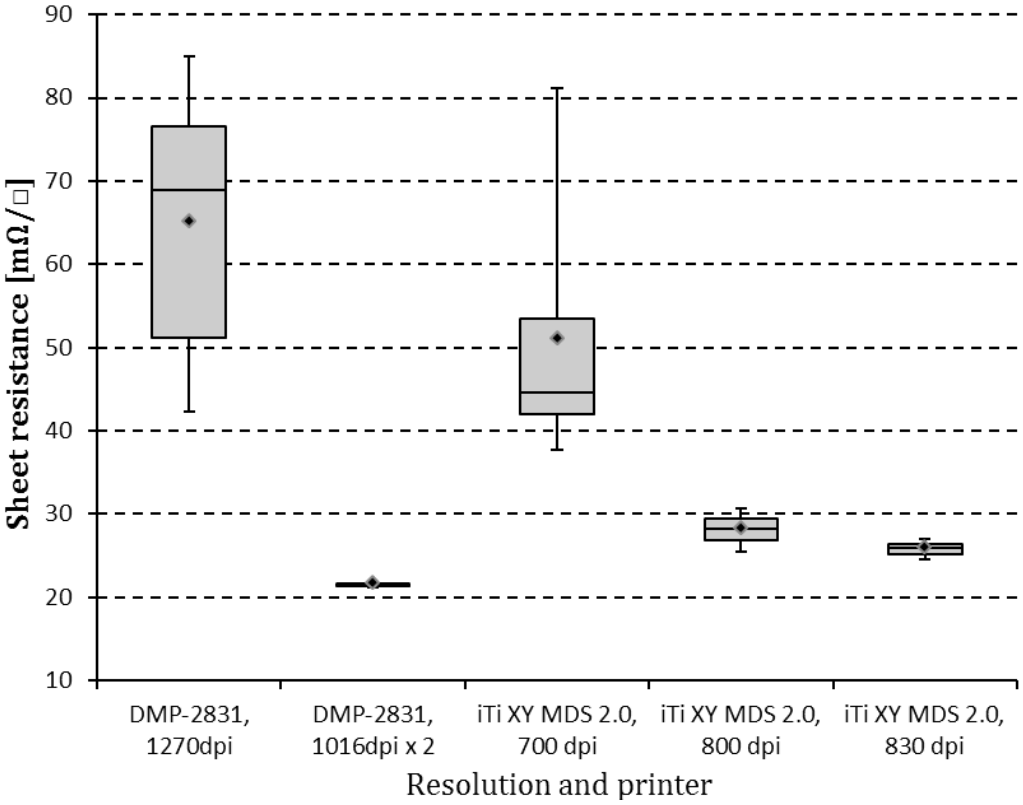

Figure 31. *Measured sheet resistances of samples printed with different printers and different parameters. Grey boxes illustrate the standard deviation and horizontal lines across boxes are the median values. Vertical lines illustrate minimum and maximum values of measurements and the black dots are the averages.*

The first measured samples were printed with Dimatix DMP-2831 and image resolution of 1270 dpi, which is the same resolution as has been previously used with PEN film. As can be seen in Figure 31, the results had fairly high variance, although the printed surface was continuous in visual inspection. The highest measured sheet resistance was more than double the lowest measured sheet resistance. The average of measured sheet resistances would be an acceptable value for printed structures, but the high variance makes it difficult to design circuits with the sheet resistance taken into account and this variance is likely to decrease yield of the manufacturing process. The surface roughness of thermoplastic polyurethane film is notably higher than of PEN film and therefore it was seen as the most probable cause for higher sheet resistance variance than has been seen before with the same printing parameters.

Since the first samples suffered from high variance in sheet resistance presumably because of surface roughness, the amount of ink per surface area was chosen to be increased. However, image resolution could not be increased because 1270 dpi already caused some flooding in printed patterns. Therefore ink amount per surface area was increased by using a lower resolution, but printing two layers with it. As described in Chapter 5.1, resolution of 1016 dpi was the smallest resolution, which produced continuous ink coverage in a single layer and with two layers deposited ink amount was approximately 27 % higher than with 1270 dpi resolution. Samples printed with these parameters showed significantly narrower distribution of sheet resistance and the average

value was a little over 20 mΩ/□, as can be seen in Figure 31. This very low variance in sheet resistance was considered to be caused by thicker and more homogenous structure of printed patterns.

Next samples for sheet resistance measurement were printed with iTi XY MDS 2.0 pilot scale inkjet printer. Because of the bigger nominal drop size, the printing parameters had to be optimized again for printability. Continuous structures were successfully printed with resolution of 700 dpi, which is nominally fairly close to 1270 dpi resolution with DMP-2831, as already explained in Chapter 5.1.3. The results of sheet resistance measurements were also similar to the first results with DMP-2831, but the standard deviation of results was smaller and the average value of sheet resistance was lower. Since sheet resistance variation was effectively minimized with DMP-2831 by increasing amount of deposited ink, next samples with iTi XY MDS 2.0 were printed with 800 dpi resolution. These samples showed significantly narrower sheet resistance distribution as can be seen in Figure 31, but the results were not as good as seen before with DMP-2831. Although deposited ink amount per surface area was nominally almost the same, printed structures were not as homogenous because of different deposition process, which is most probably the reason for slightly higher sheet resistances.

Finally image masking algorithm described in Chapter 5.1 was introduced to speed up printing process and the amount of ink also increased a little since the algorithm produces an ink amount equal to approximately 830 dpi resolution. As expected, samples printed with this algorithm showed lower sheet resistances with less variation than with 800 dpi resolution. Results were still not as good as samples printed with DMP-2831, but it was clear that this amount of ink was sufficient to overcome the sheet resistance variation due to surface roughness and further improvement with same film thickness would require better ink or improved sintering process. For comparison, sheet resistance of bulk silver with 1 µm film thickness would be approximately 16 mΩ/□ and average sheet resistance with these printing parameters was 25.8 mΩ/□. However, the resistivity of sintered nanoparticles is typically at least 1.5 – 2 times higher than bulk material resistivity [13]. The specifications of Harima NPS-JL shows resistivity of $6 \cdot 10^{-6}$ Ω/cm, when it is sintered at recommended temperature of 120 °C and resistivity of approximately $4 \cdot 10^{-6}$ Ω/cm, when it is sintered at temperature of 150 °C or above [23]. Placing these resistivity values and measured sheet resistance 25.8 mΩ/□ in Equation (8) gives an estimated thickness ranging from 1.6 µm to 2.3 µm for these printed structures. If the printed patterns are assumed to have resistivity of $4 \cdot 10^{-6}$ Ω/cm, the surface morphology of printed ink and substrate is still quite rough and therefore the actual film thickness was estimated to be approximately 2 µm. The use of introduced masking algorithm was considered to be the best option in viewpoints of printability and also electrical performance.

Sheet resistance measurements were also performed with printed samples on silicone rubber, but without any results. The reason for failed measurements was that contacting printed conductors with 4-point probe station turned out to be very challenging without piercing contact needles through the printed silver film and thus destroying

samples. Although thermoplastic polyurethane and silicone rubber are both relatively soft materials, the film thickness of silicone rubber samples was tenfold compared to thermoplastic polyurethane samples. Therefore contacting conductors on TPU was possible with the aid of a rigid backing plate, but thicker layer of soft material, silicone rubber in this case, deteriorated the mechanical support offered by rigid backing plate.

5.3 Mechanical and Electromechanical Performance

Mechanical performance of printed samples was evaluated after good printability was achieved on both substrate materials with the chosen ink. First, adhesion between ink and substrate material was tested with a simple scratch test. Sample patterns shown in Figure 16 were printed and strain properties were measured with custom made test bench described in Chapter 4.3.

5.3.1 Adhesion

Adhesion between ink and substrate material was evaluated simply by scratching printed patterns with the tip of a mechanical pencil. Test was performed by holding mechanical pencil in an angle of approximately 45°, pressing the tip against sample surface and sliding it across printed patterns several times with constant velocity. All tested samples were placed side by side so that pressure against the surface of every sample could be kept as same as humanely possible. Figure 32 illustrates the test setup with a single sample.

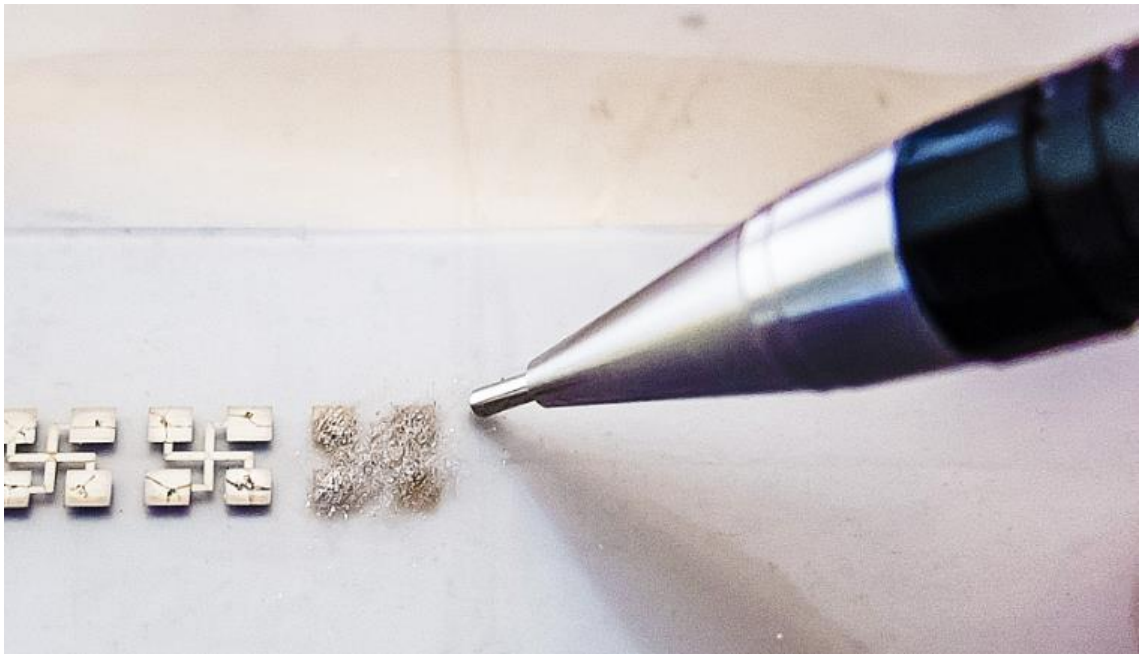

Figure 32. *Scratch test for testing adhesion between ink and substrate material.*

Patterns that were used for adhesion testing were the same patterns, which were printed for sheet resistance measurements. Adhesion was tested on both chosen substrate materials. Results were analyzed visually and compared to known good ink-substrate pair, which was Harima NPS-JL ink and PEN film as a substrate. Figure 33 shows microscope images taken from scratched samples.

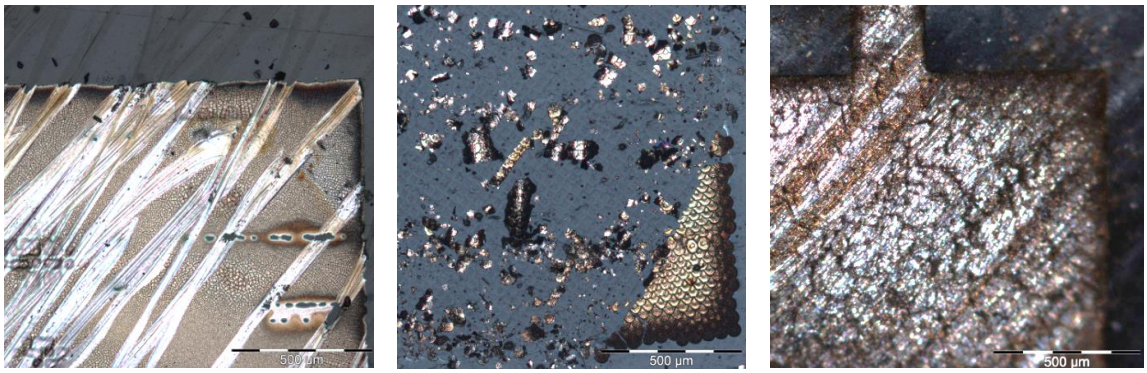

Figure 33. *Microscope images of scratched samples. Substrate on the left is PEN, the middle one is silicone rubber and on the right is TPU. All samples are scratched roughly in the same direction.*

As can be seen in Figure 33, scratching has a clear visible effect on sintered silver ink on PEN film, but ink stays firmly attached to the substrate. On silicone rubber scratching has more radical consequences as the sintered ink completely detaches from substrate, which is a clear indication that adhesion is far worse than in PEN samples. However, on TPU scratching has less pronounced effects than on PEN, which means that adhesion between ink and substrate is on good level. It must also be taken into account that this test tells very little about the actual adhesion and can be used only for rough comparison between samples.

5.3.2 Resistance in Linear Strain

Samples for strain testing were printed with iTi XY MDS 2.0 using image masking algorithm, which produces ink amount equal to resolution of 830 dpi, and sintering was performed in convection oven at temperature 150 °C for 60 minutes. Printed pattern is shown in Figure 16 with the exception of different trace widths between rectangular contact pads. Four types of samples were manufactured for strain testing with different substrate materials, deposition methods and trace widths. Thickness of printed conductors was estimated based on measured sheet resistance as described in Chapter 5.2. Manufactured samples are listed in Table 6.

Table 6. *Different sample types manufactured for strain testing.*

Property	**Test case 1**	**Test case 2**	**Test case 3**	**Test case 4**
Substrate material	Silicone rubber	TPU	TPU	TPU
Conductor material	Silver	Silver	Silver	Silver
Deposition method	Inkjet	Inkjet	Inkjet	Evaporation
Length	61 mm	61 mm	61 mm	61 mm
Trace width	1 mm	1 mm	100 µm	1mm
Thickness (approx..)	2 µm	2 µm	2 µm	50 nm

Measurement wires with diameter of 255 µm (30 AWG) were attached to samples' contact pads with isotropic conductive adhesive, Creative 124-08C, which was initially cured in convection oven at temperature 120 °C for 15 minutes. However, it was observed that because TPU softens at high temperatures, film ruptured around the outline of conductive adhesive. Therefore curing temperature was decreased to 80 °C and curing time was increased to 90 minutes, which enabled successful wire attachment.

Attaching samples to the test bench so that all lines remained operational proved to be a bit of a challenge, which was the first indication of a modest durability. Due to the low adhesion of silicone rubber, which was observed in Chapter 5.3.1, all samples with silicone rubber as substrate (test case 1) broke before any measurements could be done. Although adhesion on TPU is significantly better, samples with trace width 100 µm (test case 3) also proved to be so fragile, that only one printed line was successfully tested. It was observed that the 100 µm line broke almost immediately as strain increased, but its conductivity restored when strain was released although it had been stretched by 5 %. Peak strain in the first test run was approximately 0.31 % of initial length, which means only 12 points of measurement data with 15 µm movement resolution of the test bench. In order to achieve better characterization of the sample's resistance behavior in linear strain, the line was measured 10 times. The average of those results is shown in Figure 34.

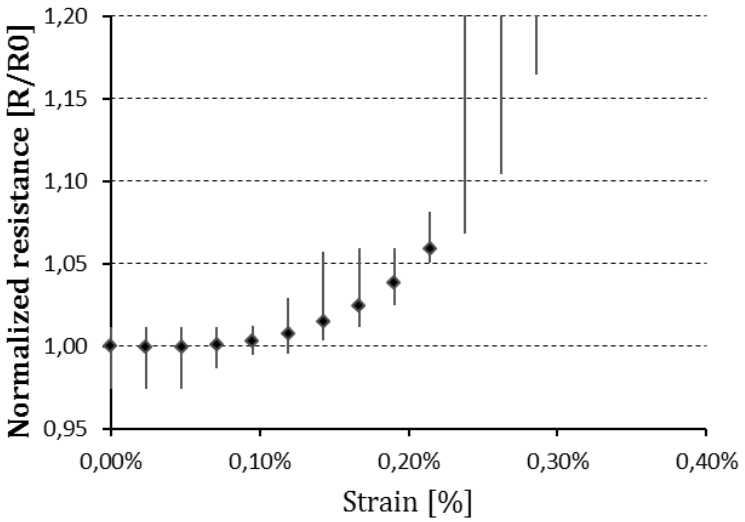

Figure 34. *Normalized resistance of 100 µm wide trace on TPU during linear strain. Data points are average of 10 measurements and vertical lines illustrate maximum and minimum values.*

Following test runs showed a bit lower peak strain than the first test run and the average peak strain in 10 test runs was approximately 0.24 %. According to Equation (5) minimum bending radius of 50 µm thick TPU film with printed conductors' peak strain of 0.24 % can be calculated to be:

$$r_{min} = \frac{50 \cdot 10^{-6}\, m/2.4 \cdot 10^{-3} - 50 \cdot 10^{-6} m}{2} = 10.39 \cdot 10^{-3} m \quad (15)$$

Although Equation (5) assumes the whole material homogenous, which in this case it is not, this calculation gives a rough estimate, since results are distorted towards the safe side due to stiffness of printed conductors. This calculated minimum bending strain of 10.39 mm is still explanatory for the fragility of these conductors, because TPU film itself is so soft and flexible that such bending radius is easily inflicted unless special care is taken to keep film flattened. Even the slightest bending caused by measurement wires combined with the sharp edge of rigid adhesive can be enough to cause smaller bending radius than the calculated minimum value. Because measured peak strain was too small for the sample to be even considered as stretchable, no reasonable strain could be chosen for cyclic strain testing. Based on the observed restoring phenomenon of conductivity when strain is released, cyclic testing was focused on analysis of this phenomenon as will be explained in Chapter 5.3.3.

The next tested samples were printed lines with 1 mm trace width on TPU (test case 2). These samples had notably higher survival rate during test bench attachment, which was partly due to greater care that was taken in handling. In the first test run samples showed a lot of variation in durability and some traces even regained conductivity for a while after breaking at some point. Some of the variation was identified to be caused by uneven tension i.e. samples' initial flatness. The smallest observed peak

strain was 0.27 %, the highest 1.50 % and the average was 1.00 % with standard deviation, σ, of 0.42 percentage point. The highest measured resistance at peak strain was over 12 times higher than the initial resistance of the trace in question. For better characterization of resistance in linear strain with this trace width average values of every measurement point were calculated and are shown in Figure 35.

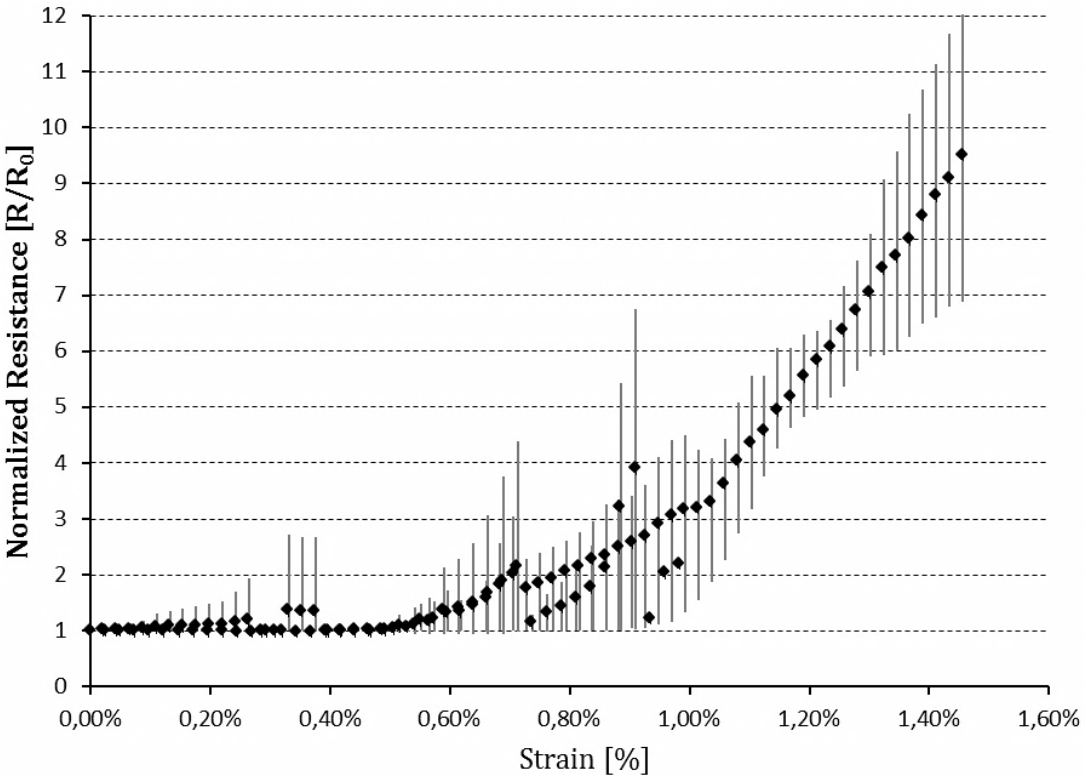

Figure 35. *Normalized resistance of 1 mm wide traces on TPU during linear strain. Data points are averaged from all measured values and the vertical lines illustrate maximum and minimum values. Infinite values in measurement data were ignored to enable calculation of averages. All traces were considered broken after the last data point.*

Interestingly traces showed notable hysteresis when the strain was decreased. For example trace, which had the smallest peak strain, 0.27 %, regained its conductivity at strain of 1.15 % and trace, which had the highest peak strain, 1.50 %, regained its conductivity at strain of 3.18 % with resistance reaching up to 20 times the initial resistance. Resistances were generally smaller in decreasing strain than in the increasing strain at the same strain values, but resistances did not reach the initial values at relaxed state. However, the relaxed state resistances after first test run had only increased by 15.9 % on average with standard deviation of 10.5 percentage points. In the following test runs samples showed more monotonic, but steeper strain-resistance curve. The hysteresis phenomenon was smaller, but still noticeable. Difference between the first and the second test run was much more prominent than differences between second and following test runs. Similarly as before, minimum bending radius with the observed average peak strain of 1.00 % can be calculated to be:

$$r_{min} = \frac{50 \cdot 10^{-6}\, m/1.00 \cdot 10^{-2} - 50 \cdot 10^{-6} m}{2} = 2.475 \cdot 10^{-3} m \quad (16)$$

This minimum bending radius of approximately 2.5 mm also explains the better survivability of samples during handling and attaching to test bench and it also means that these samples with 1 mm trace width could probably conform to all shapes of e.g. human body, but the conductivity would be intermittent if any stretching occurs.

Behavior of printed conductors under tensile strain was further analyzed visually with the aid of microscope. It was observed that clearly visible lateral cracks form during stretching along the whole length of tested traces. Crack formation is relatively sparse and distribution seems random, which can be seen in Figure 36A.

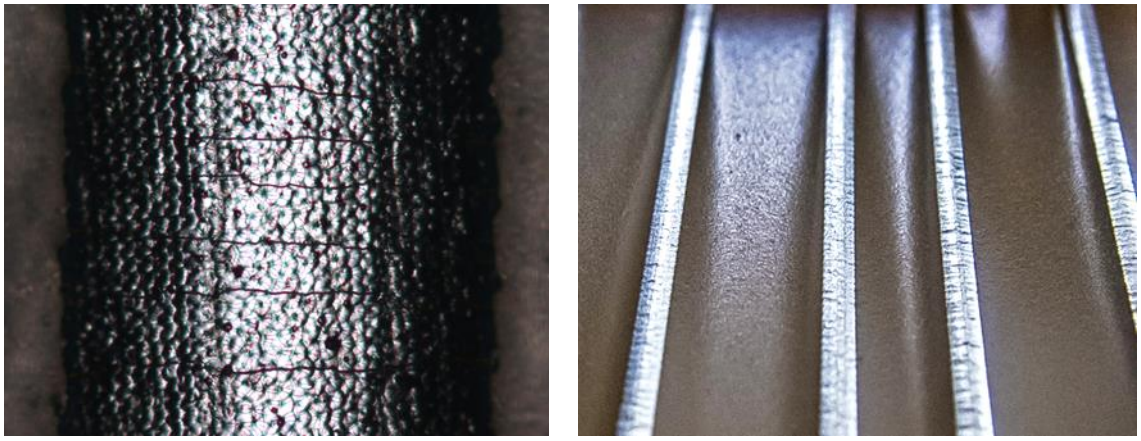

(A) **(B)**

Figure 36. *Microscope image (A) and photo (B) of printed 1 mm wide traces in strain.*

Lateral cracks form relatively straight through printed traces and effectively break the conductive path without forming a percolating conductive network, which has been observed [76] with thin gold films. Significantly different strain-resistance behavior of samples in increasing and decreasing strain on the first test run is however explained by this crack formation; on the first time as strain increases, cracks begin to form gradually along the length of conductors, but as strain is decreased multiple cracks exist in the structure and the amount of strain is distributed among them. Therefore with more existing cracks the total strain can be higher while local strain in a single crack is lower, which enables conductive path to form with higher strains than with a single existing crack. Figure 36B shows the effect of Poisson's ratio mismatch between substrate material and conductor material. Substrate film contracts notably in directions perpendicular to direction of strain, but this effect is weaker in conductor material, which causes substrate material to squeeze conductors so that conductors become curved around the axis of strain.

Lastly, 1 mm wide traces with were manufactured by evaporating silver on TPU (test case 4). Thickness of evaporated conductors was approximately 50 nm, which is less than the surface roughness of TPU film and therefore the surface structure of the film is still visible in visual inspection unlike with thicker conductive ink. All manufactured traces survived handling and attachment to test bench. Averaged strain testing results of these traces are shown in Figure 37.

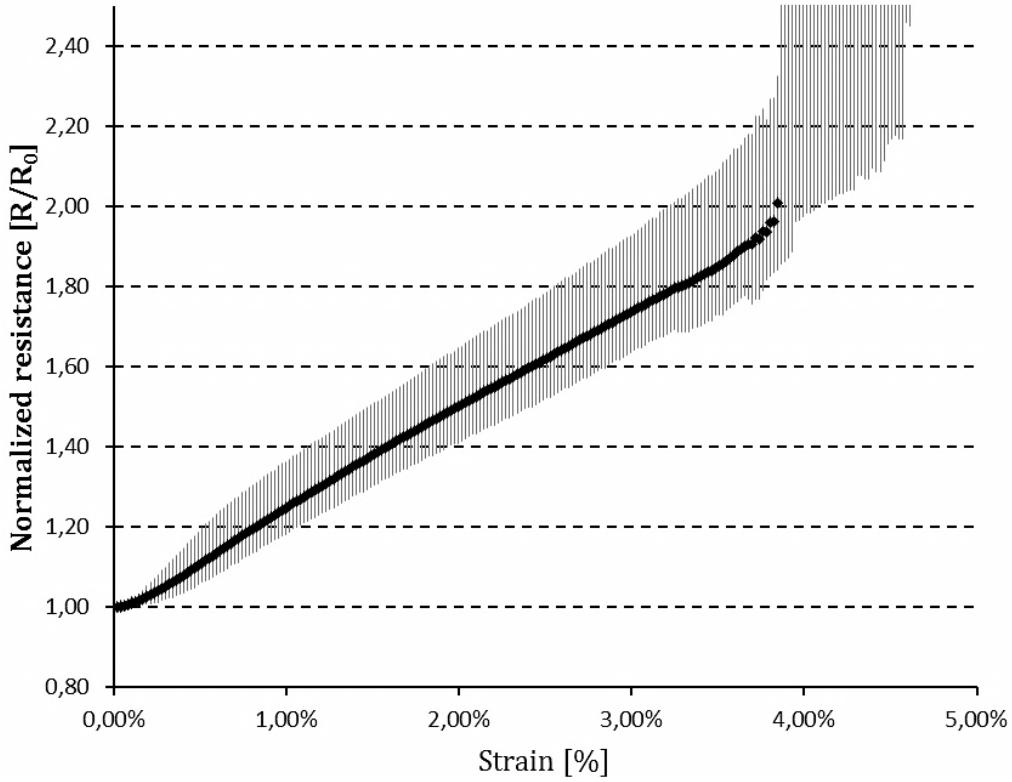

Figure 37. *Normalized resistance of 1 mm wide evaporated silver traces on TPU during linear strain. Data points are averaged from all measured values and the vertical lines illustrate maximum and minimum values.*

As can be seen in Figure 37, evaporated traces endured much greater strain with less increase in resistance when compared to printed samples. Average of highest measured strain of evaporated traces was 4.05 % with standard deviation of 0.29 percentage points. Just before losing conductivity the average resistance of conductors was only 2.16 times the initial resistance. Strain-resistance behavior of traces was very linear and more uniform than those manufactured by printing. Interestingly, at highest measured strain actual traces still remained intact, but conductivity was lost due to sudden rupture of TPU film, which meant that measurement wires were torn apart from the samples. Although thermoplastic polyurethane film can deform elastically much higher strains and the area around contact pads was stiffened with Kapton tape, sharp edge of conductive adhesive and rigid fixing of wires was enough to tear the film, which can be seen in Figure 38. Since samples were destroyed during testing, the actual peak strain of conductors and behavior in decreasing strain could not be measured.

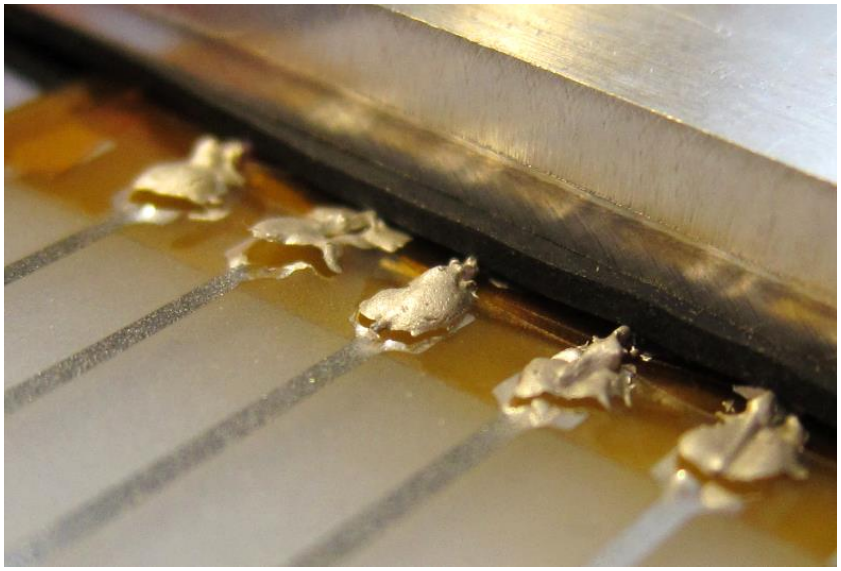

Figure 38. *Torn measurement wires' contact pads due to rupture of TPU film.*

Nevertheless, minimum bending radius with a strain of 4.05 % can be calculated to be:

$$r_{min} = \frac{50 \cdot 10^{-6}\, m/4.05 \cdot 10^{-2} - 50 \cdot 10^{-6} m}{2} = 5.923 \cdot 10^{-4} m \quad (17)$$

Evaporated 50 nm thick silver traces on TPU can therefore be safely bended with a radius of at least 590 µm, but it is most probable that the minimum radius is even smaller, since the actual peak strain is unknown.

As a conclusion, 4 different sample types were manufactured; one of which could not be tested due to fragility of samples. All manufactured samples on TPU substrate were tested with custom made test bench and peak strain the results for printed samples were notably lower than evaporated samples. Based on this, it was assumed that microcracking does not occur with approximately 2 µm thick printed conductors, which was also confirmed with visual analysis. Direct comparison to stress-strain behavior of bulk metal is not applicable since stress values were not measured, but based on the resistance values it is probable that sintered nanoparticle silver can withstand larger strains than bulk metal, as assumed. Evaporated silver conductors however showed similar results that have been reported in literature [76], which implies that also microcracking occurs respectively. It was suggested that cracks help to distribute the strain and therefore local strains remain smaller, which helps to maintain conductivity at larger strains. Based on the results shown here, smaller trace width results in smaller peak strain and thicker conductors inhibit cracking, which leads to more locally focused strain also resulting in smaller peak strains.

5.3.3 Cyclic Deformation

As stated in previous chapter, the peak strain of printed conductors on thermoplastic polyurethane film was too low to reasonably choose any appropriate strain level for cyclic testing, but conductors regained conductivity when strain was released. Therefore cyclic deformation testing was performed to analyze the lifetime of conductors in such use case where conductivity is only needed in relaxed state, but interconnects can mechanically conform to dynamic environment. Since the printed samples on silicone rubber and evaporated samples on TPU were destroyed, cycling testing was performed with 100 µm and 1 mm wide printed conductors on TPU. Implementation of control software for test bench in cyclic testing is illustrated in Figure 39.

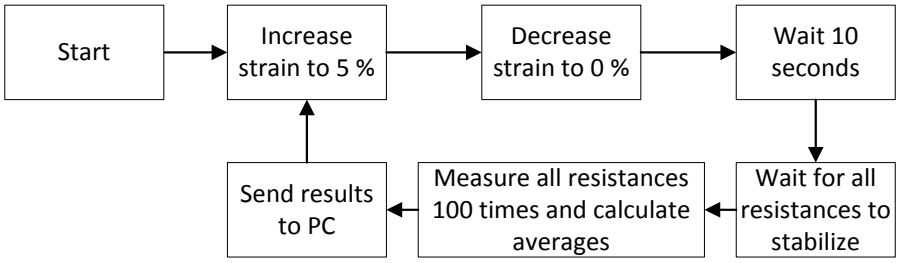

Figure 39. *Flowchart of software implementation for cyclic deformation testing.*

Results for cyclic testing are shown in Figure 40. Multiple traces with 1 mm width were measured, but only one 100 µm wide trace due to difficulties with sample attachment. Therefore results of 100 µm wide trace are not statistically as comprehensive as results of 1 mm wide traces, which limits their comparison.

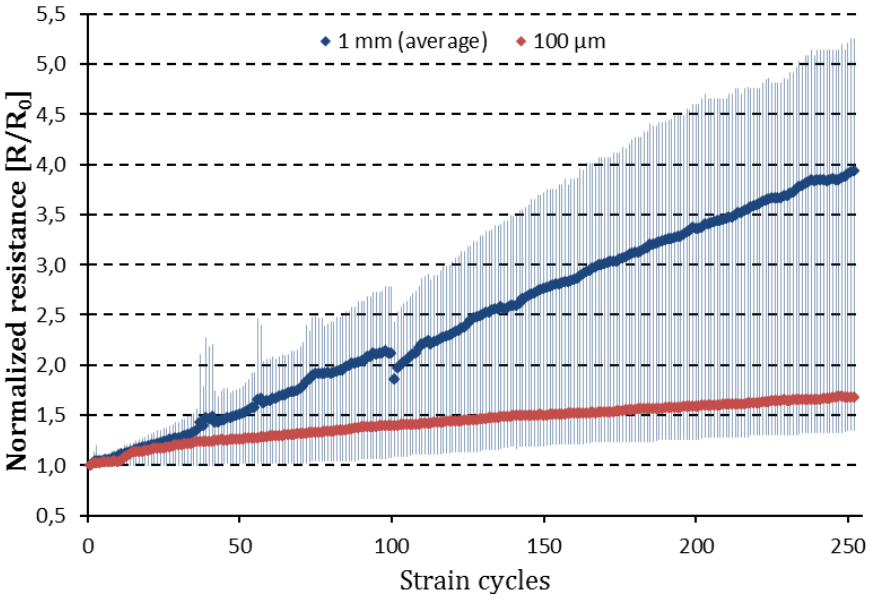

Figure 40. *Normalized resistance of 1 mm (blue) and 100 µm (red) traces in relaxed state after a number of 5 % strain cycles. Data points for 1 mm traces are averages and blue vertical lines illustrate minimum and maximum values.*

As can be seen in Figure 40, samples' resistance in relaxed state has risen by a percentage ranging from 35 % to 425 % after 250 strain cycles. Average resistance of 1 mm wide traces was 3.93 times initial resistance with standard deviation of 1.41. Resistance of 100 µm trace was 1.68 times its initial resistance after 250 cycles, which is still in the range of variation seen with 1 mm traces.

After cycling was stopped, it was seen that resistance of samples continued to decrease slowly, which was assumed to be caused by substrate material's time dependent recovery i.e. viscoelastic behavior. As suspected, rate of resistance change decreased continuously with time and after one hour the resistance values were considered to be stabilized. These final values were considerably lower than the values at the end of cycling test run, which gives a reason to suspect that results are highly dependent on the timeframe in which the resistance is measured after stretching. Average resistance of 1 mm wide traces after one hour was 1.30 times the initial resistance with standard deviation of 0.19 and resistance of 100 µm trace was 1.47 times the initial resistance. If it is assumed that the underlying failure mechanism causes damage to conductors at a rate represented by these one-hour-values after 250 cycles, it would take more than 500 cycles to even double the resistance of conductors.

5.4 Demonstrator Device Comparison

The feasibility of inkjet-printed circuits on stretchable substrates was evaluated by manufacturing demonstrator design described in Chapter 2.4.2 on thermoplastic polyurethane film. Demonstrator design contains e.g. SoC-IC in a wafer level chip scale package, WLCSP, with ball pitch of 400 µm and surface-mount passive components with sizes 0201, 0402 and 0603. Smallest trace widths and gaps are in the range of 75 – 100 µm and size of the whole layout is approximately 45 mm by 22 mm. Circuits were printed with iTi XY MDS 2.0 using Harima NPS-JL silver nanoparticle ink. Printing parameters were:

- Nominal drop volume 30 pl
- Nozzle plate temperature 34 °C
- Vacuum plate temperature 70 °C
- Printing speed 80 mm/s
- Droplet ejection voltage 55 V
- Image resolution 5050 dpi
- Masking algorithm for ink amount equal to 830 dpi

Substrate film was pre-stretched approximately 10% and attached to a rigid aluminum plate with Kapton tape. Printed circuits were sintered in convection oven at temperature 150 °C for 60 minutes. At first, pre-stretch was released after sintering, but it was observed that it changed the circuit dimensions so that pads for WLCSP balls were misa-

ligned. Therefore with next circuits pre-stretch was kept until component assembly was finished. Components were attached with isotropic conductive adhesive Creative 124-08C, which was applied with pneumatic hand-held dispenser, and components were placed with Finetech Fineplacer. Conductive adhesive was cured in convection oven at temperature 80 °C for 90 minutes and after that Epotek OE121 epoxy underfill was applied to further secure component attachment. Epoxy underfill was also cured in convection oven at 80 °C for 60 minutes and after that at room temperature for 24 hours.

After device was fully assembled and detached from aluminum carrier plate, it was observed from reverse side that substrate film had warped during component assembly. This was considered to be caused by epoxy underfill, since such warping had not occurred with just conductive adhesive. Figure 41 shows fully assembled device on skin contact. It can be easily observed that demonstrator device on stretchable substrate is much more conformable to irregular shapes of human body than device on flexible substrate.

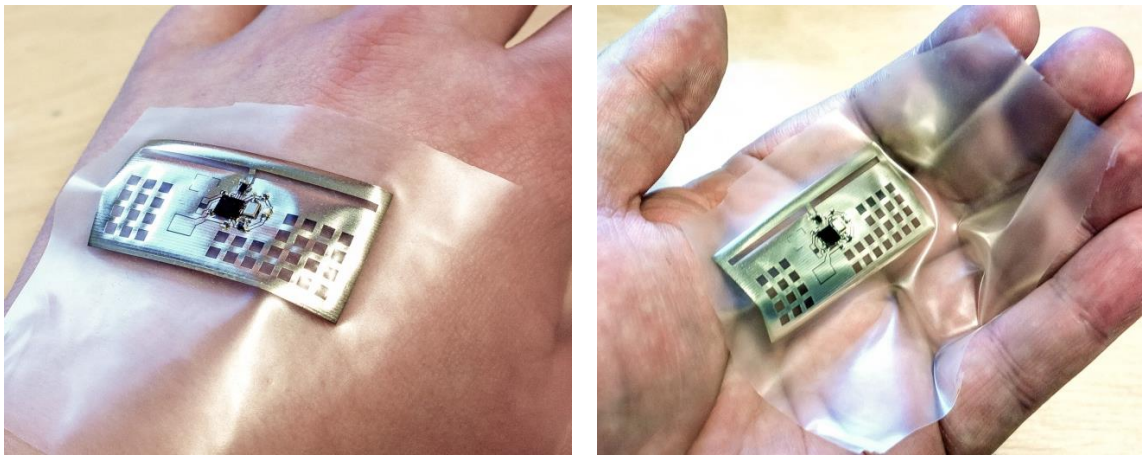

(A) **(B)**

Figure 41. *Fully assembled demonstrator device on (A) convex and (B) concave surface of human body.*

Programming of assembled device was tried with same custom-built fixture as flexible demonstrator device had been programmed with, but without success. Closer analysis revealed that one of programming traces had been cracked in the proximity of SoC-IC edge. Programming was tried with other manufactured devices, but they were also defective. Due to this observation it was assumed that warping caused by epoxy underfill inflicts significant stresses to printed traces and consequently causes crack formation. Substrate warping around components is clearly visible from the backside of device, as can be seen in Figure 42.

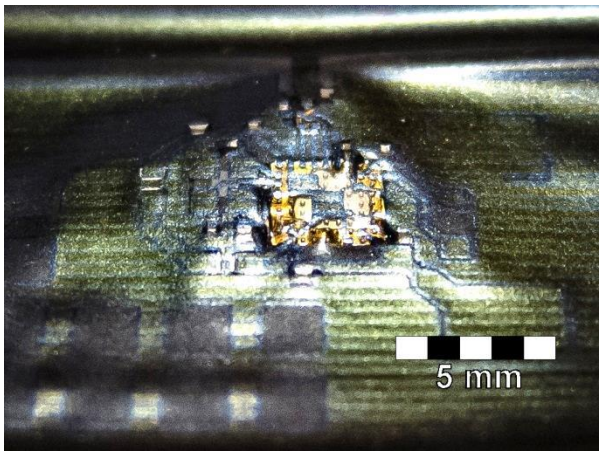

Figure 42. *Backside of demonstrator device component assembly.*

This same warping phenomenon was not seen with devices on PEN film, since more rigid substrate offers significantly better mechanical support for printed traces and possibly better chemical resistance. For further development of stretchable demonstrator device is it suggested, that epoxy underfill is replaced with more compatible substance, such as polyurethane based adhesive, and component area could also be reinforced with a stiff backing plate. Local reinforcing of the thinnest traces could also be one option worth researching. This could be for example done by printing a polymer dielectric layer before the actual circuits are printed or by using a thin layer of polyimide, which can be spin-coated and patterned with UV-light.

6 CONCLUSIONS AND PROPOSALS FOR FUTURE WORK

In this thesis feasibility of inkjet printing in manufacturing of stretchable interconnects has been evaluated through literature review and experimental analysis. In Chapter 2 basic principles of printed electronics and advantages of inkjet technology compared to conventional methods and other printing methods are presented. Low process temperatures, low materials waste and contactless deposition method enable a wide variety of novel materials to be used, which makes inkjet technology attractive option for conventional manufacturing processes. Digitally controlled process enables fast and cost-effective manufacturing of prototypes and small production batches, but inkjet technology can also be scaled up to mass production. Feasibility of inkjet technology in manufacturing of flexible electronics is demonstrated in this thesis by successfully manufacturing highly integrated Bluetooth –device on flexible PEN film.

In Chapter 3 basic methods for manufacturing of stretchable electronics are reviewed along with applications enabled by stretchability. Challenges involved in using inkjet technology to manufacture stretchable interconnects are estimated through material properties analysis and comparison to manufacturing of flexible circuits. Stretchable electronics is such new class of electronics that most of the activities are currently in academic laboratories. Stretchability can enable a wide range of applications – most of them related to wearable or near-body applications. Advantages of inkjet technology in manufacturing of stretchable electronics are the same as in manufacturing of flexible electronics, but especially benefits from contactless deposition method are more pronounced.

Experimental methods for evaluating inkjet printing in manufacturing of stretchable interconnects are presented in Chapter 4, which is followed by results of these experiments in Chapter 5. Good printing results are achieved with silver nanoparticle ink on two different elastomers, silicone rubber and thermoplastic polyurethane, using two different inkjet printers. However, silicone rubber is considered as more challenging substrate due to lack of adhesion and greater softness. Therefore it is suggested that silicone rubber needs further research in order to be used as a substrate for inkjet printing. Hydrophobic nature of both substrate materials was seen as a challenge when larger continuous areas are printed. Therefore a surface treatment, such as UV-ozone, is needed to enable good printing quality, but this has a negative effect on printing accuracy of finer details. Alternative method for printing fine details and large areas simultaneously on hydrophobic surface is presented in a form printing sequence modification, which is achieved with an image masking algorithm. It was also observed that challenges caused

by thermal expansion mismatch between substrate and nanometal can be balanced out with sufficient pre-stretch during manufacturing process. Conductors printed with optimized process parameters on thermoplastic polyurethane had approximate sheet resistance 25.8 mΩ/□ with low variance, which can be considered as good value.

A strain testing system was designed and built along with the software needed for control unit to enable automatic measurement operation. Samples with straight 1 mm and 100 µm wide lines were printed on thermoplastic polyurethane and measured peak strains were on average 1.0% and 0.24% respectively. Evaporated 1 mm wide silver lines with 50 nm thickness were also tested as a reference, but peak strain could not be determined since measurement contacts were torn off substrate film at strain of 4.05%. Evaporated 50 nm gold films have been reported [59; 76] to exhibit microcracking during stretching, which enables peak strains of over 10%. Considering strain testing results for printed conductors, it is obvious that similar microcracking does not occur as assumed. Although actual peak strain could not be determined with evaporated silver conductors, measured strain-resistance curve was similar as reported with gold films, which suggests that microcracking occurs correspondingly. A recent article by Kim *et al.* [54] presented strain testing results for screen printed silver nanoparticle conductors on thermoplastic polyurethane. Measured peak strains for straight line were approximately same as measured in this thesis for inkjet-printed straight lines. Kim *et al.* had also tested other planar interconnect geometries and the best results of approximately 8% peak strain was achieved with horseshoe shaped patterning. It is therefore presumable that similar results can be achieved with inkjet-printed conductors if horseshoe geometry is utilized.

In addition to peak strain measurements of inkjet-printed conductors, cyclic strain testing was also performed. It was observed that even though inkjet-printed conductors fractured at low strains, conductivity was almost fully restored when strain was released. Printed conductors were exposed to 5% strain for over 250 cycles and conductivity was maintained in relaxed state. It was observed that conductors exhibit time-dependent recovery after stretching and the resistance values continued to decrease for approximately one hour. Final resistance values for 1 mm and 100 µm wide lines after 250 strain cycles and one hour relaxing period had increased from initial values by factors 1.30 and 1.47, respectively.

Same demonstrator device design, which was manufactured on flexible substrate in Chapter 2, was manufactured on thermoplastic polyurethane substrate. Main observation was that epoxy underfill is not compatible with thermoplastic polyurethane substrate and it causes warping of substrate. This warping combined with fragility of printed conductors caused cracked conductors and therefore operational device could not be manufactured during this thesis.

For future work it is proposed that stretchability of printed conductors is researched with different in-plane patterned geometries, but also with micropatterned substrate surfaces. Additionally these highly conductive nanometal conductors could be combined with intrinsically stretchable conductive material, such as conductive polymer. This

would enable maintaining high conductivity and achieving sufficient peak strain since conductive polymer would offer conductive path over cracks formed in metal layer. For further work on demonstrator device it is proposed that optional materials for epoxy underfill are studied to avoid incompatibility problems. Utilizing more elastic component attachment materials and use of stiffener plates under component assemblies also deserve further attention. As such, printed conductors on stretchable substrate presented in this thesis are not suitable for typical stretchable applications. The ease of manufacturing and relatively low cost of these conductors may still make them an attractive option for some applications. Proposals for these applications are that critical features are manufactured on flexible islands and these islands are connected with inkjet-printed stretchable conductors using a robust serial bus protocol, such as 1-wire, I^2C or CAN, with some built-in redundancy and software algorithms for recognizing conductive/non-conductive interconnections.

REFERENCES

[1] Fjelstad, J. Flexible Circuit Technology 4th Edition. Seaside 2006, BR Publishing, Inc. 613 p.

[2] Koskinen, S., Pykari, L., & Mantysalo, M. Inkjet printed flexible user interface module. Proceedings of 62nd Electronic Components and Technology Conference (ECTC), San Diego, CA, USA, May 29 – Jun. 1, 2012. IEEE. pp. 1009-1014.

[3] Someya, T. Stretchable Electronics. Weinheim 2013, Wiley-VCH Verlag GmbH & Co. KGaA. 484 p.

[4] Gilleo, K. The Circuit Cetennial. [WWW] West Greenwich, ET-Trends LLC. 2003. [Accessed on 2.1.2014] Available at: http://www.et-trends.com/files/Circuits_100Years.pdf

[5] Khaleel, H., Al-Rizzo, H. & Abbosh, A. Design, Fabrication, and Testing of Flexible Antennas. In: Kishk, A. (ed.). Advancement in Microstrip Antennas with Recent Applications. 2013, InTech. DOI: 10.5772/3385

[6] Halonen, E., Kaija, K., Mantysalo, M., Kemppainen, A., Osterbacka, R., & Bjorklund, N. Evaluation of printed electronics manufacturing line with sensor platform application. In Microelectronics and Packaging Conference, Rimini, June 15-18, 2009. EMPC 2009. IEEE. pp. 1-8.

[7] Halonen, E. Integration of Inkjet-Printing and Processing into Manufacturing for Flexible Electronics. Dissertation. Tampere 2013. Tampere University of Technology. Publication 1179. 53 p.

[8] Pekkanen, V. Characteristics of Inkjet Material Deposition for Microelectronics Packaging. Dissertation. Tampere 2011. Tampere University of Technology. Publication 959. 60 p.

[9] Lin, L. & Bai, X. Ink-jet technology: status quo and future – relevance to surface coatings. Pigment & Resin Technology 33(2004)4, pp. 238-244. DOI: 10.1108/03699420410546926

[10] Le, H. P. Progress and trends in ink-jet printing technology. Journal of Imaging Science and Technology 42(1998)1, pp. 49-62. Available at http://www.imaging.org/ist/resources/tutorials/inkjet.cfm [Accessed on 2.1.2014]

[11] Hon, K.K.B., Li, L. & Hutchings, I.M. Direct writing technology—Advances and developments. CIRP Annals - Manufacturing Technology 57(2008)2, pp. 601-620. DOI: 10.1016/j.cirp.2008.09.006.

[12] Xu, B. Inkjet Printing of Silver for Direct Write Applications. Dissertation. Manchester 2010. University of Manchester, School of Materials. 169 p. Available at: https://www.escholar.manchester.ac.uk/item/?pid=uk-ac-man-scw:94655 [Accessed on 2.1.2014]

[13] Kamyshny, A., Steinke, J., & Magdassi, S. Metal-based inkjet inks for printed electronics. Open Applied Physics Journal 4(2011), pp. 19-36. Available at: http://www.benthamscience.com/open/toapj/articles/V004/SI0001TOAPJ/19TOAPJ.pdf [Accessed on 2.1.2014]

[14] Buffat, P. & Borel, J. P. Size effect on the melting temperature of gold particles. Physical Review A 13(1976)6, pp. 2287-2298.

[15] Fuller, S. B., Wilhelm, E. J., & Jacobson, J. M. Ink-jet printed nanoparticle microelectromechanical systems. Microelectromechanical Systems, Journal of 11(2002)1, pp. 54-60. DOI: 10.1109/84.982863

[16] Laakso, P., Ruotsalainen, S., Halonen, E., Mäntysalo, M., & Kemppainen, A. Sintering of printed nanoparticle structures using laser treatment. In: Ostendorf, A., Graf, T., Petring, D. & Otto, A.(eds.). Proceedings of the Fifth International WLT-Conference on Lasers in Manufacturing, Munich, Germany, June 15-18, 2009. LIM 2009. pp. 1360-1366.

[17] Perelaer, J., de Gans, B. J., & Schubert, U. S. Ink-jet Printing and Microwave Sintering of Conductive Silver Tracks. Advanced materials 18(2006)16, pp. 2101-2104. DOI: 10.1002/adma.200502422

[18] Reinhold, I., Hendriks, C. E., Eckardt, R., Kranenburg, J. M., Perelaer, J., Baumann, R. R., & Schubert, U. S. Argon plasma sintering of inkjet printed silver tracks on polymer substrates. Journal of Materials Chemistry 19(2009)21, pp. 3384-3388. DOI: 10.1039/B823329B

[19] Allen, M. L., Aronniemi, M., Mattila, T., Alastalo, A., Ojanperä, K., Suhonen, M. & Seppä, H. Electrical sintering of nanoparticle structures. Nanotechnology 19(2008)17. DOI: 10.1088/0957-4484/19/17/175201

[20] Magdassi, S., Grouchko, M., Berezin, O., & Kamyshny, A. Triggering the sintering of silver nanoparticles at room temperature. ACS nano 4(2010)4, pp. 1943-1948. DOI: 10.1021/nn901868t

[21] Perelaer, J., de Laat, A. W., Hendriks, C. E., & Schubert, U. S. Inkjet-printed silver tracks: low temperature curing and thermal stability investigation. Journal of Materials Chemistry 18(2008)27, pp. 3209-3215. DOI: 10.1039/B720032C

[22] Tekin, E., Smith, P. J., & Schubert, U. S. Inkjet printing as a deposition and patterning tool for polymers and inorganic particles. Soft Matter 4(2008)4, pp. 703-713. DOI: 10.1039/B711984D

[23] Nano Paste®Series datasheet [WWW]. Harima Chemicals Group. [Accessed on 2.1.2014] Available at: http://www.harima.co.jp/en/products/electronics/pdf/E_P21.pdf

[24] Metalon Conductive Inks [WWW]. Novacentrix®. [Accessed on 10.12.2013]. Available at: http://www.novacentrix.com/products/metalon-inks

[25] Conductive Metallic Inks [WWW]. Applied Nanotech Holdings, Inc. [Accessed on 10.12.2013]. Available at: http://www.appliednanotech.net/Products/Nanoelectronics/conductive_inks.php

[26] Intrinsiq Materials, Our Products [WWW]. Intrinsiq Materials, Inc. [Accessed on 10.12.2013]. Available at: http://intrinsiqmaterials.com/our-products/

[27] Soltman, D., & Subramanian, V. Inkjet-printed line morphologies and temperature control of the coffee ring effect. Langmuir 24(2008)5, pp. 2224-2231. DOI: 10.1021/la7026847

[28] Pekkanen, V., Mäntysalo, M., Kaija, K., Mansikkamäki, P., Kunnari, E., Laine, K., Niittynen, J., Koskinen, S., Halonen, E. & Caglar, U. (2010). Utilizing inkjet printing to fabricate electrical interconnections in a system-in-package. Microelectronic Engineering 87(2010)11, pp. 2382-2390. DOI: 10.1016/j.mee.2010.04.013

[29] Goldschmidt, A., & Streitberger, H. J. BASF handbook on basics of coating technology. Hannover 2003, Vincentz. 792 p.

[30] Oláh, A., Hillborg, H., & Vancso, G. J. Hydrophobic recovery of UV/ozone treated poly (dimethylsiloxane): adhesion studies by contact mechanics and mechanism of surface modification. Applied Surface Science 239(2005)3, pp. 410-423. DOI: 10.1016/j.apsusc.2004.06.005

[31] Ma, M., & Hill, R. M. Superhydrophobic surfaces. Current Opinion in Colloid & Interface Science 11(2006)4, pp. 193-202. DOI: 10.1016/j.cocis.2006.06.002

[32] 3M™ Novec™ 1720 Electronic Grade Coating datasheet [WWW] 3M. [Accessed on 2.1.2014]. Available at: http://multimedia.3m.com/mws/mediawebserver?mwsId=SSSSSuH8gc7nZxtUMxmZMY_1evUqe17zHvTSevTSeSSSSSS--&fn=prodinfo_nvcegc1720.pdf

[33] Jurvetson, S. Olympus Stylus [Photograph]. 2004. [Accessed on 19.12.2013]. Available at: http://www.flickr.com/photos/44124348109@N01/2265519

[34] Halonen, E., Halme, A., Karinsalo, T., Iso-Ketola, P., Mantysalo, M., & Makinen, R. Dynamic bending test analysis of inkjet-printed conductors on flexible substrates. In 62nd Electronic Components and Technology Conference (ECTC), San Diego, CA, USA, May 29 – Jun. 1, 2012. 2012, IEEE. pp. 80-85. DOI: 10.1109/ECTC.2012.6248810

[35] Yang, L., Rida, A., Vyas, R., & Tentzeris, M. M. RFID tag and RF structures on a paper substrate using inkjet-printing technology. IEEE Transactions on Microwave Theory and Techniques 55(2007)12, pp. 2894-2901. DOI: 10.1109/TMTT.2007.909886

[36] Wong, W. S., & Salleo, A. (Eds.). Flexible electronics: materials and applications. Vol. 11. New York 2009, Springer. 480 p.

[37] Choi, M. C., Kim, Y., & Ha, C. S. Polymers for flexible displays: from material selection to device applications. Progress in Polymer Science 33(2008)6, pp. 581-630. DOI: 10.1016/j.progpolymsci.2007.11.004

[38] High performance FR-4 for Multi-layered PWB [WWW] Mitsubishi Gas Chemical Company, Inc. [Accessed on 2.1.2014]. Available at: http://www.mgc.co.jp/eng/products/lm/btprint/lineup/fr4.html

[39] FR-4 Glass / Epoxy Phenolic datasheet [WWW]. Plastics International. [Accessed on 19.12.2013]. Available at: http://www.plasticsintl.com/datasheets/Phenolic_G10_FR4.pdf

[40] Weick, B. L., & Bhushan, B. Characterization of magnetic tapes and substrates. Magnetics, IEEE Transactions on 32(1996)4, pp. 3319-3322. DOI: 10.1109/20.508397

[41] Jagt, J. C., Beris, P. J. M., & Lijten, G. F. C. M. Electrically conductive adhesives: A prospective alternative for SMD soldering?. Components, Packaging, and Manufacturing Technology, Part B: Advanced Packaging, IEEE Transactions on 18(1995)2, pp. 292-298. DOI: 10.1109/96.386264

[42] Ogunjimi, A. O., Boyle, O., Whalley, D. C., & Williams, D. J. (1992). A review of the impact of conductive adhesive technology on interconnection. Journal of Electronics Manufacturing 2(1992)03, pp. 109-118. DOI: 10.1142/S0960313192000145

[43] nRF51822 [WWW] Nordic Semiconductor. [Accessed on 22.12.2013]. Available at: http://www.nordicsemi.com/eng/Products/Bluetooth-R-low-energy/nRF51822

[44] Sosin, S. Interconnect schemes for stretchable array-type microsystems. Dissertation. Delft 2011. Delft University of Technology. ISBN: 978-90-5335-390-5. 106 p.

[45] Mark, J. E., (ed.). Polymer Data Handbook. New York, 1999. Oxford University Press, Inc. 1012 p.

[46] Online Materials Information Resource – MatWeb [WWW] MatWeb, LLC. [Accessed on 26.12.2013] Available at: http://www.matweb.com

[47] Wargo, C. Characterization of Conductors for Printed Electronics. [WWW] PChem Associates, Inc. [Accessed on 2.1.2014] Available at: http://www.nanopchem.com/pdf/understanding.pdf

[48] Smith, D. R., & Fickett, F. R. Low-temperature properties of silver. Journal of Research of National Institute of Standards and Technology 100(1995)2, pp. 119-171. DOI: 10.6028/jres.100.012

[49] Roylance, David. 3.11 Mechanics of Materials, Fall 1999 [WWW] MIT OpenCourseWare: Massachusetts Institute of Technology. [Accessed on 19.8.2013]. Available at: http://ocw.mit.edu/courses/materials-science-and-engineering/3-11-mechanics-of-materials-fall-1999 License: Creative Commons BY-NC-SA

[50] Khaled, T. Calculation of Bend Radii from Tensile Elongation Data [WWW]. USA, Federal Aviation Admistration. 17.9.2003. [Accessed on 2.1.2014]. Available at: http://www.faa.gov/aircraft/air_cert/design_approvals/csta/publications/media/calc_bend_radii_tensile_elong_data.pdf

[51] Khang, D. Y., Jiang, H., Huang, Y., & Rogers, J. A. A stretchable form of single-crystal silicon for high-performance electronics on rubber substrates. Science, 311(2006)5758, pp. 208-212. DOI: 10.1126/science.1121401

[52] Jiang, H., Sun, Y., Rogers, J. A., & Huang, Y. Mechanics of precisely controlled thin film buckling on elastomeric substrate. Applied physics letters 90(2007)13, pp. 133119-133119-3. DOI: 10.1063/1.2719027

[53] Shin, G., Bae, M. Y., Lee, H. J., Hong, S. K., Yoon, C. H., Zi, G., Rogers, J. A. & Ha, J. S. (2011). SnO2 Nanowire Logic Devices on Deformable Nonplanar Substrates. ACS nano 5(2011)12, pp. 10009-10016. DOI: 10.1021/nn203790a

[54] Kim, K. S., Jung, K. H., & Jung, S. B. Design and fabrication of screen-printed silver circuits for stretchable electronics. Microelectronic Engineering (2013). http://dx.doi.org/10.1016/j.mee.2013.07.003

[55] Kim, D. H., & Rogers, J. A. Stretchable electronics: Materials strategies and devices. Advanced Materials, 20(2008)24, pp. 4887-4892. DOI: 10.1002/adma.200801788

[56] Rogers, J. A., Someya, T. & Huang, Y. Materials and mechanics for stretchable electronics. Science 327(2010)5973, pp. 1603-1607. DOI: 10.1126/science.1182383

[57] Park, C. W., Jung, S. W., Lim, S. C., Oh, J. Y., Na, B. S., Lee, S. S., Chu, H. Y. & Koo, J. B. Fabrication of well-controlled wavy metal interconnect structures on stress-free elastomeric substrates. Microelectronic Engineering 113(2014), pp. 55-60. DOI: 10.1016/j.mee.2013.07.012

[58] Graudejus, O., Görrn, P., & Wagner, S. (2010). Controlling the morphology of gold films on poly (dimethylsiloxane). ACS Applied Materials & Interfaces, 2(7), 1927-1933. http://dx.doi.org/10.1021/am1002537

[59] Lambricht, N., Pardoen, T., & Yunus, S. Giant stretchability of thin gold films on rough elastomeric substrates. Acta Materialia 61(2013), pp. 540–547. DOI: 10.1016/j.actamat.2012.10.001

[60] Robinson, A. P., Minev, I., Graz, I. M., & Lacour, S. P. Microstructured silicone substrate for printable and stretchable metallic films. Langmuir 27(2011)8, pp. 4279-4284. DOI: 10.1021/la103213n

[61] Sterken, T., Vanfleteren, J., Torfs, T., Op de Beeck, M., Bossuyt, F., & Van Hoof, C. Ultra-thin chip package (UTCP) and stretchable circuit technologies for wearable ECG system. In Engineering in Medicine and Biology Society, EMBC, 2011 Annual International Conference of the IEEE, Boston, MA, USA, Aug. 30 – Sept. 3, 2011. IEEE. pp. 6886-6889

[62] Ko, H. C., Stoykovich, M. P., Song, J., Malyarchuk, V., Choi, W. M., Yu, C. J., Geddes, J. B., Xiao, J., Wang, S., Huang, Y. & Rogers, J. A. A hemispherical electronic eye camera based on compressible silicon optoelectronics. Nature 454(2008)7205, pp. 748-753. DOI: 10.1038/nature07113

[63] Jablonski, M., Bossuyt, F., Vanfleteren, J., Vervust, T., & de Vries, H. Reliability of a stretchable interconnect utilizing terminated, in-plane meandered copper conductor. Microelectronics Reliability 53(2013), pp. 956–963. DOI: 10.1016/j.microrel.2013.04.002

[64] Kim, D. H., Lu, N., Ma, R., Kim, Y. S., Kim, R. H., Wang, S., Wu, J., Won, S. M., Tao, H., Islam, A., Yu, K. J., Kim, T., Chowdhury, R., Ying, M., Xu, L., Li, M., Chung, H. J., Keum, H., McCormick, M., Liu, P., Zhang, Y. W., Omenetto, F. G., Huang, Y., Coleman, T. & Rogers, J. A. Epidermal electronics. Science, 333(2011)6044, pp. 838-843. DOI: 10.1126/science.1206157

[65] MC10 | Extending human capabilities through stretchable electronics [WWW]. MC10 Inc. [Accessed on 30.12.2013]. Available at: http://www.mc10inc.com/

[66] Wereszczak, A. A., Vuono, D. J., Wang, H., Ferber, M. K., & Liang, Z. Properties of Bulk Sintered Silver As a Function of Porosity. Tennessee 2012. Oak Ridge National Laboratory (ORNL), ORNL/TM-2012/130. 31 p. DOI: 10.2172/1041433

[67] Technical Data Platilon® U [WWW] Germany, Epurex Films GmbH & Co. KG. Feb. 2012. [Accessed 2.1.2014]. Available at: http://www.epurex.com/fileadmin/downloads/Platilon_U_EN_2012-02.pdf

[68] NewMet60 Series datasheet [WWW] UK, New Metals & Chemicals Ltd. [Accessed on 2.1.2014] Available at: http://www.newmetalsandchemicals.com/downloads/ss_newmet60.pdf

[69] Dimatix Materials Printer DMP-2831 datasheet [WWW] USA, Fujifilm Dimatix, Inc. 19.4.2013. [Accessed on 2.1.2014]. Available at: http://www.fujifilmusa.com/shared/bin/PDS00085-DMP2831.pdf

[70] Smith, S. Sheet Resistance and Electrical Linewidth Test Structures for Semiconductor Process Characterisation. Dissertation. Edinburgh 2003. The University of Edinburgh. 224 p. Available at: http://www.see.ed.ac.uk/~ssmith13/thesis.pdf [Accessed 2.1.2014]

[71] Van der Pauw, L. J. A Method of Measuring Specific Resistivity and Hall Effect of Discs of Arbitrary Shape. Philips Research Reports 13(1958)1, pp. 1-9.

[72] Enderling, S., Brown, C.L. III., Smith, S., Dicks, M.H., Stevenson, J., Mitkova, M., Kozicki, M.N., Walton, A.J. Sheet resistance measurement of non-standard cleanroom materials using suspended Greek cross test structures. Semiconductor Manufacturing, IEEE Transactions on 19(2006)1, pp. 2-9. DOI: 10.1109/TSM.2005.863248

[73] ASTM Standard D 3359-09e2. Standard test method for measuring adhesion by tape test. Philadelphia 1995, American Society for Testing and Materials. 8 p. DOI: 10.1520/D3359-09E02

[74] ASTM Standard D4541-09e1. Standard Test Method for Pull-Off Strength of Coatings Using Portable Adhesion Testers. Philadelphia 2004. American Society for Testing and Materials. 16 p. DOI: 10.1520/D4541-09E01

[75] Hopcroft, M. A., Nix, W. D., & Kenny, T. W. What is the Young's Modulus of Silicon?. Microelectromechanical Systems, Journal of 19(2010)2, pp. 229-238. DOI: 10.1109/JMEMS.2009.2039697

[76] Robinson, A. P., Minev, I., Graz, I. M., & Lacour, S. P. Microstructured silicone substrate for printable and stretchable metallic films. Langmuir 27(2011)8, pp. 4279-4284. Supplementary information. [Accessed on 2.1.2014]. Available at: http://pubs.acs.org/doi/suppl/10.1021/la103213n/suppl_file/la103213n_si_002.pdf

[77] Nanotec ST5709S1208 datasheet [WWW]. [Accessed on 2.1.2014]. Available at: http://www.farnell.com/datasheets/81056.pdf

[78] ME EN 7960 – Precision Machine Design, Topic 4: Ball Screw Selection and Calculations [WWW] USA, The University of Utah. 30.11.2006. [Accessed 2.1.2014]. Available at: http://www.mech.utah.edu/~me7960/lectures/Topic4-BallscrewCalculations.pdf

[79] Technical Calculations, Selection of Ball Screws 1 [WWW]. Misumi Corporation. [Accessed on 2.1.2014]. Available at: http://us.misumi-ec.com/pdf/tech/mech/p2799.pdf

[80] McNier, T. & Johnson, J. G. Specifying, Selecting and Applying Linear Ball Screw Drives [WWW]. Wood Dale, IL, USA, Thomson Industries, Inc. [Accessed on 2.1.2014]. Available at: http://www.thomsonlinear.com/downloads/articles/Specifying_Selecting_Applying_Linear_Ball_Screw_Drives_taen.pdf

[81] ATmega48PA/88PA/168PA/328P datasheet [WWW] Atmel Corporation. 2009. [Accessed on 2.1.2014]. Available at: http://www.atmel.com/Images/doc8161.pdf

[82] Koskinen, S. Analysis of Inkjet-Printed Flex-Module in a Mobile Phone. Master of Science Thesis. Tampere 2011. Tampere University of Technology. 63 p.

A. APPENDIX

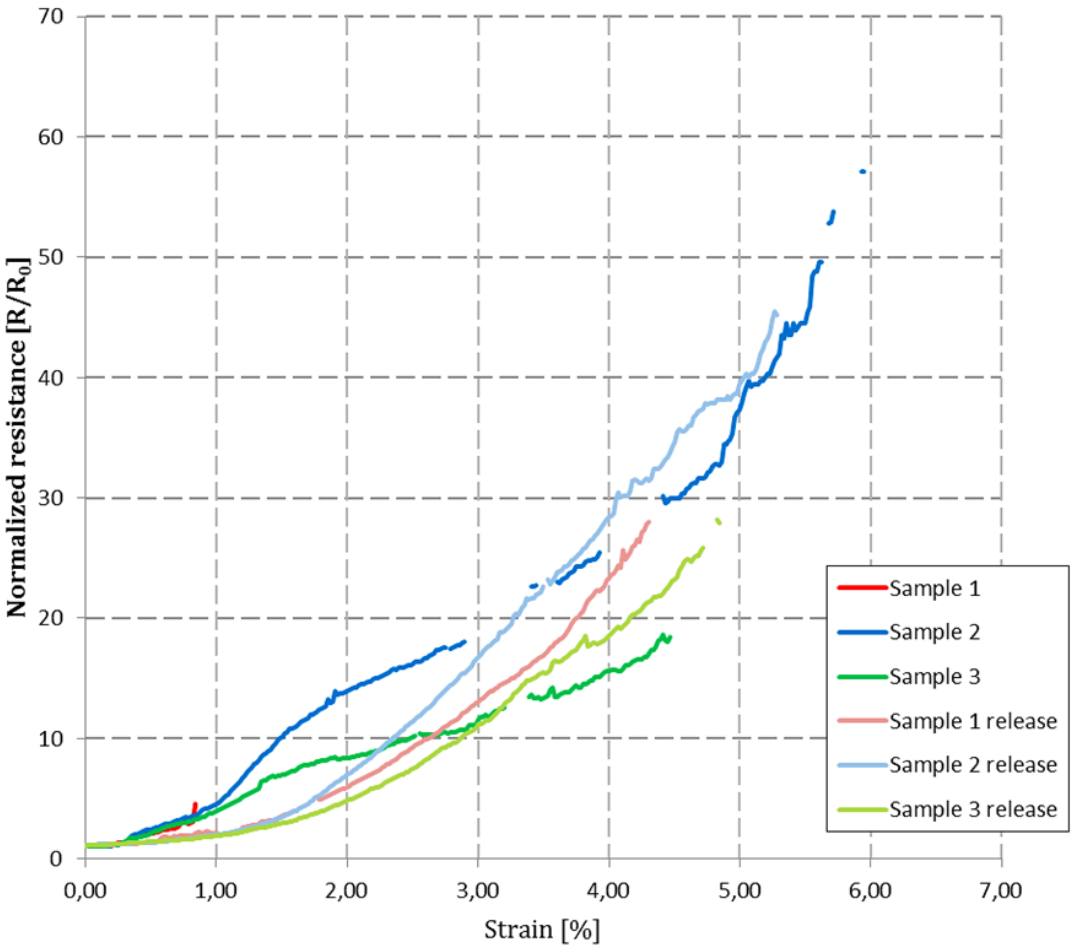

***Figure A.1**: Example of strain testing result with 1 mm wide inkjet-printed conductors on TPU when results are distorted due to incorrect sample attachment. Strain is not properly focused on conductors and therefore results are too optimistic.*